12-2018

Speleogenesis in Turbulent Flow

Max P. Cooper
University of Arkansas, Fayetteville

Speleogenesis in Turbulent Flow

A dissertation submitted in partial fulfillment
of the requirements for the degree of
Doctor of Philosophy in Geosciences

by

Max Cooper
State University of New York at New Paltz
Bachelor of Science in Geology, 2011
Mississippi State University
Master of Science in Geosciences, 2014

December 2018
University of Arkansas

This dissertation is approved for recommendation to the Graduate Council

Matthew Covington, Ph.D.
Dissertation Director

Jackson Cothren, Ph.D.
Committee Member

John Shaw, Ph.D.
Committee Member

Jill Marshall, Ph.D.
Committee Member

ABSTRACT

Existing models of speleogenesis neglect the shape of cross-sections, which can hold information related to climate, tectonics, and sediment supply in their widths. The first study of this dissertation simulates cross-sections of phreatic tubes, vadose canyons, and paragenetic galleries using a method developed for bedrock channels. Successful simulation of these cross-sections depends on erosion scaling with shear stress, in conflict with speleogenesis theory. Scaling of equilibrium width in paragenetic galleries was explored through analytical derivation and simulations, showing that width scales positively with discharge to the 1/2 power, and negatively with a weak power of sediment supply. Negative scaling of width to sediment supply is the opposite of scaling in surface bedrock channels.

Mechanisms of erosion were explored in Parks Ranch Cave, New Mexico, and Copperhead Cave, Arkansas by comparing simulated relationships between scallop ratios and incision angles varying with an exponent in the erosion model, and field data measured from 3D scans of meandering passages. Data indicate that the exponent is between 0.5 and 2.5, with a best fit of 0.5 for Copperhead, and 1 for Parks Ranch. These values arise due to a mixing of dissolution and abrasion. This study also developed a tool to estimate discharge in partially air-filled passages by minimizing the discrepancy between measured and calculated scallop size.

The last study extends the cross-section model into multiple cross-sections simulating a single conduit, with flow calculated using a stormwater management code. This model includes the ability for base level to change, and erosion weighted by the probability of a particular discharge. Single cross-section simulations with weighted erosion shows that equilibrium width in vadose canyons scales similarly when only the mean discharge is simulated, though the magnitude of widths is lower. Magnitude is controlled by an extremity parameter in the probability distribu-

tion, with distributions with less extreme events having larger widths. The multiple cross-section model simulates vadose canyon formation from a phreatic tube, and simulates vadose canyons propagating downstream, the opposite of knickpoint propagation in surface channels. The model also shows that keyhole passages are only successfully simulated when mean discharge lowers during conduit formation.

TABLE OF CONTENTS

LIST OF FIGURES

LIST OF TABLES

1 Introduction

Most studies on the formation of caves and karst features have largely focused on dissolution as the dominant mechanism of erosion (Covington et al., 2015). In contrast, geomorphologists studying insoluble bedrock channels have largely ignored the dissolution process and instead focus on erosion by mechanical processes (e.g. Chatanantavet and Parker, 2009; Lamb et al., 2008; Sklar and Dietrich, 2004; Whipple et al., 2000). Current mathematical models of *speleogenesis* (cave formation) in *epigene* caves, caves connected to surface hydrology and chemistry, are reflective of this disparity as they seek to understand the time scale and geometry of caves in the *pre-breakthrough* stage, before the onset of turbulent flow through the entire cave (e.g. Dreybrodt, 1996; Dreybrodt et al., 2005; Groves and Howard, 1994; Palmer, 1984, 1991; Szymczak and Ladd, 2011). These models cease at the centimeter scale in the dimension of passage width/diameter, treat cross-sections as either fractures or tubes, and neglect mechanical erosion as there would be little, if any, sediment transport through the incipient cave. Past the breakthrough stage models of cave evolution are conceptual, with few mathematical models existing (Covington and Perne, 2015; Grm et al., 2017; Hammer et al., 2011; Perne et al., 2014b), despite the bulk of morphology, particularly in the cross-section view (Lauritzen and Lundberg, 2000), being set in this stage.

Cave passages can be considered bedrock channels under the definition of Turowski et al., 2008b, as adjustments to channel morphology is due to erosion of bedrock. Such channels are well known to preserve records of past conditions such as climate in their geometry (e.g Amos and Burbank, 2007; Finnegan et al., 2005; Stark, 2006; Turowski et al., 2007, 2009; Wobus et al., 2008, 2006; Yanites and Tucker, 2010). The geometry of cave passages is thus a powerful tool for understanding climate, tectonics, and paleohydrology over long time periods as they can persist in

a landscape for millions of years (Broak, 2008; Gabrovšek, 2002; Osborne, 2007; Palmer, 2007; Plotnick et al., 2015). Additionally, caves are used as records for climate and landscape evolution through dating of sediment deposits preserved at discrete cave levels (Anthony and Granger, 2004, 2006, 2007; Granger et al., 2001, 1997; Granger and Siame, 2006). To address the lack of models I develop several process based models of cave evolution, including the cross-section and profile view, as well as explore the erosional mechanisms of cave formation past the breakthrough stage.

1.1 Current understanding of erosion in turbulent flow

The reason few attempts to model post-breakthrough speleogenesis have been conducted is due to the complexity of speleogenesis in turbulent flow. Turbulent flow creates complex flow structures that control shear stress on the walls, requiring computationally expensive estimations of the Navier-Stokes equations (e.g., Grm et al., 2017; Hammer et al., 2011). Turbulent flow can also transport sediment, which in turn can either armor caves from erosion or aid in it. While both dissolution and mechanical erosion is known to occur in caves and soluble bedrock channels, the relative amounts have only begun to be explored (Covington et al., 2015). Perhaps the largest issue in modeling speleogenesis in turbulent flow is a conundrum relating to the type of dissolution that occurs. This conundrum arises as speleogenetic theory, built upon experiments of Plummer et al., 1978, predicts that only surface reaction rate limited dissolution occurs in turbulent flow (Covington, 2014; Dreybrodt and Buhmann, 1991; Liu and Dreybrodt, 1997), resulting in an erosion law that does not scale with shear stress, and as a consequence, does not produce bedforms that require such scaling. The hypothesis of scallop formation by Curl, 1966, requires erosion to scale with shear stress. Despite this conundrum, scallops, a cuspate bedform (Fig. 1.1), are abundant in many cave settings.

Figure 1.1: A photograph of a set of scallops, a cuspate speleogen. The length of scallops is proportional to shear stress, with higher shear stresses resulting in smaller scallops. The geometry of scallops also indicates flow direction, with the point of the cusp indicating downstream direction, in this case from right to left.

Dissolution of minerals when interacting with water can occur with two rate limiting end members, or, if the rates are close enough, undergo mixed kinetics (Berner, 1978). These end members are surface reaction rate limited dissolution, where the chemical reaction at the surface limits the rate, and transport limited dissolution, where the rate at which ions involved in the reaction diffuse across a diffusion boundary layer (DBL). Surface reaction rate limited dissolution depends solely on the bulk chemistry of the water and a rate constant for the conversion of the mineral to dissolved ions. These rate constants are determined empirically through experiments. Transport limited dissolution depends on the bulk chemistry, and on the ratio between the thickness of the diffusion boundary layer (ϵ) and the diffusion rate of a particular ion. These extremes produce two differing erosion laws; surface reaction rate limited dissolution erosion only depends on chemistry, with no dependence on shear stress. On the other hand, transport limited dissolution depends on shear stress as DBL thickness can be written in terms of boundary shear stress, e.g.,

$$\epsilon = \frac{5\nu}{\sqrt{\tau_b/\rho_w}} \cdot Sc^{-1/3}, \tag{1.1}$$

where ν is kinematic viscosity, τ_b is boundary shear stress, ρ_w is water density, and Sc is the Schmidt number (ν/D) (Perne et al., 2014a). In this formulation, ϵ depends on τ_b to the $-1/2$ power, and as erosion rate is proportional to the inverse of ϵ it is related to $\tau_b^{1/2}$.

Most caves formed by dissolution are within limestone, which is composed primarily of calcite. The dissolution of calcite is a slow reaction when compared to the dissolution of gypsum and salt, two other cave forming minerals. By analyzing the possible rates of calcite dissolution due to surface reaction limited dissolution as determined by experiments of Plummer et al., 1978, compared to thickness of the DBL in a large parameter space calculated from the hydraulic parameters diameter and gradient (Fig. 1.2), Covington, 2014 determined that in almost no case is dissolution of calcite transport limited. As such, any speleogen (cave formation formed by erosion) that requires erosion to scale with shear stress must be formed by some mechanical process, such as abrasion or grain plucking, or the rate constants determined from Plummer et al., 1978 are not true surface reaction rates. One issue in the experiments of Plummer et al., 1978 is that the hydrodynamics of the system, in this case powdered calcite in a batch reactor, are not known, and the ratio of surface reaction rate to transport rate can not be determined. Experiments where hydrodynamics are known, and ϵ can be computed, show higher surface reaction rates in calcite (Rickard and Sjöberg, 1983; Sjöberg, 1976; Sjöberg and Rickard, 1983). Thus, in some cases, dissolution of calcite can be transport limited. While these experiments show that transport limited dissolution or mixed kinetics can occur for calcite, the rates obtained do not greatly increase the cave settings in which dissolution is transport limited ($min(\epsilon_{crit,Sj})in$Fig. 1.2).

In other media, such as gypsum, dissolution rates have been shown to be transport limited of mixed in turbulent flow. The mixed kinetics of gypsum (Raines and Dewers, 1997) allow erosion in this media to scale with a fractional power of shear stress (Opdyke et al., 1987). While this

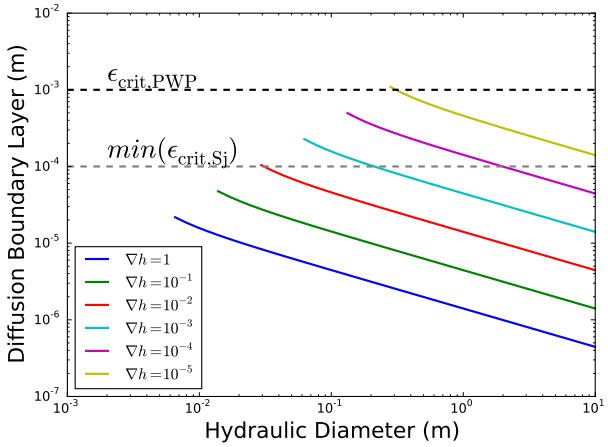

Figure 1.2: Graph of boundary layer thickness given a hydraulic diameter and gradient. Lines indicate the critical thickness, above which transport limited dissolution can occur considering data from Plummer et al., 1978 (PWP), and Sjöberg, 1976 (Sj).

is the case in experiment, it is unknown what conditions produce transport limited dissolution in caves formed in gypsum. Additionally, the relative importance of mechanical erosion is unknown in these caves.

As erosion in non-soluble, surface bedrock channels is well understood (Chatanantavet and Parker, 2009; Sklar and Dietrich, 2004; Whipple et al., 2000) compared to caves and surface soluble bedrock channels, models of bedrock channel formation are more developed for turbulent flow. To model speleogenesis in turbulent flow methods developed for studying bedrock channel evolution can be adapted.

1.2 Bedrock channels

1.2.1 Erosion in bedrock channels

Erosion in bedrock channels is most largely due to processes of mechanical erosion such as plucking of jointed blocks, abrasion, and cavitation (e.g., Whipple and Tucker, 1999). To model erosion in bedrock channels a simplified equation is often used. Equations include the stream power

erosion model,

$$E = K_s A_b^m S^n, \tag{1.2}$$

where K_s is a constant encapsulating erodibility, A_b is contributing basin area, S is slope, and m and n are exponents related to process, or a shear stress erosion model,

$$E = K\tau_b^a \tag{1.3}$$

where K is a constant and a is an exponent related to process. When shear stress is formulated as the depth-slope product,

$$\tau_b = \rho g H S \tag{1.4}$$

where ρ is density of the fluid, g is acceleration due to gravity, and H is the depth of flow, the exponents are translatable with $n = 2a/3$. Known relationships between processes and a include $1 \leq a \leq 3/2$ for plucking of jointed blocks, $a = 5/2$ for abrasion, and $q/2$ where q is a positive integer up to 7 for cavitation. Erosion can also be modeled by physically derived equations for plucking and abrasion (Chatanantavet and Parker, 2009; Sklar and Dietrich, 2004).

While considering only stream power and shear stress erosion laws allow generalizations at the landscape scale, sediment effects become important at the scale of individual channels and cross-sections due to cover protecting some of the bed from erosion.

1.2.2 Role of sediment

Sediment plays two roles in bedrock channels. The first role is supplying *tools* for eroding, the second is providing a *cover* from further erosion.

Sediment cover has many effects. Cover in bedrock channels is known to widen channels (Turowski, 2018; Turowski et al., 2007), and an increase in sediment supply increases cover and

width (Yanites and Tucker, 2010). This widening is due to sediment armoring the center of the channel, where without cover most erosion would occur, forcing erosion to proceed laterally. Lateral erosion may also cause meandering (Turowski et al., 2008a). Cover can also set the efficacy of erosion, and lower long term incision rates (Lague, 2010).

Another effect of sediment is the setting of thresholds. The ability to transport sediment requires an initial threshold to be met at which the force of drag on a sediment particle can overcome frictional forces. This threshold is known as the threshold for sediment motion and can be expressed as a critical shear stress τ_c, and is typical in sediment transport laws such as that of Fernandez Luque and Beek, 1976. As there is a threshold for sediment motion, it follows that in order for erosion to occur this threshold must be exceeded, and that under the threshold the cover effect dominates. The shear stress threshold also creates a discharge (Q) threshold, as τ_b is a function of discharge. At low Q sediment is immobile and a cover persists. At high Q, such as during flooding, the cover can become mobile and provide tools for erosion. From this threshold effect it is interpreted that most geomorphic work occurs in floods of high return time (Barbour et al., 2009; Hartshorn et al., 2002; Lague, 2010; Turowski et al., 2008a). The recognition of this threshold has led to modeling of erosion using probabilistic models of erosion past simple expressions such as the stream power erosion law by including discharge probability distributions and the likelihood of exceeding (e.g, Lague, 2014; Lague et al., 2005; Molnar et al., 2006). Such models have increasingly shown the importance of discharge probability on scaling relationships between geometry, climate, tectonics, and sediment supply.

1.2.3 Geometry scaling and cross-section models

Models of bedrock channel evolution are commonly explored to build scaling relationships between measurable parameters such as slope and width to climate and tectonics (Amos and Burbank, 2007; DiBiase and Whipple, 2011; Finnegan et al., 2005; Stark, 2006; Whipple and Tucker, 1999; Wobus et al., 2008, 2006), as they can be used to constrain unknowns such as uplift rate (e.g., Kirby and Whipple, 2012; Lague, 2014; Miller et al., 2013; Roberts and White, 2010; Whittaker et al., 2007). Common scalings are between width and discharge ($W \propto Q^{0.3-05}$), and slope and discharge ($S \propto Q^{-3/16}$) (e.g., Finnegan et al., 2005). Such models can be analytical (e.g., Finnegan et al., 2005; Wobus et al., 2008), starting with a set of assumptions, or can simulate geometry with a freely changing cross-section shape (e.g., Stark, 2006; Wobus et al., 2008, 2006). Common assumptions in analytic derivations are a constant shape, characterized by width-to-depth ratio, and erosion governed by the stream power erosion law or linear shear stress erosion law equaling base level drop, also known as steady state (e.g., Finnegan et al., 2005).

The speleogenesis models in this dissertation use a freely updating cross-section. To update the cross-section a shear stress erosion model is used, and shear stress is estimated using the method of Wobus et al., 2006, termed the WTA method. The WTA method treats the cross-section as a series of points that define the perimeter and updates the cross-section through time proportional to shear stress to an exponent reflective of process. Shear stress in the WTA is approximated with a modified law of the wall equation that references the point of maximum velocity. The speleogenesis model developed in this dissertation modifies the original WTA method which considers the maximum velocity position to be the center of the free-surface, to the centroid of the perimeter for conduit-full conditions (phreatic conditions). The normal WTA method is also used to simulate vadose canyons,

where the cave passage is partially air filled. The WTA method also includes a method to find the height of the water in the cross- section by minimizing the difference between a prescribed discharge and discharge calculated using the Chézy equation with a height dependent wetted perimeter, P, and wetted cross-sectional area, A. The WTA method allows the simulation of a cross-section given only the geometry of the channel, roughness length, discharge, and slope in the free-surface case. In the phreatic case slope becomes an energy slope and is calculated with the Chézy equation and roughness length.

1.3 Cave cross-sections

Unlike the morphology of bedrock channels, cave morphology has been largely limited to conceptual models. One aspect of cave morphology, the cross-section, can be very complex and range from simple tubes and canyons, to ruggedly sculpted shapes with features such as ceiling anastomoses and pendants. These cross-sections can also record multiple stages of development such as the switch from phreatic to vadose conditions, or the changing of discharge reflected by narrowing or the formation of notches. Lauritzen and Lundberg, 2000 presents a thorough review of cross-sectional geometries in caves.

The cross-section geometries explored in this dissertation are phreatic tubes, meandering and non-meandering vadose canyons, paragenetic galleries, and keyholes where a narrower vadose canyon incises into a phreatic tube. Phreatic tubes are simple elliptical or circular shapes. These form when hydraulic head is above the cave passage and the passage is in conduit-full conditions, causing erosion to occur entirely throughout the perimeter. Vadose canyons are typically taller than they are wide, and often have a constant, or little varying width from floor to ceiling. Canyons form

when a free-surface is in the passage. As the cave is partially air-filled the upper portions do not erode, and erosion is focused on the walls below the free-surface and the floor of the passage.

Paragenetic galleries are also are typically taller than they are wide. These form in the phreatic zone and therefore the conduit is filled with water. This interesting process occurs when sediment armors the floor of the passage, protecting the floor and lower parts of the walls from erosion (e.g., Farrant and Smart, 2011; Renault, 1968). As water is in contact with the ceiling, and it is not protected by cover, erosion occurs upwards towards the water table. As this erosion is directed upwards, against the direction of gravity, it is sometimes termed antigravite erosion (Pasini, 2009). Again, like vadose canyons, paragenetic galleries commonly feature constant widths. Paragenesis can also form many complex cross-sections when the sediment interface is near the ceiling, including ceiling anaostomeses and ceiling pendants (Farrant and Smart, 2011; Lauritzen and Lundberg, 2000).

The last type of cross-section explored are keyholes. Keyholes are shaped like their namesake and have a narrower vadose canyon cut into a phreatic tube. There are several possible explanations for keyholes including only requiring base level to drop, transitioning from conduit-full conditions to having a free-surface with conduit-full conditions existing long enough to enlarge the cross-section to be greater than the equilibrium width of a canyon given particular discharge, combined with base level dropping. Another hypothesis is that discharge must change at some point, causing the smaller width to occur.

1.4 Goals of the dissertation

The overall goal of this dissertation is to develop an understanding of speleogenesis in turbulent flow and to provide tools for determining erosive mechanisms in soluble bedrock channels.

This dissertation is organized into three separate, but connected chapters that stand as papers on their own. The first paper details a simple, single cross-section model of speleogenesis in turbulent flow and focuses on modeling the process of paragenesis. The goal of this paper is to see if it is possible to model cave cross-sections in phreatic tubes, vadose canyons, and paragenetic galleries, and to elucidate the dynamics of paragenesis.

The second paper explores mechanisms of erosion in two caves, Parks Ranch Cave, a gypsum cave in New Mexico, and Copperhead Cave, a limestone cave in Arkansas. To explore erosion mechanisms 3D scans are performed around well scalloped meander bends. The scallops and incision angles within the meander bends are measured, and compared to relationships simulated using the cross-section model built in the first paper. The goal of this paper is to see if it is possible to constrain erosion method from these data and modeled relationships.

The last paper extends the cross-section model into a multiple cross-section model with multiple discharges, erosion weighted by the probability of a discharge occurring, and base level drop. The goal of the last paper is to explore cross-section and profile geometry in the transition from phreatic to vadose conditions, and to test hypotheses of keyhole type passage formation.

1.5 References

Amos, C. B. and D. W. Burbank (2007). "Channel width response to differential uplift". In: *Journal of Geophysical Research: Earth Surface* 112.F2.

Anthony, D. M. and D. E. Granger (2004). "A Late Tertiary origin for multilevel caves along the western escarpment of the Cumberland Plateau, Tennessee and Kentucky, established by 26Al and 10Be". In: *Journal of Cave and Karst Studies* 66.2, pp. 46–55.

— (2006). "Five million years of Appalachian landscape evolution preserved in cave sediments". In: *Perspectives on karst geomorpology, hydrology, and geochemistry - A tribute volume to Derek C. Ford and William B. White*. Ed. by R. S. Harmon and C. M. Wicks. Vol. 404. Special Paper. Geological Society of America, pp. 39–50.

Anthony, D. M. and D. E. Granger (2007). "A new chronology for the age of Appalachian erosional surfaces determined by cosmogenic nuclides in cave sediments". In: *Earth Surface Processes and Landforms* 32.6, pp. 874–887.

Barbour, J. R., C. P. Stark, C. W. Lin, H. Chen, M. J. Horng, C. P. Ko, T. C. Yi, T. T. Tsai, W. S. Chang, S. P. Lee, et al. (2009). "Magnitude-frequency distributions of boundary shear stress along a rapidly eroding bedrock river". In: *Geophysical Research Letters* 36.4.

Berner, R. A. (1978). "Rate control of mineral dissolution under earth surface conditions". In: *American Journal of Science* 278.9, pp. 1235–1252.

Broak, P. (2008). "Karst processes and time". In: *Geologos* 14, pp. 19–36.

Chatanantavet, P. and G. Parker (2009). "Physically based modeling of bedrock incision by abrasion, plucking, and macroabrasion". In: *J. of Geophys. Res.* 114.F4, F04018.

Covington, M. D. (2014). "Calcite dissolution under turbulent flow conditions: a remaining conundrum". In: *Acta Carsologica* 43.1, pp. 195–202.

Covington, M. D., J. D. Gulley, and F. Gabrovšek (2015). "Natural variations in calcite dissolution rates in streams: Controls, implications, and open questions". In: *Geophysical Research Letters* 42.8, pp. 2836–2843.

Covington, M. D. and M. Perne (2015). "Consider a cylindrical cave: A physicist's view of cave and karst science". In: *Acta Carsologica* 44.3, pp. 363–380.

Curl, R. L. (1966). "Scallops and Flutes". In: *Transactions of the Cave Research Group of Great Britain* 7.2, pp. 121–160.

DiBiase, R. A. and K. X. Whipple (2011). "The influence of erosion thresholds and runoff variability on the relationships among topography, climate, and erosion rate". In: *Journal of Geophysical Research: Earth Surface* 116.F4.

Dreybrodt, W. (1996). "Principles of early development of karst conduits under natural and man-made conditions revealed by mathematical analysis of numerical models". In: *Water Resources Research* 32.9, pp. 2923–2935.

Dreybrodt, W. and D. Buhmann (1991). "A mass transfer model for dissolution and precipitation of calcite from solutions in turbulent motion". In: *Chemical Geology* 90.1, pp. 107–122.

Dreybrodt, W., F. Gabrovšek, and D. Romanov (2005). *Processes of Speleogenessis: A Modeling Approach*. Vol. 4. Ljubljana, Slovenia: ZRC Publishing, p. 376.

Farrant, A. R. and P. L. Smart (2011). "Role of sediment in speleogenesis; sedimentation and paragenesis". In: *Geomorphology* 134.1, pp. 79–93.

Fernandez Luque, F. and R. van Beek (1976). “Erosion and transport of bed-load sediment”. In: *Journal of Hydraulic Engineering* 14.2, pp. 127–144.

Finnegan, N. J., G. Roe, D. R. Montgomery, and B. Hallet (2005). “Controls on the channel width of rivers: Implications for modeling fluvial incision of bedrock”. In: *Geology* 33.3, pp. 229–232.

Gabrovšek, F. (2002). *Evolution of karst: from prekarst to cessation*. Založba ZRC.

Granger, D. E., D. Fabel, and A. N. Palmer (2001). “Pliocene- Pleistocene incision of the Green River, Kentucky, determined from radioactive decay of cosmogenic 26Al and 10Be in Mammoth Cave sediments”. In: *Geological Society of America Bulletin* 113.7, pp. 825–836.

Granger, D. E., J. W. Kirchner, and R. C. Finkel (1997). “Quaternary downcutting rate of the New River, Virginia, measured from differential decay of cosmogenic 26Al and 10Be in cave-deposited alluvium”. In: *Geology* 25, pp. 107–110.

Granger, D. E. and L. Siame (2006). “A review of burial dating methods usingˆ 2ˆ 6Al andˆ 1ˆ 0Be”. In: *Special Papers-Geological Society of America* 415, p. 1.

Grm, A., T. Šuštar, T. Rodič, and F. Gabrovšek (2017). “A numerical framework for wall dissolution modeling”. In: *Mathematical Geosciences* 49.5, pp. 657–675.

Groves, C. G. and A. D. Howard (1994). “Early development of karst systems: 1. Preferential flow path enlargement under laminar flow”. In: *Water Resources Research* 30.10, pp. 2837–2846.

Hammer, Ø., S.-E. Lauritzen, and B. Jamtveit (2011). “Stability of dissolution flutes under turbulent flow”. In: *Journal of Cave and Karst Studies* 73.3, pp. 181–186.

Hartshorn, K., N. Hovius, W. B. Dade, and R. L. Slingerland (2002). “Climate-driven bedrock incision in an active mountain belt”. In: *Science* 297.5589, pp. 2036–2038.

Kirby, E. and K. X. Whipple (2012). “Expression of active tectonics in erosional landscapes”. In: *Journal of Structural Geology* 44, pp. 54–75.

Lague, D. (2010). “Reduction of long-term bedrock incision efficiency by short-term alluvial cover intermittency”. In: *Journal of Geophysical Research: Earth Surface* 115.F2.

— (2014). “The stream power river incision model: evidence, theory and beyond”. In: *Earth Surface Processes and Landforms* 39.1, pp. 38–61.

Lague, D., N. Hovius, and P. Davy (2005). “Discharge, discharge variability, and the bedrock channel profile”. In: *Journal of Geophysical Research (Earth Surface)* 110.F9, pp. 4006–+. DOI: 10.1029/2004JF000259.

Lamb, M. P., W. E. Dietrich, and L. S. Sklar (2008). “A model for fluvial bedrock incision by impacting suspended and bed load sediment”. In: *Journal of Geophysical Research (Earth Surface)* 113.F12, pp. 3025–+. DOI: 10.1029/2007JF000915.

Lauritzen, S.-E. and J. Lundberg (2000). “Solutional and erosional morphology of caves”. In: *In: Klimchouk, A., Ford, DC, Palmer, Arthur N. & Dreybrodt, Wolfgang,(eds), Speleogenesis. Evolution of Karst Aquifers. National Speleological Society, Huntsville*, pp. 408–426.

Liu, Z. and W. Dreybrodt (1997). “Dissolution kinetics of calcium carbonate minerals in H2O-CO2 solutions in turbulent flow: the role of the diffusion boundary layer and the slow reaction H2O + CO2 -> H+ + HCO3-”. In: *Geochimica Cosmochimica Acta* 61.14, pp. 2879–2889. URL: http://www.imedea.uib-csic.es/master/cambioglobal/Modulo_3_02/Tema_8-acidificaci%C3%B3n/pH/geochim%20cosmochim61pp2879-2889.pdf.

Miller, S. R., P. B. Sak, E. Kirby, and P. R. Bierman (2013). “Neogene rejuvenation of central Appalachian topography: Evidence for differential rock uplift from stream profiles and erosion rates”. In: *Earth and Planetary Science Letters* 369, pp. 1–12.

Molnar, P., R. S. Anderson, G. Kier, and J. Rose (2006). “Relationships among probability distributions of stream discharges in floods, climate, bed load transport, and river incision”. In: *Journal of Geophysical Research: Earth Surface* 111.F2.

Opdyke, B. N., G. Gust, and J. R. Ledwell (1987). “Mass transfer from smooth alabaster surfaces in turbulent flows”. In: *Geophysical Research Letters* 14.11, pp. 1131–1134. ISSN: 0094-8276. DOI: 10.1029/GL014i011p01131.

Osborne, A. R. L. (2007). “The World’s Oldest Caves:-How-Did They Survive and What Can They Tell Us?” In: *Acta carsologica* 36.1.

Palmer, A. N. (1984). “Geomorphic interpretation of karst features”. In: *Groundwater as a geomorphic agent. Allen and Unwin, Boston, Massachusetts. 390pp*, pp. 173–209.

— (1991). “Origin and morphology of limestone caves”. In: *Geological Society of America Bulletin* 103.1, pp. 1–21.

— (2007). “Variation in Rates of Karst Processes”. In: *Acta Carsologica* 36 (1).

Pasini, G. (2009). “A terminological matter: paragenesis, antigravitative erosion or antigravitational erosion?” In: *International Journal of Speleology* 38.2, p. 4.

Perne, M., M. D. Covington, and F. Gabrovšek (2014a). “Evolution of karst conduit networks in transition from pressurised flow to free surface flow”. In: *Hydrology and Earth System Sciences Discussions* 11.6, pp. 6519–6559. DOI: 10.5194/hessd-11-6519-2014. URL: http://www.hydrol-earth-syst-sci-discuss.net/11/6519/2014/.

Perne, M., M. D. Covington, and Franci Gabrovšek (2014b). “Evolution of karst conduit networks in transition from pressurized flow to free-surface flow”. In: *Hydrology and Earth System Sciences* 18.11, pp. 4617–4633.

Plotnick, R. E., F. Kenig, and A. C. Scott (2015). “Using the voids to fill the gaps: caves, time, and stratigraphy”. In: *Geological Society, London, Special Publications* 404.1, pp. 233–250.

Plummer, L. N., T. M. L. Wigley, and D. L. Parkhurst (1978). “The kinetics of calcite dissolution in CO2-water systems at 5 degrees to 60 degrees C and 0.0 to 1.0 atm CO2”. In: *American Journal of Science* 278.2, p. 179.

Raines, M. A. and T. A. Dewers (1997). “Mixed transport/reaction control of gypsum dissolution kinetics in aqueous solutions and initiation of gypsum karst”. In: *Chemical Geology* 140.1-2, pp. 29–48.

Renault, P. (1968). “Contribution à l’étude des actions mécaniques et sédimentologiques dans la spéléogenèse”. In: *Annales de spéléologie*. Vol. 22. 1, pp. 5–21.

Rickard, D. and E. L. Sjöberg (1983). “Mixed kinetic control of calcite dissolution rates”. In: *American Journal of Science* 283.8, pp. 815–830.

Roberts, G. G. and N. White (2010). “Estimating uplift rate histories from river profiles using African examples”. In: *Journal of Geophysical Research: Solid Earth* 115.B2.

Sjöberg, E. L. (1976). “A fundamental equation for calcite dissolution kinetics”. In: *Geochimica et Cosmochimica Acta* 40.4, pp. 441–447.

Sjöberg, E. L. and D. Rickard (1983). “The influence of experimental design on the rate of calcite dissolution”. In: *Geochimica et cosmochimica acta* 47.12, pp. 2281–2285.

Sklar, L. S. and W. E. Dietrich (2004). “A mechanistic model for river incision into bedrock by saltating bed load”. In: *Water Resour. Res.*

Stark, C. P. (2006). “A self-regulating model of bedrock river channel geometry”. In: *Geophysical Research Letters* 33.4.

Szymczak, P. and A. J. C. Ladd (2011). “The initial stages of cave formation: Beyond the one-dimensional paradigm”. In: *Earth and Planetary Science Letters* 301.3, pp. 424–432.

Turowski, J. M. (2018). “Alluvial cover controlling the width, slope and sinuosity of bedrock channels”. In: *Earth Surface Dynamics* 6.1, p. 29.

Turowski, J. M., N. Hovius, H. Meng-Long, D. Lague, and C. Men-Chiang (2008a). “Distribution of erosion across bedrock channels”. In: *Earth Surface Processes and Landforms: The Journal of the British Geomorphological Research Group* 33.3, pp. 353–363.

Turowski, J. M., N. Hovius, A. Wilson, and M.-J. Horng (2008b). “Hydraulic geometry, river sediment and the definition of bedrock channels”. In: *Geomorphology* 99, pp. 26–38.

Turowski, J. M., D. Lague, and N. Hovius (2007). “Cover effect in bedrock abrasion: A new derivation and its implications for the modeling of bedrock channel morphology”. In: *Journal of Geophysical Research: Earth Surface* 112.F4.

— (2009). “Response of bedrock channel width to tectonic forcing: Insights from a numerical model, theoretical considerations, and comparison with field data”. In: *Journal of Geophysical Research: Earth Surface* 114.F3.

Whipple, K. X., G. S. Hancock, and R. S. Anderson (2000). “River incision into bedrock: Mechanics and relative efficacy of plucking, abrasion, and cavitation”. In: *Bulletin of the Geological Society of America* 112.3, pp. 490–503.

Whipple, K. X. and G. E. Tucker (1999). “Dynamics of the stream-power river incision model: Implications for height limits of mountain ranges, landscape response timescales, and research needs”. In: *Journal of Geophysical Research* 104.B8.

Whittaker, A. C., P. A Cowie, M. Attal, G. E. Tucker, and G. P. Roberts (2007). “Bedrock channel adjustment to tectonic forcing: Implications for predicting river incision rates”. In: *Geology* 35.2, pp. 103–106.

Wobus, C. W., J. W. Kean, G. E. Tucker, and R. S. Anderson (2008). “Modeling the evolution of channel shape: Balancing computational efficiency with hydraulic fidelity”. In: *Journal of Geophysical Research: Earth Surface (2003–2012)* 113.F2.

Wobus, C. W., G. E. Tucker, and R. S. Anderson (2006). “Self-formed bedrock channels”. In: *Geophysical Research Letters* 33.18.

Yanites, B. J. and G. E. Tucker (2010). “Controls and limits on bedrock channel geometry”. In: *Journal of Geophysical Research* 115.F04019, pp. 1–17.

2 Modeling Cross-Section Evolution

MODELING CAVE CROSS-SECTION EVOLUTION INCLUDING SEDIMENT TRANSPORT AND PARAGENESIS

2.1 Abstract

The geometry of cave cross-sections is an important indicator of its formative processes. While speleogenesis (cave formation) has been modeled extensively, cross-sections have nearly entirely been treated as simple tubes or fractures. In this study we build a model for the evolution of cross-sections by adapting methods developed in the bedrock channel literature.

To model cross-section development in caves we adapt a method developed to estimate boundary shear stress along a perimeter of discrete points for surface bedrock channels to closed shapes. The geometry of the cross-section is updated with an erosion law that scales with shear stress. As a first test of the model we simulate phreatic tubes, vadose canyons, and paragenetic galleries with two erosion rules: scaling with shear stress to the 1/2 power, and not scaling with shear stress. Simulations where erosion does not scale with shear stress, in-line with current speleogenesis theory, do not produce realistic cross-sections, indicating our knowledge of erosion in caves is incomplete. Secondly, we duplicate the scaling relationship between discharge and width modeled in the original study that developed the shear stress method, and simulated the effect of changing power in the erosion law, reflecting a change in erosional mechanism. Changing the erosional power does not affect the scaling relationship, though does change the magnitude of width.

We also use this model to explore the dynamics and scaling relationships that form paragenetic galleries. The model successfully duplicates the hypothesized dynamics that these galleries,

and produces equilibrium widths that scale identically with an analytically derived relationship. The scaling law predicts that increased sediment supply results in smaller widths to balance shear stress and sediment transport. This scaling is opposite of that within surface channels.

2.2 Introduction

Cave cross-sections have long been understood to record information about the formative processes of caves (Bretz, 1942). Cross-section shape can indicate the position of a cave passage with respect to the water table during development. Water-filled passages forming in the phreatic zone have a tube or enlarged fracture shape, typically of similar width to height. Vadose passages, which are partially air-filled, tend to be canyon shaped and have a greater height than width. However, superficially similar geometries can also arise through entirely different genetic origins; paragenetic galleries have a greater height than width, but unlike vadose canyons they form in the phreatic zone when sediment armors the floor and walls of the cave (Farrant and Smart, 2011).

It is important to be able to identify the formative location of particular passages, because cave levels, and age dates of sediments deposited within them, are often used to reconstruct base level history and constrain landscape evolution rates (e.g. Anthony and Granger, 2004, 2006, 2007; Granger et al., 2001, 1997; Granger and Siame, 2006; Palmer, 1987; Stock et al., 2005). For instance, misidentifying a paragenetic passage as vadose would lead to an underestimation of the elevation of base level, and thus an improper value for erosion rate. Additionally, cave passages can be considered to be bedrock channels (Turowski et al., 2008), as morphological adjustments of a cave channel require the erosion of bedrock. Since the geometry of bedrock channels is known to vary with parameters such as uplift rate, discharge, and sediment supply (e.g., Amos and Burbank, 2007; Finnegan et al., 2005; Stark, 2006; Turowski et al., 2007, 2009; Wobus et al., 2008, 2006;

Yanites and Tucker, 2010), the geometry of cave cross-sections may also hold information about hydrological, tectonic, and sediment supply conditions during the time of formation. Despite the usefulness of cave cross-sections, and a broad conceptual understanding of the relationships between cave passage shape and formative conditions (e.g., Bretz, 1942; Farrant and Smart, 2011; Lauritzen and Lauritsen, 1995; Lauritzen and Lundberg, 2000; Palmer, 1984), no mathematical models have been developed to quantitatively explore the relationships between cave passage shape and the conditions during cave development. Consequently, we also have little understanding of the dynamics and timescales associated with adjustments in cross sectional shape.

Here we simulate the evolution of cross-sectional shapes using a simple, physically based model, and explore the development of phreatic tubes, vadose canyons, and paragenetic galleries. We test the conceptual model of paragenesis, capture the dynamics of the process, and determine scaling relationships between equilibrium geometry, discharge, and sediment supply. We also test the effect of different erosion mechanisms on scaling relationships and cross-section shape.

2.3 Background

The morphology of surface bedrock channels has been well studied quantitatively and has been modeled both physically in flumes (e.g., Finnegan et al., 2007; J. P. Johnson and Whipple, 2010) and numerically (e.g., Finnegan et al., 2005; Nelson and Seminara, 2011; Stark, 2006; Wobus et al., 2008, 2006). Bedrock channel studies have focused on how geometry scales with parameters such as discharge, contributing basin area, sediment supply, and lithology. Geometrical parameters include the width of the channel, the width-to-depth (aspect) ratio, and slope. Well known relationships include the scaling of width ($W \propto Q^{0.3-0.5}$) and slope to discharge, and how width-to-depth ratio changes with lithology (e.g., Amos and Burbank, 2007; Finnegan et al., 2005). These studies

have also focused on the response of the geometry to changes in uplift rates and lithology (e.g. Amos and Burbank, 2007; Finnegan et al., 2005; Stark, 2006; Wobus et al., 2006), and sediment supply (e.g., Yanites and Tucker, 2010).

Bedrock channel models often start with an erosion law, typically the stream power erosion model,

$$E = K_s A_b^m S^n \,, \tag{2.1}$$

or a shear stress erosion model,

$$E = K \tau_b^a \,. \tag{2.2}$$

The parameters for these models are: K_s, a constant that encapsulates erodibility factors with units $[L^{1-2m}T^{-1}]$, A_b, contributing basin area, S, the slope of the channel, and τ_b, boundary shear stress. K in the shear stress model is also a constant, though is different than K_s in the stream power erosion model. The powers m, n, and a are values that depend on erosional processes. These two models of erosion are near identical in their formulation, as shear stress in most models is estimated with the depth-slope product,

$$\tau_b = \rho_w g H S \,, \tag{2.3}$$

where ρ_w is the density of water, g is acceleration due to gravity, and H is the depth of water. When the depth-slope product is used to estimate boundary shear stress, the exponents in these models are related by $n = 2a/3$. Values in the shear stress erosion law are typically $1 \lesssim a \lesssim 7/2$ for mechanical/physical processes such as plucking of jointed blocks, abrasion, and cavitation (Whipple et al., 2000).

Landscape evolution models including bedrock channels treat channels as having simple geometry that does not evolve in shape. While this is sufficient for modeling at the landscape

scale, it neglects the ability for cross-sections to freely evolve in shape. Cross-section models treat the geometry as a series of points that can erode at independent rates that are function of shear stress. Available models use a shear stress approximation such as the Ray-Isovel Method (Kean et al., 2009; Kean and Smith, 2004; Nelson and Seminara, 2011) or a modified version of the law of the wall equation (Wobus et al., 2008, 2006) to estimate shear stress and erode the channel cross-section using the shear stress erosion law (e.g., Eq. 2.2).

While mathematical models of speleogenesis (cave formation) have been around since the 1980s (Dreybrodt, 1988; Palmer, 1984), they have primarily focused on the pre-breakthrough stage, during initial network development, typically with individual conduit widths at the centimeter scale. These models have neglected evolution of passage cross-sectional shape and instead treat incipient cave passages as fractures or tubes (e.g., Dreybrodt et al., 2005). There are several barriers to the development of models for cross section evolution. The first barrier is the complexity of calculating flow structures and shear stress for passage shapes more complicated than a simple planar fracture or circular tube. Such calculations are needed to estimate contrasts in erosion rates along the passage wall. Some attempts to model flow structures and shear stress use computational fluid dynamics (CFD) to solve the Navier-Stokes equation for incompressible flow (Covington and Perne, 2015; Grm et al., 2017; Hammer et al., 2011). While these methods can calculate flow structures, they are computationally expensive and are not currently suitable for cross-section evolution over thousands of time steps. Perne et al., 2014 used a simplified version of the Navier-Stokes equations, the 1-D Saint-Venant equations in a storm water management software, SWMM, to simulate cave formation over long periods of time, however, this simplified equation is depth averaged and neither captures small scale flow structures nor produces a robust method of shear stress estimation. Simpler approximations such as the depth-slope product have been used to estimate shear stress in

caves for the purposes of quantifying sediment transport (e.g., Dogwiler and Wicks, 2004; Herman, 2006; Springer, 2004; E. L. White and W. B. White, 1968). While this formulation may be adequate for generalizations, it is not adequate for simulating channel development (Wobus et al., 2008).

A second problem is the poor understanding of the dissolution of calcite in turbulent flow. The theory of speleogenesis in turbulent flow is built on the calcite dissolution experiments of Plummer et al., (1978), and assumes the measured rates in the experiments represent true surface reaction rate limited dissolution. If these experimental results are applied within the turbulent dissolution model developed by Dreybrodt and Buhmann, (1991), results suggest that dissolution rates are limited by the rate of the surface reaction under most turbulent flow conditions Covington, (2014). If this is the case, dissolution rate, E_D, is only controlled by a rate constant and the degree of undersaturation with respect to calcite. Below 80% saturation the rate is

$$E_D = \alpha_C(C_{Eq} - C_b), \tag{2.4}$$

where α_C is a rate constant that does not depend on flow and is determined by experiment, C_{Eq} is the equilibrium concentration of calcium in the fluid, and C_b is the concentration of calcium in the bulk fluid.

Though this formulation of erosion rate based on experimental results suggests that calcite dissolution rates should be independent of shear stress under turbulent conditions, the presence of scallops, a sculpted bedrock form with a size that scales with shear stress (Curl, 1966), within natural limestone channels requires that erosion rates vary as a function of shear stress (Covington, 2014). This contradiction suggests that there is some problem with either the calcite dissolution model or with the interpretation of the experimental results. In terms of the shear stress erosion

model, Eq. 2.2, this reaction-limited case would be represented by $a = 0$, with K adjusted according to the saturation state of the water.

The opposite limit, transport limited dissolution, occurs when dissolution rates are entirely controlled by the rate at which species can be transported to and from the dissolving surface. For transport limited dissolution the erosion rate is

$$E_D = \frac{D}{\epsilon}(C_{Eq} - C_b), \tag{2.5}$$

where D is the diffusion coefficient for ions in the solution, and ϵ is the thickness of the diffusion boundary layer (DBL). DBL thickness can be written in terms of flow parameters, e.g.,

$$\epsilon = \frac{5\nu}{\sqrt{\tau_b/\rho_w}} \cdot Sc^{-1/3}, \tag{2.6}$$

where ν is kinematic viscosity, τ_b is boundary shear stress, ρ_w is water density, and Sc is the Schmidt number (ν/D) (Perne et al., 2014). This equation is valid for flow over a planar surface. For transport limited dissolution the exponent in the shear stress erosion model becomes $a = 1/2$. Mixed kinetics can also occur, where transport and reaction rate both play a role. This can produce an intermediate value of the exponent a. For instance, gypsum, unlike calcite, follows mixed kinetics and experiments have shown a between $1/3$ and $1/2$ (Opdyke et al., 1987).

A third confounding issue is the role of sediment in determining cross sectional shape. Sediment is known to impact the width of bedrock channels (e.g., Yanites and Tucker, 2010). Sediment has two effects, a 'tool' effect where sediment provides tools for erosion, and a 'cover' effect where deposited sediment shields a channel from further erosion (Sklar and Dietrich, 2001). In cave passages, the cover effect can have dramatic impacts, as it is hypothesized to lead to a process of upward channel erosion called paragenesis (Farrant and Smart, 2011). Paragenesis, also termed antigravitative erosion (Pasini, 2009), occurs when cave development is forced upwards in the phreatic

zone due to sediment armoring of passage floors and walls that protects them from dissolution (Farrant and Smart, 2011; Lauritzen and Lundberg, 2000; Renault, 1968). Paragenesis results in features such as ceiling half-tubes and anastomoses, wall tubes, pendants, and paragenetic galleries (Lauritzen and Lundberg, 2000). These features can be very complex in cross-section view.

Farrant and Smart, 2011 review the role of sediment in speleogenesis, including a conceptual model of paragenetic passage evolution (Fig. 2.1). The paragenetic process is hypothesized to occur in the following sequence:

1. Sediment influx armors the floor and walls of a passage under phreatic conditions.

2. Passage growth is forced upwards as only the upper walls and ceiling of the passage can be eroded.

3. The passage reaches an equilibrium cross-sectional area, where sediment deposition occurs at the rate of upward incision and flow velocity remains near the threshold for sediment transport.

4. The process continues until the passage reaches the water table, or there is a halt in sediment supply and erosion on the walls can resume, forcing lateral growth.

The passages formed by this process are termed paragenetic galleries. These galleries tend to have a greater height than width, and the width above the incipient phreatic tube is constant when subjected to similar average conditions (Farrant and Smart, 2011). The balance between upward growth and sedimentation in the conceptual model represents an equilibrium condition, and the constant passage width (herein termed *equilibrium width*) established may be indicative of average conditions, similar to those in other bedrock channels.

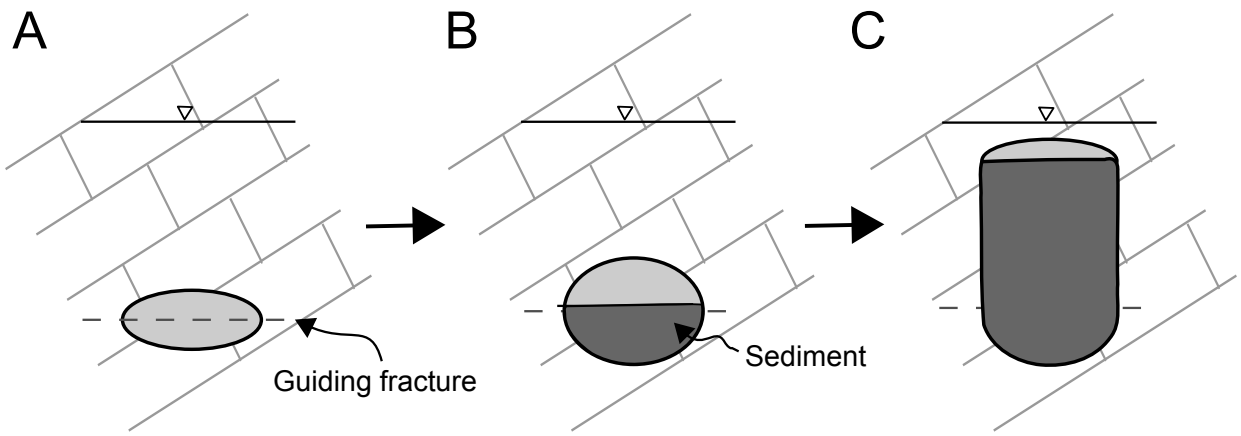

Figure 2.1: The conceptual model of paragenetic gallery formation under constant average conditions, i.e., same average discharge and sediment supply.

Some paragenetic speleogens (dissolutional cave forms) have been physically modeled including paragenetic meanders, anastomoses (braided ceiling channels), ceiling half-tubes, and pendants (Lauritzen, 1981). The conclusions from these hardware models are that these speleogens result from water flow along the sediment-rock interface and pendants require erosion rate to vary with local velocity. These models only simulated the development of speleogens, rather than the development of paragenetic galleries outlined in the conceptual model.

2.4 Model description

To simulate cross-section evolution we develop a model consisting of several components: 1) a cross-section discretized into a series of x, z points defining the perimeter, 2) a method to estimate shear stress, and 3) an erosion model that updates the cross-section geometry with each time step. In paragenesis simulations a sediment transport and alluviation component is also added to the model.

2.4.1 Cross-section

A cross-section consists of a series of n_p x, z points, with l_i representing an individual pair of points. The set of points are arranged counter-clockwise from the top-most point.

At each time step a second, wetted cross-section is generated as a subset of l. The wetted cross-section is defined with respect to a horizontal reference line. Vadose wetted cross-sections are the subset of wall points below the line representing a free-surface. Paragenetic wetted cross-sections are the subset of wall points above the line representing the sediment-water interface, as well as an added set of points representing the sediment-water interface. In the phreatic case with no sediment, the wetted cross-section and general cross-section are the same. Wetted cross-sections have the following associated parameters: A, the cross-sectional area, P, the perimeter, R, the hydraulic radius (A/P), dL_i, the distance from a point to the previous point in the cross-section, and $r(l_i)$, the distance between a reference point and the point l_i. The reference point represents the position of maximum velocity, which we consider to be the center of the free-surface in vadose cases or the centroid in phreatic cases.

At each time step cross-sections are updated by moving the subset of points defining the wetted portion outwards perpendicular to their current position by a per-point erosion rate, E_i. E_i is calculated from the boundary shear stress estimation and the shear stress erosion law. Simulations are stopped when either the channel equilibrates, staying the same width over 100 time steps, or when a certain number of time steps is reached if no equilibration occurs.

2.4.2 Estimating boundary shear stress

We choose the method developed by Wobus et al., 2006 (WTA method), for calculating boundary shear stress, as it is relatively accurate and computationally inexpensive compared other available methods (Wobus et al., 2008). The WTA method approximates boundary shear stress along the channel perimeter using a modification of the law of the wall for open channels with a free surface. As the law of the wall applies equally in full pipes (George, 2007), we implement and modify the WTA method for use in conduit-full conditions, allowing the cross-section model to simulate phreatic passages.

The WTA method allows the computation of boundary shear stress (τ_b) for an arbitrary channel geometry given only a set discharge (Q_w), roughness length (z_0) and hydraulic gradient (S). The steps of the algorithm are:

1. Find water height in free-surface conditions, or energy slope in the case of conduit-full conditions,

2. Calculate the near bed velocity gradient at each point along the perimeter that describes a cross-section,

3. Solve an equation that ensures force balance around the perimeter, and

4. Calculate τ_b from the force balance and velocity gradients.

To determine water height in the free-surface case three equations are solved by varying the reference line height above the channel bottom until the calculated discharge equals prescribed discharge,

$$Q_w = \bar{u} \cdot A, \tag{2.7}$$

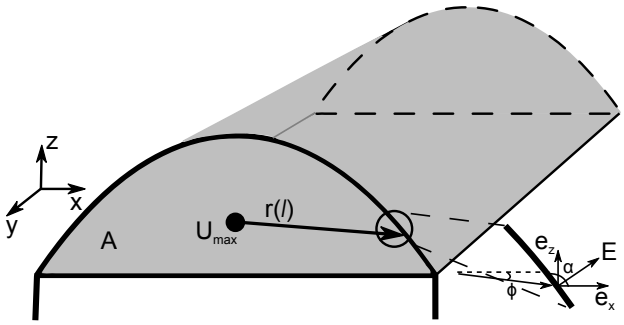

Figure 2.2: Schematic of model parameters in the conduit-full/phreatic case. Velocity gradient is calculated from U_{max}, and $r(l)$, the distance from the maximum velocity position to point l on the perimeter. The bed-normal velocity gradient and τ_b are calculated from velocity gradient, the angle of the bed-normal vector to horizontal (α), and the angle of the vector $r(l)$ to horizontal (ϕ).

$$\bar{u} = C\sqrt{R \cdot S}, \text{ and} \tag{2.8}$$

$$C = 2.5\sqrt{g}\ln\left(\frac{0.37R}{z_0}\right), \tag{2.9}$$

where $\bar{u}$ is mean velocity in the downstream direction, and C is the Chézy friction factor (Wobus et al., 2008). For conduit-full (phreatic) conditions A and P are known, and the energy slope, S, is solved for using these equations.

Velocity gradients are computed using a modified the law of the wall equation with a reference point at the maximum velocity (U_{max}) position,

$$\left.\frac{du}{dr(l_i)}\right|_{z_0} = \frac{U_{max}}{z_0} \cdot \frac{1}{ln(r(l_i)/z_0)} \cdot sin(\phi_i - \alpha_i), \tag{2.10}$$

The term $sin(\phi_i - \alpha_i)$ projects the velocity gradient onto a bed- normal vector (Fig. 2.2). The value of U_{max} is determined by integrating equation 2.10, and assuming the sum of the integrated velocity gradients divided by area equal $\bar{u}$. A full derivation and algorithm is presented in Appendix 1.

Finally, boundary shear stress at each point is calculated via

$$\tau_b(l) = \varphi\rho_w A\left(\left.\frac{du}{dr(l)}\right|_{z_0}\right)^2, \tag{2.11}$$

with φ being a factor to ensure force balance,

$$\varphi = \frac{gS}{\sum_{i=1}^{n_p} \left(\left. \frac{du}{dr(l_i)} \right|_{z_0} \right)^2 dL_i}. \tag{2.12}$$

2.4.3 Erosion

During each time step, erosion at each point of the wetted cross-section is calculated using shear stress erosion (Eq. 2.2). We use a range of a values in the cross-section model runs for simulating different types of erosion and dissolution. For reaction rate limited dissolution $a = 0$, while for transport limited dissolution $a = 1/2$. We also simulate mixed kinetics dissolution with $a = 0.3$. Sediment transport is a vital part of paragenesis and also occurs in the vadose zone. As such we also model mechanical erosion in both paragenesis and vadose channels with several values of $a > 1/2$.

2.4.4 Sediment dynamics

The sediment dynamics model includes components for both transport and alluviation. The alluviation method implemented is that of Nelson and Seminara, 2011, which assumes that if the bed-load layer is thicker than five times the sediment diameter (D_s), the channel alluviates, adding one sediment diameter thickness. The alluviation rule of Nelson and Seminara, 2011 is derived from flume experiments (Finnegan et al., 2007; J. P. Johnson and Whipple, 2010).

Bed-load sediment transport capacity along the perimeter is calculated using the transport equation of Fernandez Luque and Beek, 1976,

$$q_t(l_i) = 5.7(\tau_b^*(l_i) - \tau_c^*)^{3/2} \rho_s (\rho_b D_s^3)^{1/2} \tag{2.13}$$

where τ_c^* is critical Shields stress, ρ_s is sediment density, and $\rho_b = \rho_s/\rho_w - 1$. The form of τ_b used in this equation is the dimensionless Sheilds stress ($\tau_b^* = \frac{\tau_b}{(\rho_s - \rho_w)gD_s}$). τ_c^* is calculated from D_s using linear functions fit to data in Julien, (2010, Table 7.1). Sediment transport capacity is then integrated along the bottom of the channel from equidistant points from the center iteratively until the integral equals the prescribed sediment supply, Q_s:

$$Q_s = \int_{l_{Ls}}^{l_{Rs}} q_t(l_i) dL_i \tag{2.14}$$

where l_{Ls} and l_{Rs} are points that indicate the left side and right side of the bed-load layer, respectively. Bed-load thickness is calculated from the z component of l_{Ls} and l_{Rs} and the current sediment reference line. If the thickness is $> 5D_s$ the reference line is raised by D_s and flow is recalculated. This process is repeated until alluviation ceases.

2.5 Results

2.5.1 Initial tests of the model

Initial tests were run to determine the ability of our implementation of the WTA method to duplicate the shapes of cave cross-sections seen in the field, including phreatic tubes, vadose canyons (Fig. 2.3), and paragenetic galleries (Fig. 2.4). We also test our model compared to the scaling results from Wobus et al., 2006.

Phreatic tube type cross-sections were simulated starting from a bedding plane fracture geometry with an aperture of 0.01m and a breadth of 0.5m. We use a wall roughness value of 0.01m given by Palmer, 2007 for scalloped walls. Wall roughness values can be translated to z_0 by dividing by 30 for hydraulically rough flow (Nikuradse, 1950), and thus $z_0 = 3.3 \cdot 10^{-4} m$ in this case. A discharge of $1 m^3/s$ is used in these simulations. The erosional exponents used

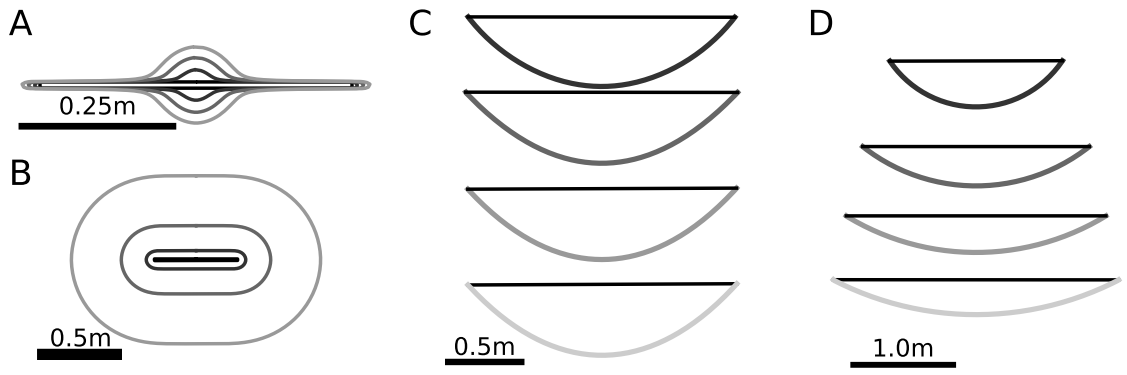

Figure 2.3: Wetted cross-section evolution of: (A) a phreatic tube with $a = 0.5$, (B) a phreatic tube with $a = 0$, (C) a vadose canyon with $a = 0.5$, and (D) a vadose canyon with $a = 0$. Lighter cross-sections indicate later times. For the phreatic tube cases, the cross-section is initialized as a bedding-plane fracture. For the vadose cases, the cross-section is initialized as a circle of 1m radius. Black lines indicate the water height in the vadose cases.

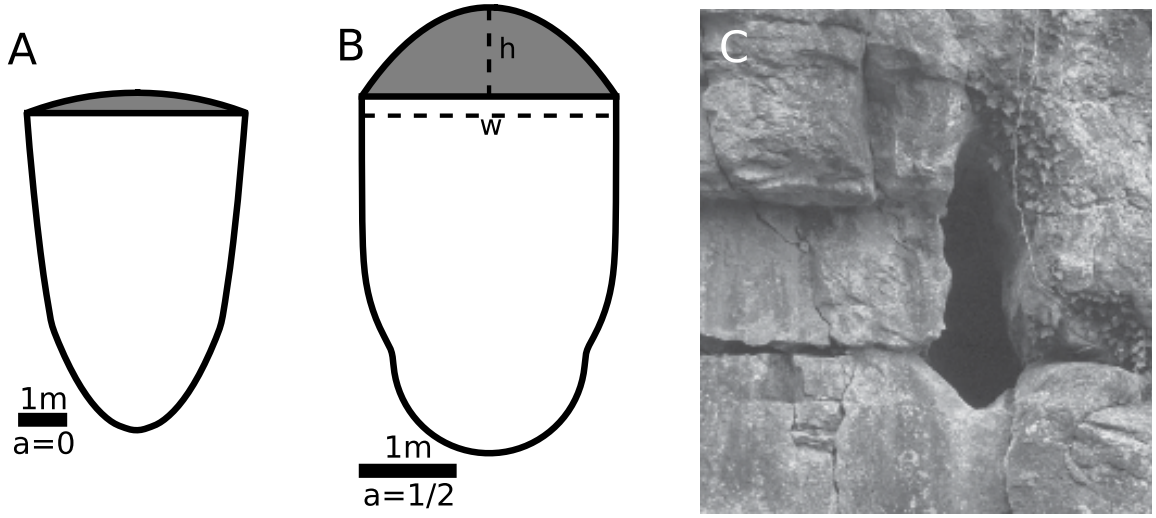

Figure 2.4: A. Simulated paragenetic gallery with erosion law $e = K$. B. Simulated paragenetic gallery with erosion law $e = K\tau_b^{1/2}$. Grey shaded region in A and B indicates water filled portion of the passage. C. A field example of a paragenetic gallery stripped of sediment from further erosion. This example shows an equilibrium width established directly above the incipient phreatic tube. Height of gallery ~2m. Photograph from Simms, 2004.

in these simulations are $a = 0$ and $a = 1/2$ (Fig. 2.3a,b). Runs where $a = 1/2$ maintain the incipient parting shape through their evolution. While simulations of $a = 0$ produce a tube shape, the incipient parting is erased after few time steps.

There are some caveats concerning the input parameters for these model runs; both Q_w and z_0 are unrealistic for the incipient 0.01m aperture fracture; however, they are applicable once the cross-section enlarges. These phreatic tube simulations are not to be taken as representative of realistic dynamics, and are instead used to illustrate the ability of the model to reproduce equilibrated geometries seen in the field.

Vadose canyon type cross-sections were simulated beginning as a closed, circular geometry with an initial radius of 1m (Fig. 2.3c,d). Parameter values are $Q_w = 1m^3/s$, $S = 0.017$ and $z_0 = 3.3 \cdot 10^{-4}m$. Runs with $a > 0$ obtain an equilibrium width after a number of time steps; however, runs with $a = 0$ do not obtain an equilibrium width or width-to-depth ratio and continue to widen indefinitely.

As a check of our implementation of the WTA algorithm we ran a set of simulations identical to those in Wobus et al., 2006, Fig. 2d, for $D_s = 0.001m$. This set of simulations starts with a broad, elliptical channel with an initial width of 8m, and a constant slope of 10^{-3}. Our independently written code produces a scaling relationship between width and discharge of $W \propto Q^{0.42}$, which is approximately the same as that found using the previous model, $W \propto Q^{0.38}$ (Wobus et al., 2006). Unlike Wobus et al., 2006 we vary a in the erosion law (Fig. 2.5). Changes in the exponent a only lead to changes in the magnitude of the erosion rates, and an identical scaling law results for all tested values of a, with $W \propto Q^{0.42}$. Higher values of a reduce the overall width.

Initial simulations of paragenesis used erosion model exponents of $a = 0$ and $a = 1/2$. Simulations were run until the channel reached an equilibrium width, or for a set number of time

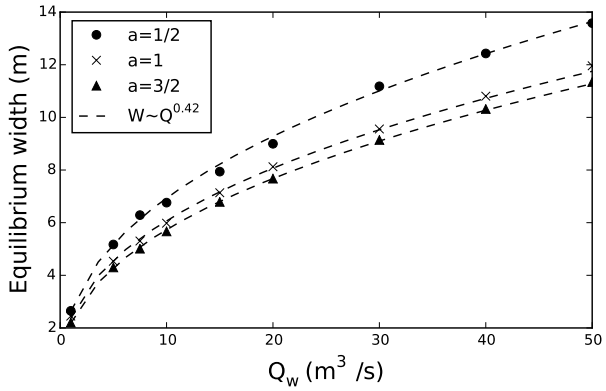

Figure 2.5: Plot of equilibrium width versus discharge in a surface channel for various values of the exponent, a. Curve fitting suggests successful duplication of the WTA algorithm as the exponent in the power law fit is similar.

steps. Runs where $a = 1/2$ reached a constant width, whereas runs with $a = 0$ always ran for all time steps (Fig. 2.4), as an equilibrium width was never reached.

2.5.2 Paragenesis dynamics

To explore the dynamics of paragenetic gallery development a simulation is selected where average shear stress, wetted cross-sectional area, and width were recorded for each time step (Fig. 2.6).

Figure 2.6 reveals the dynamics of paragenetic gallery formation. The simulated paragenetic galleries are initialized as phreatic tubes (Fig. 2.3a). They grow until they reach a cross-sectional size where the reduction in shear stress allows alluviation to occur. After a time step in which alluviation occurs the water-filled part of the passage shrinks slightly, thus increasing average shear stress. Growth in the outward and upward direction continue until an equilibrium shear stress is maintained that is sufficient to transport the available sediment. Once the equilibrium shape is established, only upward growth of the passage continues, with width being constant.

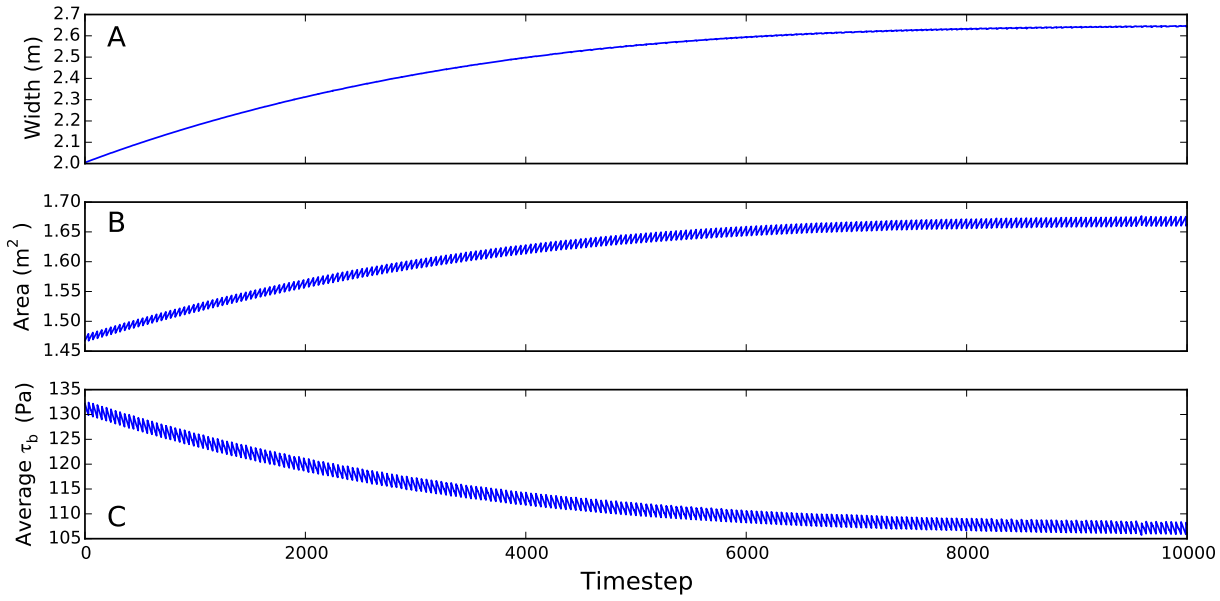

Figure 2.6: Width (A), area (B), and average shear stress (C) versus time step in a simulation run.

2.5.3 Controls on equilibrium width of paragenetic conduits

Analytical approximation of scaling relationship

An analytical approximation can be used to understand the controls on equilibrium width, particularly how equilibrium width scales with discharge, Q_w, and sediment supply, Q_s. To make the problem tractable, we assume that the channel reaches an equilibrium shape, and that this shape is the same for all equilibrium channel cross-sections with different Q_w and Q_s. Under this assumption of equilibrium shape, it follows that, for equilibrium channel cross-sections, all linear measures of channel geometry (such as radius and wetted perimeter) scale linearly with channel width, and cross sectional area scales with width squared. Consequently,

$$Q_w \propto \bar{u} w^2, \tag{2.15}$$

where w is channel width, and the constant of proportionality relates only to cross sectional shape.

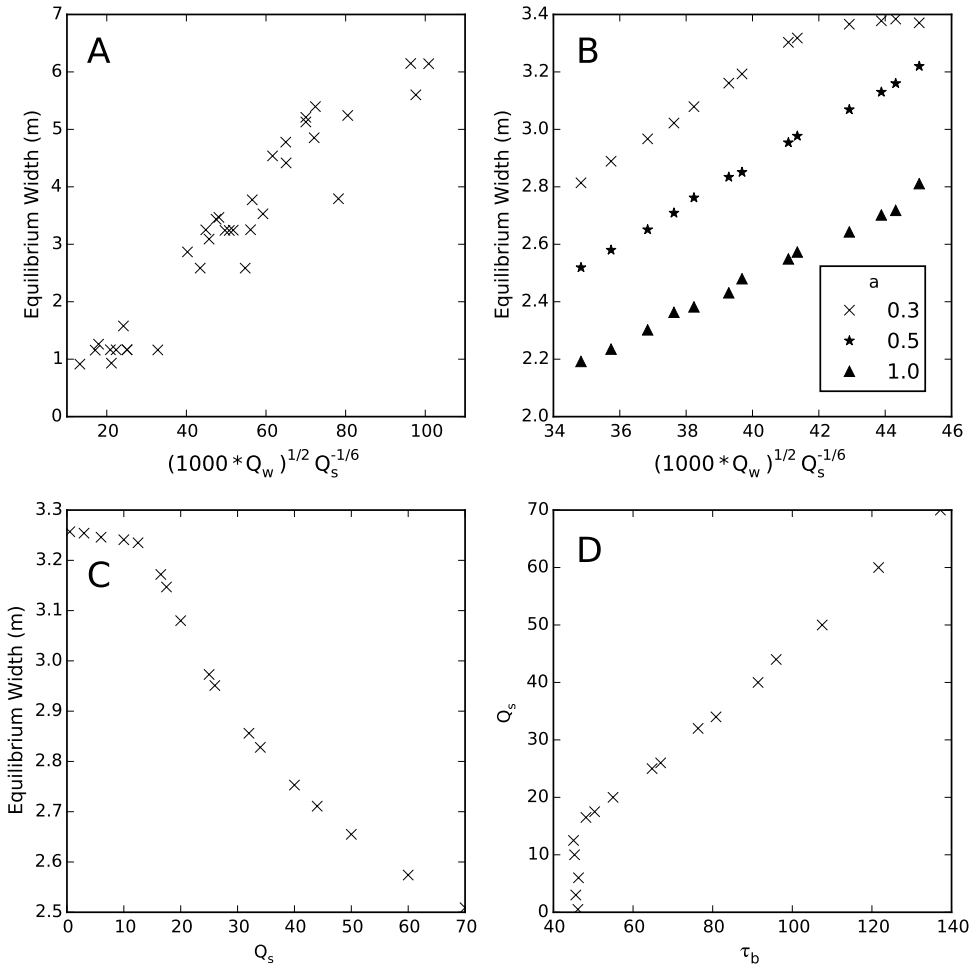

Figure 2.7: Scaling relationship with varying Q_w and Q_s with $a = 0.5$ (A) and different values of a (B). (C) Scaling of Q_s to equilibrium width with $Q_w = 0.5$. (D) Scaling of average boundary shear stress at equilibrium to sediment supply with $Q_w = 0.5$.

Combining the force balance equation at the channel wall (Stark, 2006),

$$\tau_b = \frac{\rho g A S}{P}, \tag{2.16}$$

where P is the wetted perimeter, with the Chézy Equation (2.8), leads to

$$\tau_b \propto Q_w^2 / w^4. \tag{2.17}$$

Sediment supply, Q_s, also relates to shear stress, and considering the case where bed stress is much greater than critical leads to

$$Q_s \propto \tau_b^{3/2}. \tag{2.18}$$

Eliminating τ_b, by combining Equations 2.17 and 2.18, and then solving for channel width gives

$$w \propto Q_w^{1/2} Q_s^{-1/6}. \tag{2.19}$$

From this approximate scaling relationship, we would predict that paragenetic channel width increases with the square root of discharge and decreases weakly with increased sediment supply.

Simulated scaling relationships

To understand the controls of channel width, we run a set of simulations with Q_w between 0.3 and 20.0 m^3/s and Q_s between 0.3 and 42 kg/s. All other parameters are held constant (Table 2.1). The full set of chosen Q_w and Q_s are presented in Supplemental 1. Running these simulations results in a linear fit to the analytically derived scaling relationship (Fig. 2.7a), with some scatter in low Q_s cases.

To explore the effect of erosional mechanism on channel width, we also run three sets of simulations with different erosional exponents. These simulations also result in a linear relationship

Table 2.1: Constant input parameters for scaling simulations.

Parameter	Value	Unit
a	1/2	Unitless
D_s	0.006	m
z_0	0.002	m
ρ_w	999.97	kg/m^3
ρ_s	2650	kg/m^3
g	9.81	m/s^2

between width and the scaling relationship, with higher powers of shear stress resulting in smaller widths (Fig. 2.7b).

Both of the previous simulation sets show that the analytical scaling relationship breaks down for low sediment supply. Therefore, to better understand the reason for this breakdown in scaling, we run a set of simulations with varying sediment supply. Simulations for Fig. 2.7c use the same constants as Table 2.1, with the addition of setting $Q_w = 5m^3/s$. By inspecting the relationship between Q_s and average τ_b (Fig. 2.7d) there appears to be a limit where further reduction in sediment supply does result in a reduction of τ_b. This causes a breakdown in the scaling relationship in equation 2.19 for low Q_s. This limit shifts depending on erosional power and discharge (see $a = 0.3$ runs in Fig. 2.7b. For runs in Fig. 2.7 dimensionless $\tau^*_{sc} = 0.043$, while the dimensional version, $\tau_{sc} = 4.3Pa$. Average τ_b is an order of magnitude larger than τ_{sc} for all runs in (Fig. 2.7c,d). A simulation with $a = 0.5$, $Q_w = 5m^3/s$ and $Q_s = 10kg/s$ results in a minimum $\tau_b = 4.2Pa$ at the corner between the sediment surface and the wall. Halving Q_s results in the same minimum τ_b, while setting $Q_s = 70kg/s$ results in $\tau_b = 13.1Pa$. As such, the width is limited by τ_{sc} in these cases, whereas it is ignored in the analytical derivation which only considers average shear stress.

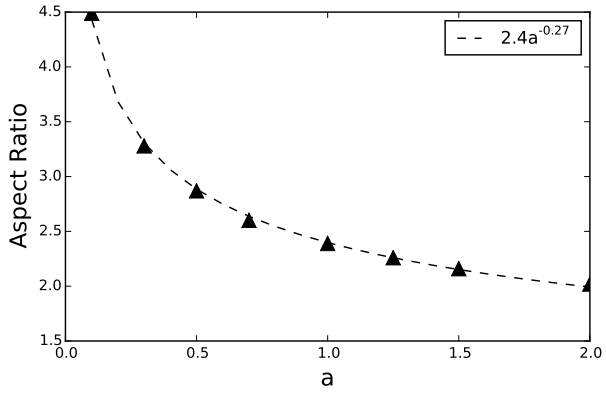

Figure 2.8: Power in the erosion law, a, versus aspect ratio as determined by model runs. Here aspect ratio is the equilibrium width of the paragenetic gallery divided by the height of the wetted portion of the cross-section.

A set of simulations were run to test the assumption of a universal equilibrium shape, which we used in the analytically derived scaling relationship. This set varied one parameter at a time from the parameters in Table 2.1. Q_w and Q_s, were also held constant except for one case at $5.0m^3/s$ and $20kg/s$, respectively. Aspect ratio, w/h, here defined as the ratio between equilibrium width and the distance between the sediment reference line and the highest point in the channel (Fig. 2.4b) was recorded as a measure of shape. These model runs reveal that aspect ratio is only dependent on a (Supplemental 2). A second set of runs varying a show the relationship between aspect ratio and a is a power law with an exponent $\approx -1/4$ (Fig. 2.8).

2.6 Discussion

2.6.1 Success of the model

Our implementation of the WTA method approximately duplicates the results of the original WTA model (Fig. 2.5). In turn, the model results of Wobus et al., 2006 match scaling relationships seen in the field and ones derived analytically for open channels. Our model also successfully

produces phreatic tubes from an initial fracture shape (Fig. 2.3a,b). Production of equilibrium width channels and phreatic tubes, as observed in the field, requires that erosion rates that vary with shear stress.

The paragenesis simulations (Fig. 2.4b) produce passage shapes that are qualitatively similar to those seen in the field (Fig. 2.4c), and the dynamics of paragenesis are similar to the available conceptual model for paragenetic passage evolution (Fig. 2.1). As for open channels, simulated passage cross sections do not approach an equilibrium width unless erosion rate varies with shear stress. The fact that paragenesis and vadose incision frequently produce constant width channels in real cave settings provides further evidence that erosion rates do vary with wall shear stress in natural cave settings. While this is in-line with the hypothesis of Lauritzen, 1981 presented for paragenetic speleogens, and with the existence of scalloped bed forms in limestone cave channels Curl, (1966), it provides further evidence that currently available models of calcite dissolution in turbulent flow require revision. Simulations where erosion is a function of shear stress develop an equilibrium width that scales with Q_w and Q_s (Fig. 2.7) as predicted by the analytical approximation. While the exact values of the scaling exponents may depend, in part, on simplifications made in the model, this scaling result provides evidence that paragenetic cave channel width records information about flow and sediment conditions during formation. The specific scaling relationship determined both by analytical approximation and simulations, $w \propto Q_w^{1/2} Q_s - 1/6$, provides a starting point for future studies.

2.6.2 Scaling relationships in bedrock channels

The derived scaling relationship and results of the paragenesis model show some commonalities and differences to scaling relationships in bedrock channels, in both assumptions used in

deriving relationships and in the scaling relationships themselves. Scaling relationships in surface bedrock channels are well known, with the relationship of width to discharge, erosion/uplift rate, and slope being derived analytically (Finnegan et al., 2005; Turowski et al., 2007; Wobus et al., 2008), modeled numerically (Turowski et al., 2009; Wobus et al., 2006; Yanites and Tucker, 2010), and observed in the field (Turowski et al., 2009; Whipple, 2004; Yanites and Tucker, 2010). Typical scaling law exponents for width as a power law function of discharge are 0.3-0.5. Analytical approximations begin with the continuity equation (Eq. 2.7) and a flow equation such as the Manning (Finnegan et al., 2005; Turowski et al., 2007) or Chézy (Wobus et al., 2008) equation. They also typically assume a constant width-to-depth (aspect) ratio and that erosion is equal to uplift (steady state). We also assume constant aspect ratio to derive the paragenesis scaling relationship (Eq. 2.19). In our numerical simulations we find that simulations reach identical aspect ratios for given value of shear stress exponent, a (Fig. 2.8). Field data (Finnegan et al., 2005) and models of cross-section evolution (Turowski et al., 2009; Wobus et al., 2006) suggest that channels in similar rock types maintain aspect ratios. However, sediment cover of the bedrock can also influence channel aspect ratio (Yanites and Tucker, 2010). Unlike equilibrium bedrock channel models, we make no steady state assumption in deriving the paragenesis scaling relationship, as phreatic cave development and paragenesis occur beneath base level.

Prior bedrock channel cross-section models often assume a linear relationship between erosion and boundary shear stress ($a = 1$) (e.g., Wobus et al., 2006; Yanites and Tucker, 2010). In contrast, pure dissolution of soluble bedrock scales with a shear stress exponent of $a \leq 1/2$, with $a = 1/2$ representing the transport-limited end member and $a = 0$ representing the surface reaction rate limited end member. Simulating vadose canyons or surface channels with the WTA method and different exponents of shear stress in the erosion equation results in the same scaling relation-

ship between width and discharge as found in Wobus et al., 2006 and Wobus et al., 2008 for each choice of exponent (Fig. 2.5). Smaller values of the exponent result in larger widths. Understanding the response of bedrock channel widths to changes in rock properties, erosion rate, and slope, is important for interpreting channel profiles and the history of landscape evolution that can be preserved within them (e.g., Kirby and Whipple, 2012; Lague, 2014; Miller et al., 2013; Roberts and N. White, 2010; Whittaker et al., 2007). However, in contrast to surface channels, caves often preserve long histories of channel width, potentially enabling cave passages to be powerful tools in reconstructing past conditions.

While the scaling of width with discharge in bedrock channels has been well explored in all types of models, the scaling of width to sediment supply has been primarily explored in numerical models (Turowski et al., 2007; Yanites and Tucker, 2010) and flume experiments (Finnegan et al., 2007). These modeling results, along with observations of natural channels, suggest that open channels respond to increasing sediment supply by widening, as cover prevents erosion in the channel center (Yanites and Tucker, 2010). In contrast, paragenetic galleries respond to increasing sediment supply by narrowing. The channels narrow to obtain a smaller cross sectional area so that a sufficient shear stress can be applied to transport the available sediment. Armoring of the central portion of the eroding channel, the process that drives widening with increased sediment in open channels, does not occur in the paragenetic case, because the center of active erosion is on the ceiling of the cave passage.

In the simulations run for Figure 2.7c there appears to be a threshold in the scaling relationship for paragenesis. This threshold is due to a breakdown in the scaling between sediment supply and boundary shear stress, arising when critical shear stress is equal to the minimum shear stress at the corners between the sediment-water interface and the gallery walls.

2.6.3 Sediment transport and alluviation

The bed-load sediment transport capacity equation used in the paragenesis model plays a vital role in the width scaling relationship. We use the equation given by Fernandez Luque and Beek, 1976, one that is commonly used in other bedrock channel models for both erosion, and alluviation (e.g., Hodge and Hoey, 2012; J. P. Johnson and Whipple, 2010; Lamb et al., 2008; Nelson and Seminara, 2011; Sklar and Dietrich, 2004; Turowski et al., 2007, 2009). While there are several choices for bed-load transport equations, (e.g. Bagnold, 1977; Meyer-Peter and Müller, 1948; Parker, 1990; Wilson, 1966) their power of excess shear stress is the same, $3/2$, and as such the derivation and model are insensitive to the choice of equation.

While there are no physically derived models of alluviation in cross-sections, they do exist for reaches (e.g., Hodge and Hoey, 2012; Inoue et al., 2016; J. P. L. Johnson, 2014; Nelson and Seminara, 2012). These models take into account mass balance and sediment transport, and successfully duplicate experimental results and observations from physical streams. As the cross-section paragenesis model is insensitive to the alluviation rule and uses the same transport equations, it is possible this scaling relationship holds to field examples.

2.6.4 Applications in speleogenesis modeling

Scaling relationships are often employed in landscape evolution models to simplify channel development (e.g., Whipple and Tucker, 1999). The paragenesis scaling relationship and other such scaling relationships that can be derived may allow simplifications in further post-breakthrough speleogenesis models. The shapes and widths formed at a set discharge and sediment supply represent an equilibrium that appears to be reached quickly in models and in the field (Fig. 2.4). If the

time scale at which average conditions change is larger than the equilibrating time scale, it may be possible to directly apply the width and shapes for a given condition and only track upward (paragenesis) or downward (vadose) growth. If this is the case, only the routing of flow and incision rate needs to be calculated.

Additionally, if a shear stress erosion law is found to apply to speleogenesis, models can be further simplified if length scales are short enough to ignore chemistry changes and only calculate erosion using shear stress. In a mature cave conduit, these lengths are typically on the order of a kilometer (Covington et al., 2012). In contrast, existing models exploring the pre-breakthrough stage of speleogenesis must track chemistry as short lengths of conduit effect saturation state, and thus erosion rate (e.g., Dreybrodt et al., 2005).

That fact that equilibrium width cave channels (vadose or paragenetic) do not develop unless erosion rate is a function of shear stress suggests that channels in caves, which often exhibit nearly constant width during incision, do not form from surface reaction rate limited dissolution alone as the models suggest. Instead either transport limited dissolution or mechanical erosion is likely playing a role. Equilibrium widths thus are further field evidence that speleogenesis under turbulent flow conditions is not purely surface reaction rate limited (Covington, 2014). However, it remains unclear whether transport-limited dissolution or mechanical erosion is the key factor, and additional work is needed to resolve this question and improve the fidelity of future speleogenesis models.

2.7 Conclusion

The model developed here provides a physically based and computationally efficient means of simulating cave cross-section evolution and is able to duplicate cross-sectional shapes that are seen in the field such as phreatic tubes, vadose canyons, and paragenetic galleries. The efficiency

of the WTA method enables simulations of the evolution of channel form through many time steps, making investigations into the morphology of post-breakthrough cave channels possible using a wide range of parameter values. Using this model, we have tested analytical relationships between discharge, sediment supply, and width and have explored dynamics not captured in the analytical relationships.

We derive an analytical relationship between discharge, sediment supply, and width in paragenetic galleries, backed with simulation results reveal that equilibrium width in paragenetic galleries scales on discharge to the half power, and weakly to the inverse of sediment supply. In surface bedrock channels the inverse has been observed, with width being positively related to sediment supply.

Equilibrium in the paragenetic case is maintained by a balance of shear stress and sediment transport capacity. Our model also demonstrates that the equilibrium shape obtained is a function of only the exponent in the erosion law, reflective of process.

These simulations also reveal that paragenetic galleries and other channel types that maintain an equilibrium width depend on erosion to scale with shear stress, in conflict with the assumption of current speleogenesis theory. Such scaling is possible due to dissolution rates being transport limited, or mechanical erosion being more important than previously thought.

2.8 References

Amos, C. B. and D. W. Burbank (2007). “Channel width response to differential uplift”. In: *Journal of Geophysical Research: Earth Surface* 112.F2.

Anthony, D. M. and D. E. Granger (2004). “A Late Tertiary origin for multilevel caves along the western escarpment of the Cumberland Plateau, Tennessee and Kentucky, established by 26Al and 10Be”. In: *Journal of Cave and Karst Studies* 66.2, pp. 46–55.

Anthony, D. M. and D. E. Granger (2006). “Five million years of Appalachian landscape evolution preserved in cave sediments”. In: *Perspectives on karst geomorpology, hydrology, and geochemistry - A tribute volume to Derek C. Ford and William B. White*. Ed. by R. S. Harmon and C. M. Wicks. Vol. 404. Special Paper. Geological Society of America, pp. 39–50.

— (2007). “A new chronology for the age of Appalachian erosional surfaces determined by cosmogenic nuclides in cave sediments”. In: *Earth Surface Processes and Landforms* 32.6, pp. 874–887.

Bagnold, R. A. (1977). “Bed load transport by natural rivers”. In: *Water resources research* 13.2, pp. 303–312.

Bretz, J. H. (1942). “Vadose and phreatic features of limestone caverns”. In: *The journal of Geology*, pp. 675–811.

Covington, M. D. (2014). “Calcite dissolution under turbulent flow conditions: a remaining conundrum”. In: *Acta Carsologica* 43.1, pp. 195–202.

Covington, M. D., A. J. Luhmann, C. M. Wicks, and M. O. Saar (2012). “Process length scales and longitudinal damping in karst conduits”. In: *Journal of Geophysical Research* 117.F1, pp. 1–19. ISSN: 0148-0227. DOI: 10.1029/2011JF002212. URL: http://www.agu.org/pubs/crossref/2012/2011JF002212.shtml.

Covington, M. D. and M. Perne (2015). “Consider a cylindrical cave: A physicist’s view of cave and karst science”. In: *Acta Carsologica* 44.3, pp. 363–380.

Curl, R. L. (1966). “Scallops and Flutes”. In: *Transactions of the Cave Research Group of Great Britain* 7.2, pp. 121–160.

Dogwiler, T. and C. M. Wicks (2004). “Sediment entrainment and transport in fluviokarst systems”. In: *Journal of Hydrology* 295.1, pp. 163–172.

Dreybrodt, W. (1988). *Processes in karst systems, physics, chemistry, and geology*. New York, USA: New York, NY (USA); Springer-Verlag, p. 288.

Dreybrodt, W. and D. Buhmann (1991). “A mass transfer model for dissolution and precipitation of calcite from solutions in turbulent motion”. In: *Chemical Geology* 90.1, pp. 107–122.

Dreybrodt, W., F. Gabrovšek, and D. Romanov (2005). *Processes of Speleogenessis: A Modeling Approach*. Vol. 4. Ljubljana, Slovenia: ZRC Publishing, p. 376.

Farrant, A. R. and P. L. Smart (2011). “Role of sediment in speleogenesis; sedimentation and paragenesis”. In: *Geomorphology* 134.1, pp. 79–93.

Fernandez Luque, F. and R. van Beek (1976). “Erosion and transport of bed-load sediment”. In: *Journal of Hydraulic Engineering* 14.2, pp. 127–144.

Finnegan, N. J., G. Roe, D. R. Montgomery, and B. Hallet (2005). “Controls on the channel width of rivers: Implications for modeling fluvial incision of bedrock”. In: *Geology* 33.3, pp. 229–232.

Finnegan, N. J., L. S. Sklar, and T. K. Fuller (2007). “Interplay of sediment supply, river incision, and channel morphology revealed by the transient evolution of an experimental bedrock channel”. In: *Journal of Geophysical Research* 112.F3, pp. 1–17. ISSN: 0148-0227. DOI: 10.1029/2006JF000569. URL: http://www.agu.org/pubs/crossref/2007/2006JF000569.shtml.

George, W. K. (2007). “Is there a universal log law for turbulent wall-bounded flows?” In: *Philosophical Transactions of the Royal Society of London A: Mathematical, Physical and Engineering Sciences* 365.1852, pp. 789–806.

Granger, D. E., D. Fabel, and A. N. Palmer (2001). “Pliocene- Pleistocene incision of the Green River, Kentucky, determined from radioactive decay of cosmogenic 26Al and 10Be in Mammoth Cave sediments”. In: *Geological Society of America Bulletin* 113.7, pp. 825–836.

Granger, D. E., J. W. Kirchner, and R. C. Finkel (1997). “Quaternary downcutting rate of the New River, Virginia, measured from differential decay of cosmogenic 26Al and 10Be in cave-deposited alluvium”. In: *Geology* 25, pp. 107–110.

Granger, D. E. and L. Siame (2006). “A review of burial dating methods usingˆ 2ˆ 6Al andˆ 1ˆ 0Be”. In: *Special Papers-Geological Society of America* 415, p. 1.

Grm, A., T. Šuštar, T. Rodič, and F. Gabrovšek (2017). “A numerical framework for wall dissolution modeling”. In: *Mathematical Geosciences* 49.5, pp. 657–675.

Hammer, Ø., S.-E. Lauritzen, and B. Jamtveit (2011). “Stability of dissolution flutes under turbulent flow”. In: *Journal of Cave and Karst Studies* 73.3, pp. 181–186.

Herman, E. K. (2006). “Quantitative Studies of Suspended Sediment in Karst Aquifers”. PhD thesis. The Pennsylvania State University.

Hodge, R. A. and T. B. Hoey (2012). “Upscaling from grain-scale processes to alluviation in bedrock channels using a cellular automaton model”. In: *Journal of Geophysical Research: Earth Surface* 117.F1.

Inoue, T., T. Iwasaki, G. Parker, Y. Shimizu, N. Izumi, C. P. Stark, and J. Funaki (2016). “Numerical simulation of effects of sediment supply on bedrock channel morphology”. In: *Journal of Hydraulic Engineering* 142.7, p. 04016014.

Johnson, J. P. L. (2014). “A surface roughness model for predicting alluvial cover and bed load transport rate in bedrock channels”. In: *Journal of Geophysical Research: Earth Surface* 119.10, pp. 2147–2173.

Johnson, J. P. and K. X. Whipple (2010). “Evaluating the controls of shear stress, sediment supply, alluvial cover, and channel morphology on experimental bedrock incision rate”. In: *Journal of Geophysical Research* 115.F02018.

Julien, P. Y. (2010). *Erosion and sedimentation*. Cambridge University Press.

Kean, J. W., R. A. Kuhnle, J. D. Smith, C. V. Alonso, and E. J. Langendoen (2009). “Test of a method to calculate near-bank velocity and boundary shear stress”. In: *Journal of Hydraulic Engineering* 135.7, pp. 588–601.

Kean, J. W. and J. D. Smith (2004). “Flow and boundary shear stress in channels with woody bank vegetation”. In: *Riparian Vegetation and Fluvial Geomorphology: American Geophysical Union Monograph, Water Science and Application* 8, pp. 237–252.

Kirby, E. and K. X. Whipple (2012). “Expression of active tectonics in erosional landscapes”. In: *Journal of Structural Geology* 44, pp. 54–75.

Lague, D. (2014). “The stream power river incision model: evidence, theory and beyond”. In: *Earth Surface Processes and Landforms* 39.1, pp. 38–61.

Lamb, M. P., W. E. Dietrich, and L. S. Sklar (2008). “A model for fluvial bedrock incision by impacting suspended and bed load sediment”. In: *Journal of Geophysical Research (Earth Surface)* 113.F12, pp. 3025–+. DOI: 10.1029/2007JF000915.

Lauritzen, S.-E. (1981). “Simulation of rock pendants–small scale experiments on plaster models”. In: *Proceedings, 8th International Speleological Congress. Bowling Green, Ky USA*. Vol. 8, pp. 407–409.

Lauritzen, S.-E. and A. Lauritsen (1995). “Differential diagnosis of paragenetic and vadose canyons”. In: *Cave and Karst Science* 21.2, pp. 55–59.

Lauritzen, S.-E. and J. Lundberg (2000). “Solutional and erosional morphology of caves”. In: *In: Klimchouk, A., Ford, DC, Palmer, Arthur N. & Dreybrodt, Wolfgang,(eds), Speleogenesis. Evolution of Karst Aquifers. National Speleological Society, Huntsville*, pp. 408–426.

Meyer-Peter, E. and R. Müller (1948). “Formulas for bed-load transport”. In: *IAHSR 2nd meeting, Stockholm, appendix 2*. IAHR.

Miller, S. R., P. B. Sak, E. Kirby, and P. R. Bierman (2013). “Neogene rejuvenation of central Appalachian topography: Evidence for differential rock uplift from stream profiles and erosion rates”. In: *Earth and Planetary Science Letters* 369, pp. 1–12.

Nelson, P. A. and G. Seminara (2011). “Modeling the evolution of bedrock channel shape with erosion from saltating bed load”. In: *Geophysical Research Letters* 38.17.

— (2012). “A theoretical framework for the morphodynamics of bedrock channels”. In: *Geophysical Research Letters* 39.6.

Nikuradse, J. (1950). *Laws of flow in rough pipes*. National Advisory Committee for Aeronautics Washington.

Opdyke, B. N., G. Gust, and J. R. Ledwell (1987). “Mass transfer from smooth alabaster surfaces in turbulent flows”. In: *Geophysical Research Letters* 14.11, pp. 1131–1134. ISSN: 0094-8276. DOI: 10.1029/GL014i011p01131.

Palmer, A. N. (1984). “Geomorphic interpretation of karst features”. In: *Groundwater as a geomorphic agent. Allen and Unwin, Boston, Massachusetts. 390pp*, pp. 173–209.

— (1987). “Cave levels and their interpretation”. In: *National Speleological Society Bulletin* 49.2, pp. 50–66.

— (2007). *Cave Geology*. Dayton, OH: Cave Books.

Parker, G. (1990). “Surface-based bedload transport relation for gravel rivers”. In: *Journal of hydraulic research* 28.4, pp. 417–436.

Pasini, G. (2009). “A terminological matter: paragenesis, antigravitative erosion or antigravitational erosion?” In: *International Journal of Speleology* 38.2, p. 4.

Perne, M., M. D. Covington, and F. Gabrovšek (2014). “Evolution of karst conduit networks in transition from pressurised flow to free surface flow”. In: *Hydrology and Earth System Sciences Discussions* 11.6, pp. 6519–6559. DOI: 10.5194/hessd-11-6519-2014. URL: http://www.hydrol-earth-syst-sci-discuss.net/11/6519/2014/.

Plummer, L. N., T. M. L. Wigley, and D. L. Parkhurst (1978). “The kinetics of calcite dissolution in CO2-water systems at 5 degrees to 60 degrees C and 0.0 to 1.0 atm CO2”. In: *American Journal of Science* 278.2, p. 179.

Renault, P. (1968). “Contribution à l’étude des actions mécaniques et sédimentologiques dans la spéléogenèse”. In: *Annales de spéléologie*. Vol. 22. 1, pp. 5–21.

Roberts, G. G. and N. White (2010). “Estimating uplift rate histories from river profiles using African examples”. In: *Journal of Geophysical Research: Solid Earth* 115.B2.

Simms, M. J. (2004). “Tortoises and hares: Dissolution, erosion and isostasy in landscape evolution”. In: *Earth Surface Processes and Landforms* 29.4, pp. 477–494.

Sklar, L. S. and W. E. Dietrich (2001). “Sediment and rock strength controls on river incision into bedrock”. In: *Geology* 29.12, pp. 1087–1090.

— (2004). “A mechanistic model for river incision into bedrock by saltating bed load”. In: *Water Resour. Res.*

Springer, G. S. (2004). “A pipe-based, first approach to modeling closed conduit flow in caves”. In: *Journal of hydrology* 289.1, pp. 178–189.

Stark, C. P. (2006). “A self-regulating model of bedrock river channel geometry”. In: *Geophysical Research Letters* 33.4.

Stock, G. M., D. E. Granger, I. D. Sasowsky, R. S. Anderson, and R. C. Finkel (2005). “Comparison of U–Th, paleomagnetism, and cosmogenic burial methods for dating caves: implications for landscape evolution studies”. In: *Earth and Planetary Science Letters* 236.1-2, pp. 388–403.

Turowski, J. M., N. Hovius, A. Wilson, and M.-J. Horng (2008). “Hydraulic geometry, river sediment and the definition of bedrock channels”. In: *Geomorphology* 99, pp. 26–38.

Turowski, J. M., D. Lague, and N. Hovius (2007). “Cover effect in bedrock abrasion: A new derivation and its implications for the modeling of bedrock channel morphology”. In: *Journal of Geophysical Research: Earth Surface* 112.F4.

— (2009). “Response of bedrock channel width to tectonic forcing: Insights from a numerical model, theoretical considerations, and comparison with field data”. In: *Journal of Geophysical Research: Earth Surface* 114.F3.

Whipple, K. X. (2004). “Bedrock Rivers and the Geomorphology of Active Orogens”. In: *Annual Review of Earth and Planetary Sciences* 32, pp. 151–185. DOI: 10.1146/annurev.earth.32.101802.120356.

Whipple, K. X., G. S. Hancock, and R. S. Anderson (2000). “River incision into bedrock: Mechanics and relative efficacy of plucking, abrasion, and cavitation”. In: *Bulletin of the Geological Society of America* 112.3, pp. 490–503.

Whipple, K. X. and G. E. Tucker (1999). “Dynamics of the stream-power river incision model: Implications for height limits of mountain ranges, landscape response timescales, and research needs”. In: *Journal of Geophysical Research* 104.B8.

White, E. L. and W. B. White (1968). “Dynamics of sediment transport in limestone caves”. In: *Natl Speleol Soc Bull* 30, pp. 115–129.

Whittaker, A. C., P. A Cowie, M. Attal, G. E. Tucker, and G. P. Roberts (2007). “Bedrock channel adjustment to tectonic forcing: Implications for predicting river incision rates”. In: *Geology* 35.2, pp. 103–106.

Wilson, K. C. (1966). “Bed-load transport at high shear stress”. In: *Journal of the hydraulics division* 92.6, pp. 49–59.

Wobus, C. W., J. W. Kean, G. E. Tucker, and R. S. Anderson (2008). “Modeling the evolution of channel shape: Balancing computational efficiency with hydraulic fidelity”. In: *Journal of Geophysical Research: Earth Surface (2003–2012)* 113.F2.

Wobus, C. W., G. E. Tucker, and R. S. Anderson (2006). “Self-formed bedrock channels”. In: *Geophysical Research Letters* 33.18.

Yanites, B. J. and G. E. Tucker (2010). “Controls and limits on bedrock channel geometry”. In: *Journal of Geophysical Research* 115.F04019, pp. 1–17.

Appendices

2.A Derivation for maximum velocity

To calculate U_{max} we assume that the average velocity, $\bar{u}$, is composed of the sum of average velocities in each triangle delineated by the rays $r(l_i)$. To find the average velocities of the triangles we first find the average velocities along $r(l)$. To do this we simplify the WTA formulation of the law of the wall by removing the U_{max} and sine terms,

$$\left.\frac{du}{dr(l_i)}\right|_{z_0} = \frac{1}{z_0} \cdot \frac{1}{ln(r(l_i)/z_0)}, \quad \texttt{and} \tag{2.20}$$

integrating, we obtain,

$$\bar{u}_i = \frac{r(l_i)}{r(l_i) - z_0}\left(1 + \frac{z_0}{r(l_i) * log(r(l_i)/z_0)}\right) - \frac{1}{log(r(l_i)/z_0}. \tag{2.21}$$

The average velocity within each triangle is,

$$\bar{u}_{T,i} = \frac{\bar{u}_i + \bar{u}_{i+1}}{2}, \tag{2.22}$$

and the area of the triangle is,

$$A_i = \left|\frac{x_c(z_{i+1} - z_i) + x_{i+1}(z_{i+1} - z_c) + x_i(z_c - z_{i+1})}{2}\right|, \tag{2.23}$$

where x_c and z_c are the x and y components of the centroid, and x_i and z_i are coordinates defining the perimeter of the wetted cross-section. If we then assume the sum of average velocities weighted by area is equal to the total area multiplied by $\bar{u}$ and reintroduce U_{max} it follows that

$$\bar{u}A = U_{max} \sum_{i}^{n_p} \bar{u}_{T,i} A_i \,. \tag{2.24}$$

Finally, by rearranging and solving for U_{max} we obtain an equation for maximum velocity,

$$U_{max} = \frac{\bar{u}A}{\sum_i^{n_p} \bar{u}_{T,i} A_i} \,. \tag{2.25}$$

3 Determining Mechanisms of Erosion

CAVE MEANDERS AS A RECORD OF EROSION MECHANISM

3.1 Abstract

The relative importance of different types of erosion in caves is poorly quantified, and, within models, dissolution has been considered the main erosive agent. Additionally, speleogenetic theory built on experiments predicts that dissolution is only reaction rate limited under turbulent flow conditions and does not depend on flow structure. Recent analysis on scallops and equilibrium widths in cave channels suggests that erosion must scale with shear stress, and either transport limited dissolution does occur, or mechanical erosion is more important than previously thought. In this study we use observations of meandering cave channels and scallops extract the exponent in a power law shear stress erosion model, reflective of erosion mechanism.

To determine the exponent the length of shear stress indicating bedforms, scallops, and an indicator of relative lateral and vertical incision rate, wall angles, are measured in meander bends in the gypsum cave, Parks Ranch in New Mexico, and the limestone cave, Copperhead, in Arkansas. These data are compared to modeled relationships between scallop ratio and incision angle that vary with the exponent, produced by shifting the position of maximum velocity in a shear stress estimation method. Field data indicate that erosional power in these caves is between values for transport limited dissolution, and abrasion. We interpret erosional mechanisms to be a combination of some type of dissolution, and abrasion in both caves.

Additionally, we test the veracity of the shear stress estimation method as it applies around meander bends by measuring the distribution of shear stress in a cross-section as indicated by scal-

lops, and minimizing the discrepancy between calculated values by changing discharge and maximum velocity position. We find that computed scallop lengths are statistically indistinguishable from measured. This method shows promise for calculating discharge in cave passages with a free-surface.

3.2 Introduction

Bedrock channels are well known to record past conditions such as climate, tectonics, and hydrology in their geometry (e.g Amos and Burbank, 2007; Finnegan et al., 2005; Stark, 2006; Turowski et al., 2007, 2009; Wobus et al., 2008, 2006; Yanites and Tucker, 2010). Cave passages, a type of soluble bedrock channel, are particularly useful in recording past conditions over long time periods as they are preserved from surface erosion, and have the ability to remain in a landscape over millions of years (Broak, 2008; Gabrovšek, 2002; Osborne, 2007; Palmer, 2007b; Plotnick et al., 2015). This preservative aspect has been used to constrain landscape evolution rates using sediment deposited in different cave levels (e.g. Granger et al., 2001, 1997). However, interpreting past conditions based on channel geometry is problematic, as erosion of soluble bedrock channels is poorly understood once turbulent flow develops (Covington, 2014).

While the process of limestone dissolution in turbulent flow has been explored through experiments and models (e.g. Dreybrodt and Buhmann, 1991; Liu and Dreybrodt, 1997), the results from the theory appear to contradict observations of dissolutional cave forms seen abundantly in the field (Covington, 2014). This contradiction is perhaps best illustrated by the conundrum of scallop formation; scallops are hypothesized to form due to turbulent eddies that cause differences in diffusion boundary layer thickness. This variation in boundary layer thickness leads to a variation in erosion rate, as transport limited dissolution rates are proportional to boundary layer

thickness (Curl, 1966). However, theoretical results suggest that transport limited dissolution of calcite does not occur in the vast majority of turbulent flow conditions, as the boundary layer is never thick enough to limit the rate (Covington, 2014). Instead, theory predicts that dissolution of calcite is surface reaction rate limited under most turbulent flow conditions, and, therefore, that dissolution rates should be independent of the boundary layer thickness. As such, scallops, and other speleogens that require dissolution rate to depend on boundary shear stress, should not form in limestone channels. This conflict between theory and observation suggests that either: 1) the experiments that measure dissolution rates are not measuring actual surface reaction rates, or 2) there is a mechanical component to the formation of scallops, such as grain detachment (Levenson and Emmanuel, 2016). While mechanical erosion is known to happen in caves and other soluble bedrock channels, the relative importance of chemical and mechanical processes is not well constrained (Covington et al., 2015). Gypsum, which follows mixed kinetics (Raines and Dewers, 1997), does not exhibit the same contradiction between theory and field observations; however, the relative importance of erosion mechanisms in gypsum caves have also not been explored. The fact that canyon passages within caves often reach stable widths is further evidence that erosion rates are not independent of shear stress (Cooper and Covington, in prep).

The magnitude of erosion perpendicular to a bedrock channel wall can be written in a generic form as a power law of boundary shear stress (τ_b),

$$E = K\tau_b^a\,, \tag{3.1}$$

where K is a constant, and a is an exponent related to the erosional process (Whipple et al., 2000). Whipple et al., (2000) give likely values of a for different erosion mechanisms such as plucking of jointed blocks ($1 \lesssim a \lesssim 3/2$) and abrasion by sediment ($a = 5/2$) While plucking of grains de-

tached following boundaries loosened by dissolution has been observed in soluble rocks (Levenson and Emmanuel, 2016) and on other corroding materials (Guo et al., 2006), it has not been mapped to a specific value of a. Transport limited dissolution, where dissolution rate is proportional to the boundary layer thickness (ϵ), scales with $a = 1/2$ (e.g. Perne et al., 2014). For surface reaction rate limited dissolution, as predicted on limestone for turbulent flow (Covington, 2014; Dreybrodt and Buhmann, 1991; Liu and Dreybrodt, 1997), $a = 0$ as this process depends solely on chemistry. Surface reaction rates can be calculated from kinetic experiments (e.g. Dreybrodt et al., 2005; Palmer, 1991; Plummer et al., 1978). Dissolution experiments on gypsum show $1/3 \leq a \leq 1/2$ (Opdyke et al., 1987) due to mixed transport/reaction rate kinetics. Erosion within bedrock channels can also be approximated using the stream power erosion model, $E = K_s A_b^m S^n$, where K_s is a constant encapsulating erodibility, A_b is contributing basin area, m is a constant depending on process, and S is channel slope. The exponent n in the stream power model is related to a by $n = 2a/3$.

Both dimensional analysis and experiments with dissolution of gypsum have shown that scallop lengths are a function of boundary shear stress, with

$$Re^* = \frac{L\sqrt{\tau_b/\rho}}{\nu}, \tag{3.2}$$

where $Re^* = 2200$ is the scallop roughness Reynolds number, L is the length of of the scallop, ρ is the fluid density, and ν is the fluid kinematic viscosity (Blumberg and Curl, 1974; Curl, 1974). Since τ_b can be estimated from scallop bedforms, a record of E could be used to constrain a in natural settings. However, most efforts to estimate E in soluble bedrock channels calculate the value from chemistry (e.g. Covington et al., 2015), and, since these values rely on the dissolution models, they cannot be used to constrain a. Methods of direct measurement include limestone tablets and micro-erosion meters (Gabrovšek, 2009). However, direct measurement also poses a problem as

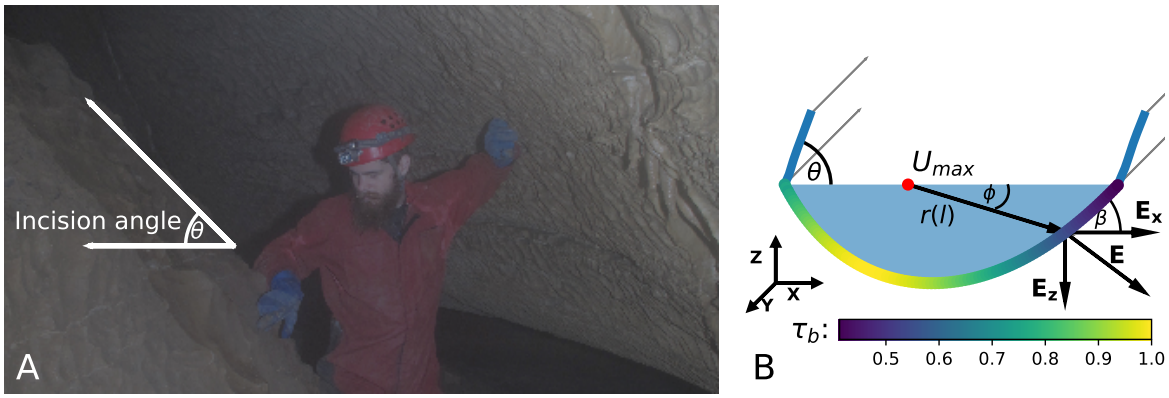

Figure 3.1: (A) A photograph in Copperhead Cave showing the incision angle around a meander bend. Scallop sizes on the outside of the bend are about half the size of those on the inside. (B) Schematic of the model. U_{max} is the position of the maximum velocity, offset from the center as a result of channel curvature in a meander. E, E_z, and E_x are the perpendicular, vertical, and horizontal erosion vectors, respectively. Colored floor indicates the current active channel, with color corresponding to τ_b normalized by its maximum value.

the rate of wall retreat is relatively slow, and may differ to that within scallops (Springer and Wohl, 2002). Additionally, the placement of limestone tablets or pins for micro-erosion measurements disrupt the flow structures required to form scallops.

Meandering cave channels preserve reaches that have incised both vertically and laterally (Fig. 3.1). The lateral migration of the channel within meanders presumably relates to contrasts in wall shear stress, with higher stresses present in the direction of channel migration. It seems plausible that the ratio of vertical to lateral incision will be sensitive to the relationship between erosion rate and wall shear stress. The stronger the dependence of erosion rate on shear stress, the greater the rate of lateral incision that will be produced for a given contrast in wall shear stresses. Consequently, while absolute erosion rates are challenging to measure and interpret, morphologies preserved in scalloped meandering cave channels may help to constrain the active erosional mechanisms.

To understand shear stress distributions and relative incision rates in meandering soluble bedrock channels we collect morphological data in the form of 3D scans in several caves. To assist in interpretations of the observed relationships between incision angle and scallop sizes we compare the field data to simulations of cross-section evolution within meander bends that employ a power law shear stress erosion model.

3.3 Site Descriptions

We collect field data in the form of incision angles and scallop lengths on opposite walls in two caves: Parks Ranch Cave (PRC) and Copperhead Cave (CHC). PRC is located in Eddy County, New Mexico, USA, and is formed within the Castile Formation, a gypsum unit (Stafford et al., 2008). Water enters PRC through several surface channels and sinkholes and drains into Chosa Draw, a tributary of the Black River. The active stream channel contains water through the entire year and some sediment. Evidence of flooding to the ceiling is visible throughout PRC, even in passages at higher elevation. Slope values are $1/2 - 3^{\circ}$. Measurements were recorded in a series of meander bends located in a tributary to the main stream near the most northwestern entrance.

CHC is located in Newton County, Arkansas, USA, and is formed in the St. Joe member of the Boone Formation. CHC contains water year round in one major stream passage that empties into a tributary of the Buffalo River (Gillip, 2007). This passage is mainly meandering canyon, with some areas having tubes near the ceiling. The stream contains chert gravel and larger clasts weathered from the Boone Fm, a unit with a high chert content. Measurements were recorded in a section of stream upstream of a knickpoint where slope is $1/2 - 1^{\circ}$ and sediment is sparse. Downstream from the measured section there are higher slopes and larger clasts.

3.4 Methods

3.4.1 Field measurements

Data were analyzed from 3D scans generated using AgiSoft Photoscan, a Structure from Motion (SfM) software package. These scans were constructed from many photographs of the cave walls from differing view points (Westoby et al., 2012). Such scans have been used to make measurements of geomorphological features (Fonstad et al., 2013; James and Robson, 2012; Westoby et al., 2012), including within caves (Mankoff et al., 2017). Markers were placed on the walls in locations that do not obscure scallops. The relative position of the markers was determined using a survey with a DistoX2 laser range finder, which measures length, azimuth, and inclination. This instrument is accurate to 2 mm for distance at up to 10 meters, and 0.5° for angular measurements (Trimmis, 2018). Survey data were logged to the cave survey software TopoDroid (Corvi, 2018b) then processed into x, y, z points in Cave3D (Corvi, 2018a). The x, y, z points from the survey were attached to markers in AgiSoft Photoscan to provide a reference coordinate system. This reference coordinate system allows measurement of incision angle and properly scaled dimensions.

Locations for morphological measurements were picked by first identifying parallel walls within a meander bend. The scan was then cropped to this area using the Cross-Section tool in the CloudCompare (*CloudCompare* 2018) software. Planes were fit to the cropped walls with RANSAC Shape Detection (Schnabel et al., 2007), which samples points repeatedly to find a model and remove outliers (Fischler and Bolles, 1987). The dip of the plane was recorded as the incision angle if the angle disparity between the walls was less than ten degrees. This to ensures the morphology has reached equilibrium and reduces variability in the statistical distribution of angles. Scallops were measured on each wall in Photoscan. The recorded scallop size (L) was the longest

distance parallel to flow as per Curl, 1974. Channel slope measurements were also taken by fitting a plane to the floor of the cave. These values were used to constrain slope within model runs for each cave setting.

Blumberg and Curl, 1974; Curl, 1974 suggest using Sauter-mean,

$$L_S = \frac{\sum L_i^3}{\sum L_i^2}, \tag{3.3}$$

as a measure of characteristic size within a scallop population, since the larger scallops are more indicative of wall shear stress. Since we seek to measure a ratio, the Sauter-mean of the inner wall, L_I, and outer wall, L_O, were computed separately. The ratio is computed as L_I/L_O, and shear stress on the outer wall is, by definition, greater than that on the inner. Scallop measurements tend to follow a log-normal to normal distribution (Lauritzen, 1982, 1989), and therefore the ratio L_I/L_O is also log-normally or normally distributed. To estimate confidence limits on the observed ratios we used bootstrap Monte Carlo with replacement. Approximately 50 scallops were randomly sampled from each wall 1000 times, and the Sauter-means were calculated for each random sample.

Scallop ratio and incision angle measurements were fit to a linear model using orthogonal distance regression, as both the ratios and angles have associated uncertainty. To compare field data to modeled meanders, confidence bands on the measured data are plotted at the 95% level.

A cross-section was also extracted from the 3D scans using the contour tool in CloudCompare (*CloudCompare* 2018). Within this cross-section, scallops were binned by distance along the channel perimeter, and Sauter-means of scallops were calculated for each bin. These values were later compared against theoretical scallop sizes produced by the shear stress estimation algorithm used in the numerical model.

3.4.2 Numerical meander model

To model relationships between erosion, channel morphology, and bed shear stress we simulate channel evolution as a function of wall shear stress. To estimate shear stress, we use the WTA method (Wobus et al., 2008, 2006) and assume that erosion rate is a power law of shear stress (Eq. 3.1). The WTA method uses the law of the wall to approximate τ_b around a channel perimeter given cross-section geometry, discharge (Q), slope (S), and roughness length (z_0). Here we use the implementation of the WTA method for open channels as developed by Cooper and Covington, in prep. To approximate the asymmetry of bed stresses found within a meander bend, we offset the position of maximum velocity from the center of the free-surface to an arbitrary position between the left wall of the channel and the center of the free-surface (Fig. 3.1). The general algorithm of the WTA method is:

1. Determine the water height, h, by minimizing the difference between prescribed Q and discharge computed by the Chézy equation with h dependent wetted area, A, and perimeter, P.

2. Calculate the maximum velocity, U_{max}, using the law of the wall over all rays, $r(l)$, from maximum velocity position to x, z points on the wall and requiring the average velocity within the cross-section to satisfy $u = Q/A$.

3. Solve the modified law of the wall equation for the bed-normal velocity gradient,

$$\left.\frac{du}{dr(l)}\right|_{z_0} = \frac{U_{max}}{z_0} ln(r(l)/z_0)^{-1} \cdot sin(\phi - \beta)\,. \tag{3.4}$$

   Angles ϕ and β are illustrated in Fig. 3.1b.

4. Calculate τ_b for all points along the perimeter via

$$\tau_b(l) = \varphi\rho A\left(\frac{du}{dr(l)}\bigg|_{z_0}\right)^2. \tag{3.5}$$

The factor, φ, ensures force balance,

$$\varphi = \frac{gS}{\sum_{i=1}^{N}\left(\frac{du}{dr(l)}\big|_{z_0}\right)^2 dl(i)}, \tag{3.6}$$

where g is gravitational acceleration, and $l(i)$ is the distance between the i and $i-1$ x, z point defining the perimeter.

At each time step this algorithm is used to calculate τ_b at each point along the perimeter. The channel is then evolved as a function of shear stress at every point along the wall, where erosion occurs in a direction perpendicular to the wall at each point. Simulations are run until the active channel width does not change over 100 time steps. Simulations are run with parameters Q, S, and z_0 that are representative of caves in this study. Roughness height, z_0, is the least constrained variable and is obtained from a distribution of scallop relief, D, that is on the order of 1cm (Palmer, 2007a). Here $z_0 = D/30$ for hydraulically rough flow (Nikuradse, 1950). For every simulation the equilibrium shear stress distribution along the channel, incision angle, and mean shear stress from the previous 100 time steps on the left and right wall are recorded along with the input parameters (a, Q, S, z_0). We use $a = 0.1$ to approximate a reaction rate limited dissolution end member, as simulations with $a = 0$ (the true reaction limited case) do not reach a constant width (Cooper and Covington, in prep).

Since the WTA method was developed for straight reaches, we test the applicability of the modified model in meander bends by calculating the shear stress distribution along a cross-section extracted from a 3D scan. Calculated shear stress is compared to scallop length using Eq. 3.2. The

maximum velocity position is found by minimizing

$$\chi^2 = \sum_{i=1}^{k} \frac{(L_{c_i} - L_{S_i})^2}{L_{S_i}}, \tag{3.7}$$

where k is the number of perimeter bins measured along the cross-section, L_S is the Sauter-mean scallop length of scallops within each bin, and L_c is scallop length scale estimated from the shear stress model for each bin. Eq. 3.7 describes the χ^2 statistic with the null hypothesis that computed and measured scallop lengths are independent.

3.5 Results

3.5.1 Field data

Scallops and incision angles were measured from scans in seven locations in CHC, and eight locations in PRC. Data were also collected by hand at one location in PRC via caliper and Brunton compass inclinometer. Scallop sizes on either wall follow normal and log-normal distributions (Supplemental Information 1). Ratios of the Sauter-mean scallop lengths on either wall versus incision angle are plotted in Figure 3.2 for CHC and PRC, along with the 95% confidence band on the orthogonal regressions, and lines fit to the simulation results for different exponents, a, in the shear stress erosion model. Confidence intervals on ratios are the standard deviation as determined by bootstrap Monte Carlo, and confidence intervals on the incision angle are the maximum and minimum values. Simulations are discussed in the following section.

For all cave sites, we find a pattern of smaller scallops (and therefore higher shear stress) on the channel wall that is being undercut in the direction of migration. Similarly, we find a general relationship of lower incision angles for larger contrasts in wall shear stress as erosion on the outer

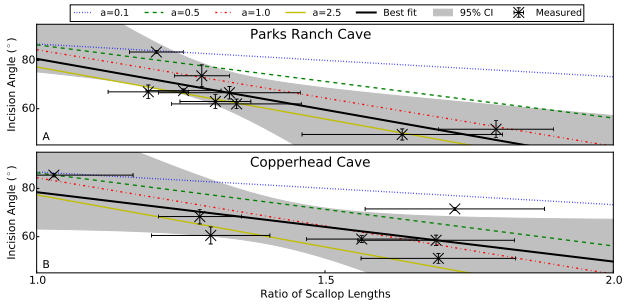

Figure 3.2: Channel incision angle versus the ratio of Sauter-mean scallop lengths on the inner and outer meander walls in Parks Ranch Cave (A) and Copperhead Cave (B). Data are fit using orthogonal distance linear regression as both incision angle and ratio have associated error values. Error bars for ratio of Sauter-means are the standard deviation, while they are the maximum and minimum values for incision angle. Colored lines are best fit lines to simulation runs with different values of the exponent, a, in the shear stress erosion model.

wall overwhelms that on the inner. The slope of this relationship differs between the two sites studied here, with PRC having a steeper negative slope than CHC.

3.5.2 Comparison between the shear stress model and measured scallop lengths

A cross-section was extracted from a 3D scan in Parks Ranch Cave. The incision angle in the cross-section is 51.5±2.5°. We measured eight groups of ten scallops distributed through the cross-section, and computed the Sauter-mean length of each group (Fig. 3.3). A channel slope of 1° is estimated using a plane fit to the floor of the cave in the reach where the cross-section is located. To estimate discharge, Q, the maximum velocity position, and to test the validity of the modified WTA approximation within meander bends, we minimize χ^2 (Eq. 3.7) calculated using the shear stress from the WTA method and the measured scallop lengths (Fig. 3.3c,d). The input parameters for the WTA algorithm are the 1 cm roughness and the measured slope. We obtain a best fit value of $Q = 0.16m^3/s$ and $\chi^2 = 0.337$, corresponding to a p-value <0.01. Minimizing the difference between measured scallop size and modeled size without a fixed value for S results in $Q = 0.16m^3/s$, $S = 0.7°$, and $\chi^2 = 0.046$, also corresponding to a p-value <0.01.

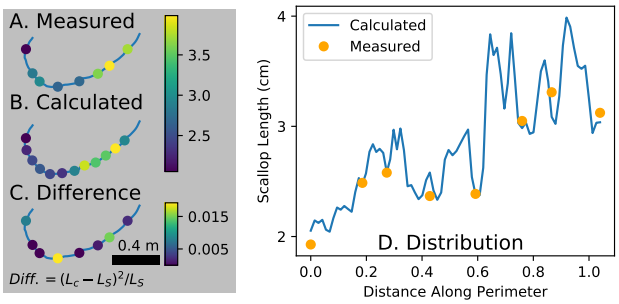

Figure 3.3: (A) Sauter-mean of scallop lengths measured within a cross section. (B) Scallop length computed using WTA method with parameters $S = 0.013$, $Q = 0.16m^3/s$, and $z_0 = 3.3 * 10^{-4}$. (C) Difference between measured and computed scallop lengths. The geometry of the cross-section in A, B, and C was measured from a 3D scan. (D) The relationship between measured and modeled scallop sizes, plotted as scallop length versus distance along the wall. Both computed and measured scallop sizes are plotted. Local peaks are due to roughness in the cross-section extracted from the scan.

The second value of S is used to test the method in recovering slope and to compensate for z_0 not being a measured value. The discharge values estimated from the measured and minimized slopes are equal and result in a water height that corresponds with the active channel below the incised meander walls (Fig. 3.3b).

Given the low p values, we conclude that the computed scallop lengths are statistically indistinguishable from the measured lengths, and that the model therefore provides a good approximation to shear stresses recorded in scallop sizes in the real channel. From the determined U_{max} positions and Q we ran simulations with varying exponents, a, in the shear stress erosion model until the modeled incision angle is the same as the measured. Using the slope value fit to the 3D scan, a simulation where $a = 0.25$ best matches the measured incision angle, whereas the best fit value of $a = 0.30$ using the slope obtained from minimization.

3.5.3 Impact of model parameters on incision angle

To explore sensitivity of the relationship between scallop ratio and incision angle to potential controlling parameters, we run four sets of simulations. In each simulation set, we vary one of the four potential controlling parameters, Q, S, z_0, and a, and keep all other parameters constant. For each value of the varied parameter a subset of 6-10 simulations are run with different positions of maximum velocity to produce a range of incision angles. (Fig. 3.4). Simulations are initiated with a circular geometry with a radius of one meter and are run until the width of the wetted channel does not change over 100 time steps. The fiducial values are $Q = 0.25$, $S = 0.035$, $z_0 = 0.0003$, and $a = 1.0$, except when they are varied. Each parameter is varied between a factor of 5 and 10. For each simulation, we record the input parameters, incision angle, calculated scallop ratio, and width at the top of the wetted channel (Supplemental Information 2). Unpaired independent t-tests between regression slopes of the minimum and maximum of the tested parameter values for each simulation set result in $p = 0.3223$, $p = 0.4062$, and $p = 0.3630$ for Q, z_0, and S, respectively. Testing at $\alpha = 0.05$ these parameters do not statistically change the relationship between ratio and incision angle.

To determine impact of the shear stress erosion exponent, a, we ran a set of simulations where parameters were chosen randomly from uniform distributions with $0.1 \leq Q \leq 0.3$, $0.01 \leq S \leq 0.052$, and $0.005 \leq D \leq 0.05$. Values of a used in the simulations were 0.1, 0.5, 1.0, and 2.5 (Fig. 3.4d, SI2). These distributions cover the range of parameters measured or determined in PRC and CHC. We choose $a = 0.1$ to represent a nearly reaction rate limited dissolution end member. We do not use $a = 0$, because such simulations do not reach a constant width but rather continue to grow wider with each time step.

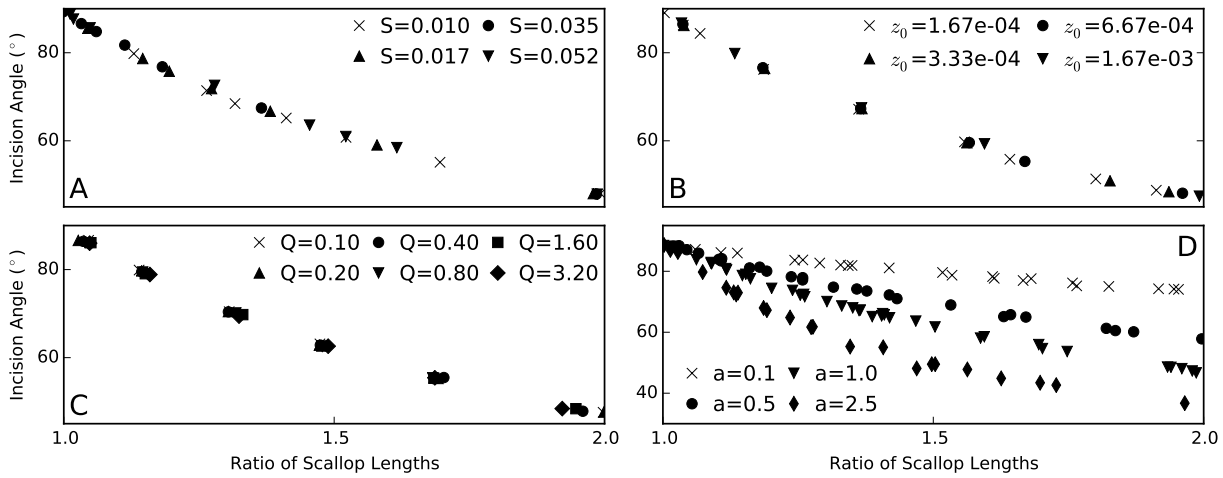

Figure 3.4: Influence of (A) slope, (B) roughness height, (C) discharge, and (D) erosion exponent on the relationship between scallop length ratio and channel incision angle. Within each panel the position of U_{max} was varied in order to produce a range of scallop lengths ratios and incision angles.

The relationship between the incision angle and the contrast in scallop sizes on the inner and outer walls is roughly linear and responds to changes in a by changing slope. For larger a, corresponding to mechanical processes, the slope increases. Despite choosing parameters randomly for these simulations little scatter occurs for each value of a, suggesting that the other parameters have little impact on this relationship (Fig. 3.4a-c).

When field data are plotted along with simulation results $a = 0.1$ and $a = 0.5$ do not fit within the 95% confidence interval for PRC, while for CHC only $a = 0.1$ does not. For Parks Ranch Cave the line of best fit for the data is nearly parallel to the relationship of $a = 1.0$. Copperhead data produce a best fit that is less steep, nearly parallel to relationship simulated for $a = 0.5$. The exponent $a = 1.0$ occurs for the mechanical process for plucking of jointed blocks, though neither PRC nor CHC contain the presence of plucked blocks.

3.6 Discussion

3.6.1 Scallops as a measure of hydraulics

This study is among the first, along with (Nance, 2007), to estimate discharge from scallops in a vadose canyon assuming free-surface conditions. The model presented here provides a valuable tool to estimate discharge in further cave studies. Other such studies that attempt to calculate discharge in vadose canyons include Checkley and Faulkner, (2014), who calculate discharge assuming that the the conduit is full during the time scallops are being formed. Charlton, (2003) performs in-situ measurements of shear stress and discharge, and while they do not perform the backwards calculation from scallop size distribution, they note the difficulty of such a procedure as the cross-section changes with discharge.

The method used here requires two easily measured parameters, scallops at certain locations within the channel, and the slope of the channel. The known relationship between shear stress and scallop length (Eq. 3.2) allows discharge to be estimated using the WTA method by minimizing the discrepancy between measured and calculated scallop lengths (or shear stress). Accuracy of this method is demonstrated by the close fit of scallop lengths along the channel perimeter (Fig. 3.3d), and recovery of the flow height of the active channel below an incised meander in Parks Ranch Cave (Fig. 3.3b) Additionally, by treating slope as a free parameter during minimization, the same discharge is calculated, and the calculated slope is similar to the measured slope.

A value of $a \approx 0.25 - 0.3$ was estimated using the distribution of shear stress and the incision angle. To estimate a, we determined the maximum velocity position in the channel using the scallop size distribution along the wall and then ran a set of simulations that used this maximum velocity position while changing a until the resulting incision angle matched the measured incision

angle. This value is outside of the 95% confidence band for PRC data and within the range that would be expected for mixed dissolution kinetics, where both surface reaction rate and transport are important.

3.6.2 Validity of the model

The WTA model has successfully duplicated observed scaling relationships between geometry and flow, such as the scaling of width to discharge (Wobus et al., 2006), with an exponent of 0.38, which falls within the range of 0.3-0.5 observed in the field (e.g., Finnegan et al., 2005). Additionally, this method has been used to model realistic cross-section shapes in conduit-full cave passages (Cooper and Covington, in prep). The WTA method has also been compared to measured shear stresses, and shear stress values calculated with more accurate methods, such as the Ray-Isovel model (Wobus et al., 2008). As such, the WTA method is valid method for estimating boundary shear stress in bedrock channel models.

The WTA model assumes that the maximum velocity is in the center of the free- surface, and the model has not previously been used to estimate shear stress in meander bends where the maximum velocity position can be offset. Here, we tested the applicability of a modified WTA method to meander bends by comparing the distribution of shear stress measured from scallop sizes within a measured channel to that estimated with the WTA method with an offset position of the velocity maximum. A statistically significant χ^2 value obtained by minimizing the discrepancy between measured and calculated scallop sizes demonstrates that the WTA method successfully estimates boundary shear stresses in a cross-section within a meander bend.

3.6.3 Erosional mechanisms

Field relationships between incision angles and scallop length ratios (Fig. 3.2) from Parks Ranch Cave and Copperhead Cave have a 95% confidence band that includes modeled relationships with several values of a. Both PRC and CHC are consistent with $a = 1$ and $a = 2.5$. These values of a would arise from mechanical processes, with $a = 1$ representing plucking of jointed blocks, and $a = 2.5$ representing abrasion by sediment. The best fit relationship to the data in PRC corresponds closely to $a = 1$. The confidence bands for the CHC data are also consistent with the model runs with $a = 0.5$, which represent transport limited dissolution. In fact, the slope of best fit line for CHC data corresponds most closely to the slope produced by this transport limited case.

Incision angle and scallop ratio data for both PRC and CH suggest that a in these caves is between 0.5 and 2.5. In contrast, $a \approx 0.25 - 0.3$ is obtained by the simulation that matches incision angle using the position of U_{max} estimated based on scallops for the full cross-section at one location in PRC. Both methods exclude $a = 0.1$, and therefore would also exclude $a = 0$, representing reaction rate limited dissolution. The presence of scallops, which require erosion to scale with boundary layer thickness/boundary shear stress, and the fact that the data are inconsistent with model runs with low values of a strongly suggest that the dominant type of erosion occurring in CH and PRC is not reaction rate limited dissolution; however, if combination of erosion processes are active, particularly if some of these are mechanical, this could explain the values obtained for a.

The value of the erosional exponent found using the incision angle within a single cross-section of PRC ($a \approx 0.25-0.3$) falls outside of the 95% confidence band and would require reaction rate limited dissolution mixed with another process. The exponent 0.25-0.3 can be interpreted

several ways: 1) the active channel reflects a different a than that of the long-term incision; 2) the data and confidence band are too sparse; 3) this a only represents one data point and no conclusions should be drawn from it; or 4) the method used to obtain this a is spurious, as it would produce a scallop ratio greater than observed in all field data in the modeled relationship.

Inferring erosional mechanism from a, no matter how well the data constrain the relationship, is not directly possible, since mixing of processes could lead to intermediate values of a. For instance, combining transport limited dissolution with abrasion by sediment might produce $0.5 < a < 2.5$, which includes the values of a for plucking of jointed blocks, where $1 \leq a \leq 3/2$. Some processes, however, can be eliminated. While there is jointing present in both PRC and CHC, neither site shows physical evidence of plucked blocks following joints. Both caves contain sediment either sourced from outside of the cave (PRC), or possibly derived from weathering of material inside the cave (CHC). These sediments can become tools for abrasion during high discharges. Neither transport limited dissolution, nor reaction rate limited dissolution can be eliminated as a possible mechanism responsible for a portion of the erosion. The value $a \approx 0.25 - 0.3$ in PRC suggests a mix of reaction rate limited dissolution and some other mechanism. This value of a is near that predicted for dissolution of gypsum dissolving by mixed kinetics ($a \in [1/3, 1/3]$, Opdyke et al., 1987). The values $0.5 < a < 2.5$ suggest a mix of abrasion and some form of dissolution, whether transport limited, reaction rate limited, or mixed kinetics.

Current models of speleogenesis in turbulent flow employ surface reaction rates measured in experiments such as Plummer et al., 1978. However, as these experiments largely do not measure hydrodynamics, the assumption that they are measuring surface reaction rates may not be correct. The experiments of Rickard and Sjöberg, 1983; Sjöberg, 1976; Sjöberg and Rickard, 1983 do use known hydrodynamics, and do show weak mixed kinetics for calcite. To truly understand the

type of dissolution occurring in limestone caves, additional experiments of this nature need to be performed. Inspection of natural dissolving surfaces via microscopy could reveal the signatures of grain detachment as seen in Emmanuel and Levenson, 2014; Levenson and Emmanuel, 2016. The rate of grain detachment is also likely to depend on shear stress, adding another possible process of erosion that has not yet been quantified.

3.6.4 Implications for meandering in bedrock channels

The cave passages that are used in this study are a form of meandering, bedrock channel, a type of channel that is not well understood (e.g. Johnson and Finnegan, 2015; Turowski, 2018). The morphology of scalloped cave channels may add additional insight into the process of bedrock meandering, as these channels contain both a history of meander incision and indicators of shear stress distribution. Turowski, 2018 suggests that the fundamental cause of meanders in bedrock is sediment cover. We suggest that meanders can form from any type of perturbation that causes a longstanding shift in maximum velocity position away from the center of the channel. Cover within the channel is a possible mechanism for this shift, though sediment cover is not the only fundamental cause of velocity distribution shifts. Meandering occurs without sediment cover, for example, in meanderkarren, a type of karst formation that is a sinuous channel in bare limestone. Meanderkarren are known to form on bare, alpine slopes with little sediment input (Veress, 2010, 2012). Sediment, while present in Parks Ranch Cave and Copperhead Cave, does not create a substantial cover in the studied meandering reaches.

The recorded shear stress distributions in the form of scallops do give an indication of the processes driving meandering, assuming the only fundamental cause of meandering is contrast in wall shear stresses. Both the simulated (Figs. 3.1b, 3.3b, d) and measured (Fig. 3.3a, d) distri-

butions of shear stress around the active channel show shear stress on the inside wall being high relative to that on the outside wall. Higher shear stresses on the outside wall result in higher erosion rates due to either mechanical erosion, or transport limited dissolution. This differential erosion could lead to meanders forming and further evolving without the need of a sediment cover.

3.7 Conclusion

This study presents a novel method to determine how erosion rates scale with shear stress within cave channels by analyzing the relationship between scallop lengths and the incision angle of the passage walls within a meander bend. Data collected from Parks Ranch Cave, a gypsum cave in New Mexico, and Copperhead Cave, Arkansas, suggest that erosion scales with shear stress with an exponent, a, between 0.5 and 2.5. Processes that result exponents in this range include transport limited dissolution ($a = 0.5$), plucking of jointed blocks ($1 \leq a \leq 3/2$), and abrasion ($a = 5/2$). However, we caution against the direct interpretation of a measured a in terms of a specific process, as mixing of processes may generate intermediate values of the exponent. The presence of sediment, lack of plucked blocks, and the meander data suggest a combination of abrasion and some type of dissolution in both Parks Ranch Cave and Copperhead Cave.

This study is among the first to reconstruct discharge values from scallop lengths in vadose/free-surface conditions. We obtain a discharge of $0.16 m^3/s$ in a tributary passage in Parks Ranch Cave by minimizing differences between scallop-estimated shear stresses and modeled shear stresses. This minimization method presents a tool that could become commonplace in studies of cave hydrology.

The minimization method also demonstrates the validity of the numerical model to simulate cross-section evolution in a meander bend. Additional modeling of this type may give greater insight to meandering processes in bedrock channels.

3.8 References

Amos, C. B. and D. W. Burbank (2007). "Channel width response to differential uplift". In: *Journal of Geophysical Research: Earth Surface* 112.F2.

Blumberg, P. and R. L. Curl (1974). "Experimental and theoretical studies of dissolution roughness". In: *Journal of Fluid Mechanics* 65.4, pp. 735–751.

Broak, P. (2008). "Karst processes and time". In: *Geologos* 14, pp. 19–36.

Charlton, R. (2003). "Towards defining a scallop dominant discharge for vadose conduits: some preliminary results". In: *Cave and Karst Science* 30, pp. 3–7.

Checkley, D. and T. Faulkner (2014). "Scallop measurement in a 10m-high vadose canyon in Pool Sink, Ease Gill Cave System, Yorkshire Dales, UK and a hypothetical post-deglacial canyon entrenchment timescale". In: *Cave and Karst Science* 41.2, pp. 76–83.

CloudCompare (2018). Version 2.10. URL: `http://www.cloudcompare.org/`.

Cooper, M. P. and M. D. Covington (in prep). "Numerical modeling of paragenetic gallery formation in caves". In:

Corvi, M. (2018a). *Cave3D*. Version 3.1.58. URL: `https://sites.google.com/site/speleoapps/home/cave3d`.

— (2018b). *TopoDroid*. Version 4.0.0h. URL: `https://sites.google.com/site/speleoapps/home/topodroid`.

Covington, M. D. (2014). "Calcite dissolution under turbulent flow conditions: a remaining conundrum". In: *Acta Carsologica* 43.1, pp. 195–202.

Covington, M. D., J. D. Gulley, and F. Gabrovšek (2015). "Natural variations in calcite dissolution rates in streams: Controls, implications, and open questions". In: *Geophysical Research Letters* 42.8, pp. 2836–2843.

Curl, R. L. (1966). "Scallops and Flutes". In: *Transactions of the Cave Research Group of Great Britain* 7.2, pp. 121–160.

Curl, R. L. (1974). “Deducing flow velocity in cave conduits from scallops”. In: *National Speleological Society Bulletin* 36.2, pp. 1–5.

Dreybrodt, W. and D. Buhmann (1991). “A mass transfer model for dissolution and precipitation of calcite from solutions in turbulent motion”. In: *Chemical Geology* 90.1, pp. 107–122.

Dreybrodt, W., F. Gabrovšek, and D. Romanov (2005). *Processes of Speleogenessis: A Modeling Approach*. Vol. 4. Ljubljana, Slovenia: ZRC Publishing, p. 376.

Emmanuel, S. and Y. Levenson (2014). “Limestone weathering rates accelerated by micron-scale grain detachment”. In: *Geology* 42.9, pp. 751–754.

Finnegan, N. J., G. Roe, D. R. Montgomery, and B. Hallet (2005). “Controls on the channel width of rivers: Implications for modeling fluvial incision of bedrock”. In: *Geology* 33.3, pp. 229–232.

Fischler, M. A. and R. C. Bolles (1987). “Random sample consensus: a paradigm for model fitting with applications to image analysis and automated cartography”. In: *Readings in computer vision*. Elsevier, pp. 726–740.

Fonstad, M. A., J. T. Dietrich, B. C. Courville, J. L. Jenson, and P. E. Carbonneau (2013). “Topographic structure from motion: a new development in photogrammetric measurement”. In: *Earth Surface Processes and Landforms* 38.421-430.

Gabrovšek, F. (2002). *Evolution of karst: from prekarst to cessation*. Založba ZRC.

— (2009). “On concepts and methods for the estimation of dissolutional denudation rates in karst areas”. In: *Geomorphology* 106, pp. 9–14.

Gillip, J. A. (2007). “The effects of land-use change on water quality and speleogenesis in Ozark cave systems: A paired cave study of Civil War and Copperhead Caves, northwestern Arkansas”. PhD thesis. University of Arkansas.

Granger, D. E., D. Fabel, and A. N. Palmer (2001). “Pliocene- Pleistocene incision of the Green River, Kentucky, determined from radioactive decay of cosmogenic 26Al and 10Be in Mammoth Cave sediments”. In: *Geological Society of America Bulletin* 113.7, pp. 825–836.

Granger, D. E., J. W. Kirchner, and R. C. Finkel (1997). “Quaternary downcutting rate of the New River, Virginia, measured from differential decay of cosmogenic 26Al and 10Be in cave-deposited alluvium”. In: *Geology* 25, pp. 107–110.

Guo, H. X., B. T. Lu, and J. L. Luo (2006). “Non-Faraday material loss in flowing corrosive solution”. In: *Electrochimica acta* 51.25, pp. 5341–5348.

James, M. R. and S. Robson (2012). “Straightforward reconstruction of 3D surface and topography with a camera: accuracy and geoscience applications”. In: *Journal of Geophysical Research* 117.F03017.

Johnson, K. N. and N. J. Finnegan (2015). “A lithologic control on active meandering in bedrock channels”. In: *Bulletin* 127.11-12, pp. 1766–1776.

Lauritzen, S.-E. (1982). “The paleocurrents and morphology of Pikhåggrottene, Svartisen, North Norway”. In:

— (1989). “Scallop dominant discharge”. In: *Proceedings of the 10th International Congress of Speleology*, pp. 123–124.

Levenson, Y. and S. Emmanuel (2016). “Quantifying micron-scale grain detachment during weathering experiments on limestone”. In: *Geochimica et Cosmochimica Acta* 173, pp. 86–96. ISSN: 0016-7037. DOI: https://doi.org/10.1016/j.gca.2015.10.024. URL: http://www.sciencedirect.com/science/article/pii/S0016703715006158.

Liu, Z. and W. Dreybrodt (1997). “Dissolution kinetics of calcium carbonate minerals in H2O-CO2 solutions in turbulent flow: the role of the diffusion boundary layer and the slow reaction H2O + CO2 -> H+ + HCO3-”. In: *Geochimica Cosmochimica Acta* 61.14, pp. 2879–2889. URL: http://www.imedea.uib-csic.es/master/cambioglobal/Modulo_3_02/Tema_8-acidificaci%C3%B3n/pH/geochim%20cosmochim61pp2879-2889.pdf.

Mankoff, K. D., J. D. Gulley, S. M. Tulaczyk, M. D. Covington, X. Liu, Y. Chen, D. I. Benn, and P. S. Glowacki (2017). “Roughness of a subglacial conduit under Hansbreen, Svalbard”. In: *Journal of Glaciology* 63.239, pp. 423–435.

Nance, R. G. (2007). “AN ANALYSIS OF HYDRAULIC GEOMETRY IN A KARST CONDUIT, PARKS RANCH CAVE, EDDY COUNTY, NEW MEXICO”. In: *2007 GSA Denver Annual Meeting*.

Nikuradse, J. (1950). *Laws of flow in rough pipes*. National Advisory Committee for Aeronautics Washington.

Opdyke, B. N., G. Gust, and J. R. Ledwell (1987). “Mass transfer from smooth alabaster surfaces in turbulent flows”. In: *Geophysical Research Letters* 14.11, pp. 1131–1134. ISSN: 0094-8276. DOI: 10.1029/GL014i011p01131.

Osborne, A. R. L. (2007). “The World’s Oldest Caves:-How-Did They Survive and What Can They Tell Us?” In: *Acta carsologica* 36.1.

Palmer, A. N. (1991). “Origin and morphology of limestone caves”. In: *Geological Society of America Bulletin* 103.1, pp. 1–21.

Palmer, A. N. (2007a). *Cave Geology*. Dayton, OH: Cave Books.

— (2007b). "Variation in Rates of Karst Processes". In: *Acta Carsologica* 36 (1).

Perne, M., M. D. Covington, and F. Gabrovšek (2014). "Evolution of karst conduit networks in transition from pressurised flow to free surface flow". In: *Hydrology and Earth System Sciences Discussions* 11.6, pp. 6519–6559. DOI: 10.5194/hessd-11-6519-2014. URL: http://www.hydrol-earth-syst-sci-discuss.net/11/6519/2014/.

Plotnick, R. E., F. Kenig, and A. C. Scott (2015). "Using the voids to fill the gaps: caves, time, and stratigraphy". In: *Geological Society, London, Special Publications* 404.1, pp. 233–250.

Plummer, L. N., T. M. L. Wigley, and D. L. Parkhurst (1978). "The kinetics of calcite dissolution in CO2-water systems at 5 degrees to 60 degrees C and 0.0 to 1.0 atm CO2". In: *American Journal of Science* 278.2, p. 179.

Raines, M. A. and T. A. Dewers (1997). "Mixed transport/reaction control of gypsum dissolution kinetics in aqueous solutions and initiation of gypsum karst". In: *Chemical Geology* 140.1-2, pp. 29–48.

Rickard, D. and E. L. Sjöberg (1983). "Mixed kinetic control of calcite dissolution rates". In: *American Journal of Science* 283.8, pp. 815–830.

Schnabel, R., R. Wahl, and R. Klein (2007). "Efficient RANSAC for Point-Cloud Shape Detection". In: *Computer Graphics Forum* 26.2, pp. 214–226.

Sjöberg, E. L. (1976). "A fundamental equation for calcite dissolution kinetics". In: *Geochimica et Cosmochimica Acta* 40.4, pp. 441–447.

Sjöberg, E. L. and D. Rickard (1983). "The influence of experimental design on the rate of calcite dissolution". In: *Geochimica et cosmochimica acta* 47.12, pp. 2281–2285.

Springer, G. S. and E. E. Wohl (2002). "Empirical and theoretical investigations of sculpted forms in Buckeye Creek Cave, West Virginia". In: *The Journal of geology* 110.4, pp. 469–481.

Stafford, K. W., R. Nance, L. Rosales-Lagarde, and P. J. Boston (2008). "Epigene and hypogene karst manifestations of the Castile Formation: Eddy County, New Mexico and Culberson County, Texas, USA". In:

Stark, C. P. (2006). "A self-regulating model of bedrock river channel geometry". In: *Geophysical Research Letters* 33.4.

Trimmis, K. P. (2018). "Paperless mapping and cave archaeology: A review on the application of DistoX survey method in archaeological cave sites". In: *JOURNAL OF ARCHAEOLOGICAL SCIENCE-REPORTS* 18, pp. 399–407.

Turowski, J. M. (2018). “Alluvial cover controlling the width, slope and sinuosity of bedrock channels”. In: *Earth Surface Dynamics* 6.1, p. 29.

Turowski, J. M., D. Lague, and N. Hovius (2007). “Cover effect in bedrock abrasion: A new derivation and its implications for the modeling of bedrock channel morphology”. In: *Journal of Geophysical Research: Earth Surface* 112.F4.

— (2009). “Response of bedrock channel width to tectonic forcing: Insights from a numerical model, theoretical considerations, and comparison with field data”. In: *Journal of Geophysical Research: Earth Surface* 114.F3.

Veress, M. (2010). *Karst environments: karren formation in high mountains*. Springer Science & Business Media.

— (2012). “Morphology and Solution Relationships of three Karren Slopes in different Environments (Totes Gebirge, Eastern Alps)”. In: *Zeitschrift für Geomorphologie, Supplementary Issues* 56.2, pp. 47–62.

Westoby, M. J., J. Brasington, N. F. Glasser, M. J. Hambrey, and J. M. Reynolds (2012). “‘Structure-from-Motion’ photogrammetry: A low-cost, effective tool for geoscience applications”. In: *Geomorphology* 179, pp. 300–314. ISSN: 0169555X.

Whipple, K. X., G. S. Hancock, and R. S. Anderson (2000). “River incision into bedrock: Mechanics and relative efficacy of plucking, abrasion, and cavitation”. In: *Bulletin of the Geological Society of America* 112.3, pp. 490–503.

Wobus, C. W., J. W. Kean, G. E. Tucker, and R. S. Anderson (2008). “Modeling the evolution of channel shape: Balancing computational efficiency with hydraulic fidelity”. In: *Journal of Geophysical Research: Earth Surface (2003–2012)* 113.F2.

Wobus, C. W., G. E. Tucker, and R. S. Anderson (2006). “Self-formed bedrock channels”. In: *Geophysical Research Letters* 33.18.

Yanites, B. J. and G. E. Tucker (2010). “Controls and limits on bedrock channel geometry”. In: *Journal of Geophysical Research* 115.F04019, pp. 1–17.

4 Modeling Speleogenesis with Varying Discharge

MODELING SPELEOGENESIS WITH VARIABLE DISCHARGE: IMPLICATIONS FOR THE WIDTHS OF VADOSE CANYONS AND KEYHOLE PASSAGES

4.1 Abstract

The distribution of discharge is an important factor in the erosion of surface bedrock channels, and increasingly has been included in models of their formation. While variable discharge is equally important in speleogenesis (cave formation) no models have yet incorporated this process. In this study we develop a speleogenesis model where erosion is weighted by the probability of discharge in both a single cross-section, and a conduit, with hydraulic calculated by the storm water management software, EPA-SWMM.

First, we successfully test the ability of SWMM to produce realistic hydraulics as base level changes, and also explore the distribution of erosion in a non-updating, keyhole shaped, conduit. The distribution of erosion is similar to that seen in bedrock channels, though in the cave case the highest erosion rates are produced by discharges close to the mean discharge, as dissolution acts at all discharges with minimal thresholding, and the mean discharge is the most probable.

Simulations of single cross-sections where erosion at varying discharges is weighted by probability of discharge result in equilibrium widths that scale similarly to simulations of single discharges, though the magnitude of such simulations are less than their single discharge counterparts. In multiple cross-sections, representing a conduit, simulations show that a canyon shape develops as head drops, either through the conduit being a more efficient route for water, or base level fall. This canyon propagates from the upstream portion, to the downstream, the opposite as

observed and modeled in surface channels. Keyhole passages are successfully simulated, though only where discharge lowers during the evolution of the conduit. Additionally, similar to surface bedrock channels, the rate of base level drop sets the slope of the conduit floor. This model shows promise for future use exploring speleogenesis past the incipient stages.

4.2 Introduction

The width and slope of bedrock channels have been used to constrain information related to climate and tectonics such as uplift rate, sediment supply, and discharge, through scaling relationships of between geometry and these parameters (e.g., Kirby and Whipple, 2012; Lague, 2014; Miller et al., 2013; Roberts and N. White, 2010; Whittaker et al., 2007). Such scaling relationships are derived through field observations, and through mathematical modeling (e.g., Finnegan et al., 2005; Wobus et al., 2008, 2006; Yanites and Tucker, 2010). Mathematical models of bedrock channels often rely on a single measure of the distribution of possible discharges, the mean (e.g., Whipple, 2004; Whipple and Tucker, 1999; Wobus et al., 2006), and as such, do not capture the effects of stochastic variability in discharge. The importance of discharge variability in bedrock channel evolution is due to erosion and sediment transport laws often containing a threshold, implying only large events with high return times cause geomorphic work (Barbour et al., 2009; Hartshorn et al., 2002; Lague, 2010; Turowski et al., 2008). Increasingly, models include variability of discharge, (e.g., DiBiase and Whipple, 2011; Lague, 2010; Lague et al., 2005; Molnar et al., 2006; Snyder et al., 2003; Stark, 2006) due to its importance. While a growing body of mathematical models exist to explore variations in discharge on surface channels, models of large scale cave morphology for the early (e.g., Dreybrodt, 1988; Dreybrodt et al., 2005; Palmer, 1984, 1991; Szymczak and Ladd, 2011) and later stages (Cooper and Covington, in prep[a],[b]; Perne et al., 2014) of cave

conduit evolution do not take discharge variation into account. Additionally, few models of cave evolution factor in base level change (Gabrovšek et al., 2014), despite the widespread use of cave levels as base level position indicators (Palmer, 1987), combined with sediment dating as a tool for constraining landscape evolution rates (e.g., Anthony and Granger, 2004, 2006, 2007; Audra and Palmer, 2011; Granger et al., 2001, 1997; Granger and Siame, 2006; Stock et al., 2005). Therefore, in this study, we mesh models for surface bedrock channels and their cave counterparts to explore the effects of these processes.

Like bedrock channels, cave conduits undergo large variations in discharge. In response, hydraulic head can greatly change, (Bonacci, 2001; Covington et al., 2009; Halihan and Wicks, 1998; Kaufmann et al., 2016; Prelovšek et al., 2008; C. C. Smart, 1988), in some cases over 100 meters (Gabrovšek et al., 2018), which raises or lowers where erosion occurs. The variability of discharges in both caves and surface bedrock channels arises from the spatial and temporal recharge in the form of rainfall or snow melt within a drainage basin (Olsson and Niemczynowicz, 1996). Discharge variability can be captured within a statistical distribution, such as exponential distributions (Tucker and Bras, 2000), power law distributions (Olsson and Burlando, 2002; Svensson et al., 1996), and gamma distributions (Crave and Davy, 2001; Davy and Crave, 2000). The study of Lague et al., 2005 showed that a two parameter, modified gamma function best explains the distribution of daily discharges for over 30 years of data from 22 discharge monitoring stations in Taiwan, and 8 in the United States, though they argue that for large events where erosion occurs a power law fit is applicable. The parameters of the distribution are daily mean discharge, and one that controls the importance of both large and small extreme events. Following Lague et al., 2005, Molnar et al., 2006 found the power law fit, $N(Q) \propto Q^{-\kappa}$, where $N(Q)$ is the number of years that exceed a threshold discharge, applicable to daily discharge variation for 440 gauges in 14

states within the United States, and explored the range of values for the extremity parameter, with more arid environments having κ between 1-3, and wetter environments with κ between 3-6. Their model also confirms that erosion rates are lower in arid environments where overall precipitation is decreasing, and that environments that switch from humid to arid can have higher or lower incision rates depending on a threshold.

Unlike surface bedrock channels in which floodwaters flood over the banks, the closed nature of caves produce several effects depending on hydraulic conditions. If water flowing through the conduit maintains a free-surface (vadose) during base flow, larger events can switch the cave to being conduit-full (phreatic). Cave passages where this switch occurs regularly are termed epiphreatic (W. B. White, 1988). Another possible condition is the diversion of water into higher cave levels during floods, termed an overflow, or the entire cave system becomes flooded when head exceeds land elevation and water is routed in intermittent streams or over land. Estimating the hydrology of these systems has been traditionally difficult in traditional porous media models due to extreme heterogeneity, and large differences in permeability. Caves also differ from surface streams as they minimal downstream discharge increase for a single conduit with no infeeders (only matrix contributions), whereas in surface bedrock channels $Q \propto y^{1.6}$ in the downstream direction (Whipple and Tucker, 1999; Wobus et al., 2006).

While traditional groundwater modeling techniques for porous media have been modified for aquifer scales (e.g., Dufresne and Drake, 1999; Gallegos et al., 2013; Ghasemizadeh et al., 2015; Hill et al., 2010; Scanlon et al., 2003; Sun et al., 2005), modeling specific caves requires a different set of equations suitable for partially or entirely full pipes undergoing turbulent flow. These equations arise as simplifications of the incompressible Navier-Stokes equations. Conduit-full pipe flow can be simulated with Euler's equation for fluid flow, which for straight pipes with

no change in cross-section shape can be simplified to the 1-D form (Covington et al., 2009). If the flow is in steady state Euler's equations can be further simplified into the Darcy-Weissbach or Chézy equations. In the case of a free-surface, and considering the same assumptions as in Euler's equations, the 1-D Saint Venant equations govern flow, and again these can be simplified for steady state. To construct a flow model caves are broken up into individual sections that have a similar shape characterized by wetted perimeter, P, and cross-sectional area, A, as well as conduit roughness characterized by a parameter such as the Darcy-Weisbach friction factor (Covington et al., 2009; Springer, 2004) or the Manning roughness coefficient (e.g. Palmer, 2007). A system of equations for each discrete section is then solved, with equations chosen depending if the sections have a free-surface or are conduit full. These models have uses from reconstructing discharge from indicators of past water level position (e.g., Springer, 2004), or attempting to duplicate hydrographs from springs (e.g, Covington et al., 2009; Halihan and Wicks, 1998), with a set of equations constructed from the given physical or hypothetical cave. A growing number of hydrological models for specific caves have been developed from the freely available EPA-SWMM (Storm Water Management Model) (Campbell and Sullivan, 2002; Gabrovšek et al., 2018; Kaufmann et al., 2016; Peterson and Wicks, 2006; Prelovšek et al., 2008), eliminating the need to write and solve a set of equations.

SWMM can calculate a number of hydraulic parameters such as discharge and head in conduits based on geometry of conduits, open channels, and surface runoff that can be prescribed a set discharge, a time series of discharge, or rainfall over a catchment (Rossman, 2010). The equation used for calculating of flow in this model is the 1-D Saint Venant equations for momentum,

$$\frac{1}{g}\Big(\frac{\partial u}{\partial t} + u\frac{\partial u}{\partial y}\Big) + \frac{\partial d}{\partial y} + S_f - S_0 = 0\,, \tag{4.1}$$

and continuity,

$$\frac{\partial A}{\partial t} + \frac{\partial Q}{\partial y} = 0\,. \tag{4.2}$$

Here g is acceleration due to gravity, t is time, u is velocity, y is the downstream direction, d is flow depth, S_f is friction slope, S_0 is floor slope, and Q is discharge. Friction (energy) slope is typically defined by an empirical equation, and in SWMM the Manning form is used,

$$S_f = \frac{n^2 u^2}{C_0^2 R^{4/3}}\,, \tag{4.3}$$

where n is the Manning roughness coefficient, C_0 is a constant depending on units (for metric the constant is 1, for US system, 1.49), and R is the hydraulic radius, A/P. In SWMM either the full 1-D Saint Venant equations are solved (dynamic wave routing), or a simplification where $S_f = S_0$ (kinetic wave routing). While the 1-D Saint Venant equations normally only apply to flows with a free-surface, SWMM uses an element called a Preissmann slot to simulate conduit-full flows. The Preissmann slot is a narrow, vertical slot applied at the top of a cross-section that allows for an artificial free-surface at the head elevation (Rossman, 2010). SWMM has been used to successfully calculate flow in a speleogenesis model by Perne et al., 2014 to explore the transition between pressurized and free-surface flows, and as such we use it in this model.

In addition to variable discharge we include base level changes to the model. Base level change is hypothesized to cause a variety of effects on cave development, including the establishment of discrete cave levels (Palmer, 1987) that can be used as records of climate and tectonics (e.g., Anthony and Granger, 2004, 2006, 2007; Audra and Palmer, 2011; Granger et al., 2001, 1997; Granger and Siame, 2006; Stock et al., 2005). Lowering of base level can also switch phreatic sections of the cave to vadose, causing entrenchment towards the water table, with canyon shaped passages (Ford and Ewers, 1978; Worthington, 2005). Typically, the changeover from phreatic to

vadose conditions changes orientation of passage development from strike-oriented, to dip-oriented (Palmer, 1984, 1991). However, in some cases canyons can entrench into formerly phreatic passages, resulting in either a vadose canyon of similar width to the phreatic tube, or one that is smaller, forming what is termed a keyhole shape (Lauritzen and Lundberg, 2000; Palmer, 2007). While both phreatic and vadose type passages have been modeled in a single cross-section, no realistic attempt has been made to simulate keyholes, as vadose keyholes in Cooper and Covington, in prep(b) start with a phreatic tube that is artificially larger than the equilibrium width at a particular discharge. In this model the introduction of multiple cross-sections and determination of flow in both phreatic in vadose conditions allows the simulation of keyhole type passages. From this ability we use the model to test two hypotheses of keyhole formation: 1) the only requirement to form a keyhole shaped passage is the transition between phreatic and vadose conditions through base level drop and a sufficient amount of time spent in phreatic conditions, or 2) a drop in discharge that requires a smaller width to maintain equilibrium.

The final component of the model in this study is erosion. Caves evolve differently from non-soluble, surface bedrock channels, as erosion is at least partially, if not fully, due to dissolution, and thus geomorphic work can occur in most discharge regimes with a minimal threshold as it depends on undersaturation of water with respect to calcite rather than energy required to mobilize sediment (Covington et al., 2015). At higher discharges the threshold for sediment motion can be reached, and mechanical erosion may occur. The relative importance of these types of erosion has only begun to be explored quantitatively in surface soluble bedrock channels (Covington et al., 2015), and within caves (Cooper and Covington, in prep[a]). Dissolution has two end members: reaction rate limited dissolution, where erosion rate is only dependent on a rate constant depending on rock properties and chemistry, with no relation to shear stresses; and transport limited dissolu-

tion where erosion rate depends on chemistry and the rate at which ions diffuse across a diffusion boundary layer. The thickness of the diffusion boundary layer is a function of flow. The type of dissolution that occurs is that of the slower rate for a particular flow and chemistry, though there are arguments that transport limited dissolution does not occur in limestone caves (Covington, 2014). While these two distinct end members exist, if the rates are close enough mixed kinetics can occur, as is seen in experiments on gypsum (e.g., Opdyke et al., 1987).

Both end members can be modeled in the same way as mechanical erosion, with a shear stress erosion law,

$$E = K\tau_b^a\,, \tag{4.4}$$

where K is a constant encapsulating erodibility, τ_b is boundary shear stress, and a is number reflecting the type of erosion. For reaction rate limited dissolution $a = 0$, and thus erosion rate does not depend on shear stress. In the case of transport limited dissolution $a = 1/2$. While the reaction rate limited case does not depend on shear stress, there may be a dependence on flow as it has been observed that higher discharges effect chemistry, and thus erodibility (Groves and Meiman, 2005), though this effect likely depends on the type of recharge (Covington et al., 2015). As K in erosion due to dissolution is a function of of chemistry, and dissolution of limestone increases the saturation state with respect to calcite, erodibility decreases in the downstream direction. While this change is important for incipient caves of small cross-sectional area in a closed system (e.g., Dreybrodt, 1996; Dreybrodt et al., 2005; Palmer, 1991), and over long lengths, for short lengths (<1km) in mature systems of large cross-sectional area, the change in saturation state is minimal (Covington et al., 2012).

While the difference in erosional mechanism and the closed nature of caves make interpretations from surface streams not directly applicable, we can adapt processes used in these models to explore effects of variable discharge can be adapted to speleogenesis (cave formation) models. In this study we develop a speleogenesis model that tracks geometry of single conduit through multiple, aligned cross-sections, calculates head and energy slope at multiple discharges using SWMM, updates the geometry of cross-sections using a shear stress erosion law weighted by the probability of a particular discharge occurring, and changes base level as the conduit evolves. To test the utility of the model several scenarios are simulated to test hypotheses of keyhole passage formation. While the model in this study is superficially similar to a previous speleogenesis model utilizing SWMM for simulating the transition between phreatic and vadose conditions (Perne et al., 2014), ours adds the multiple discharge capability, changes in base level, and a different, more realistic estimate of shear stress termed the WTA method of Wobus et al., 2008, 2006 that has been used to successfully duplicate geometry of surficial bedrock channels, and those within caves (Cooper and Covington, in prep[a],[b]). Also, unlike Perne et al., 2014 we do not track chemistry in the model and instead consider saturation state to be the same over the length scales (<1km) explored. Additionally, we use a single cross-section model to test the effects of discharge variability on equilbrium width in vadose canyons.

4.3 Model Setup

To simulate cave formation under varying discharge a model is developed with several components: 1) a set of cross-sections representing a reach of cave passage, 2) a probability function determining the percentage of time a particular discharge, Q_k, occurs, 3) an interface with Storm Water Management Model (SWMM) to compute hydraulic parameters such as head from base

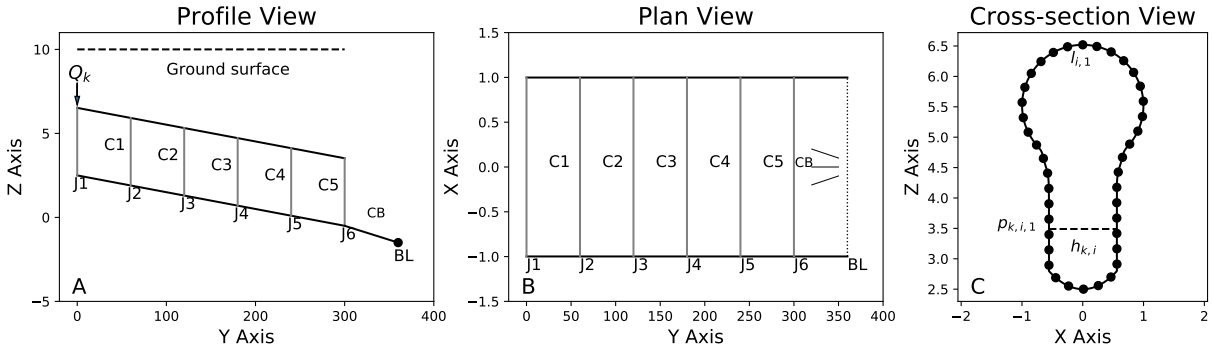

Figure 4.1: Geometry of the multiple cross-section model in the profile view (A), plan/map view (B), and cross-section view (C). Here the cross-section geometry in C is imposed throughout the conduit. J1-J6 indicate junctions, while C1-C5 indicate conduit sub-lengths. BL represents base level position (outfall in the SWMM model), while CB represents a stream run in this case. Q_k in A indicates where discharge enters the conduit. Converging lines in CB section in plan view represent the presence of a slope in the style of a cave map (e.g. Dasher, 1994). The dashed line in C indicates an example free-surface reference line.

level and passage geometry, 4) a method to estimate boundary shear stress from passage geometry and hydraulic parameters, and 5) an erosion law that weights erosion by the probability, $\mathbb{P}_k$ of a particular discharge, Q_k.

4.3.1 Model geometry

The model coordinate system is defined by x, y, z axes, with x being the cross-stream direction, y being the down/up stream direction, and z being height. Downstream is in the positive y direction. The geometry of the model is n_{cs} cross-sections along a line of length L in the y-direction representing a sub-length of the conduit, $dL = L/n_{cs}$ (Fig. 4.1). Cross-sections are a series of n_p x, z points that define their perimeter. Base level height, B, is located dL from the right-most cross-section. Geometry is initiated as a series of circular cross-sections representing a phreatic tube. The initial heights of the cross-sections are calculated from a prescribed initial passage slope with the downslope direction to the right.

Individual cross-sections contain their own properties: l_i, the set of x, z points defining the cross-section perimeter, with $l_{i,j}$ being the jth point counter-clockwise from the highest point (Fig. 4.1c), $Z_{max,i}$ is the z component of highest point, and $Z_{min,i}$ is the z component of the lowest point. Subscript i represents an individual cross-section, with $i = 1$ being the left/upstream-most cross-section, and $i = n_{cs}$ the right/downstream-most.

For every time step a wetted cross-section, $p_{k,i} \in l_i$ is created for each cross-section for all discharges. When a discharge results in conduit-full (phreatic) conditions $p_{k,i} = l_i$. In the free-surface case the subset of points is determined below a reference line that represents the height of the water (Fig. 4.1c). Wetted cross-sections have additional properties: $A_{k,i}$ is the area, $P_{k,i}$ is wetted perimeter, $R_{k,i} = A_{k,i}/P_{k,i}$ is the hydraulic radius, and $r(p_{k,i,j})$ is the distance between a reference point to each point that defines a perimeter. The reference point is the position of where velocity is maximum. For phreatic cross-sections we consider this position to be the centroid of the cross-section geometry, while for vadose cross-sections we consider this to be the the midpoint on the free-surface.

At each time step the cross-section geometry is updated perpendicular to the current geometry by an erosion rate, E_i for each point defining the perimeter, determined by weighting individual erosion rates, E_k, by $\mathbb{P}_k$. Parameters $Z_{max,i}$ and $Z_{min,i}$ are then recalculated with the evolved geometry. Erosion rates are only defined for a given discharge when the points are part of the wetted cross-section, otherwise for that discharge they are set to zero.

4.3.2 Discharge distribution

Probabilities are determined for n_Q discharges with individual discharges Q_k spaced equally in logarithmic space. Lague et al., 2005 determined that a modified gamma probability density

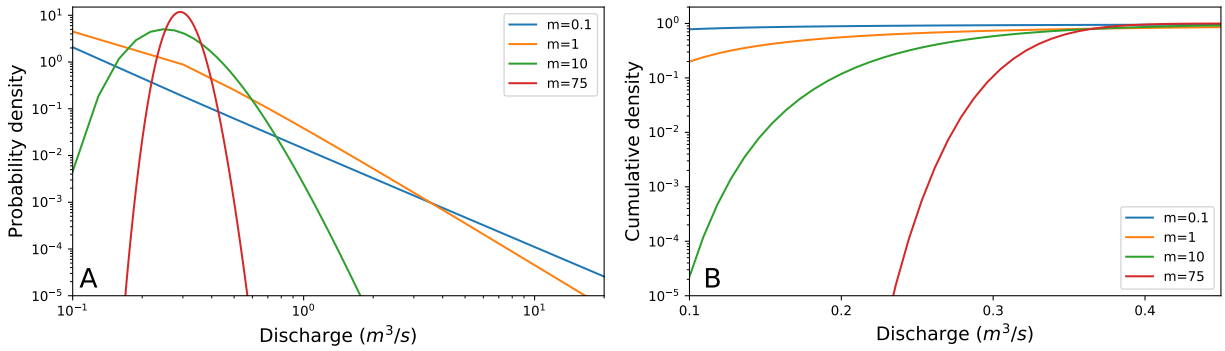

Figure 4.2: A. Probability density function of discharge with $\bar{Q} = 0.3$ for varying values of m. B. Cumulative density function with $\bar{Q} = 0.3$ for varying values of m.

function (Pdf) best fits discharge variation. This Pdf is characterized with two parameters, the mean discharge, $\bar{Q}$, and a fitting parameter, m. The modified gamma Pdf is given by Crave and Davy, 2001; Davy and Crave, 2000 as

$$Pdf_{\bar{Q},m}(Q) = \frac{(\bar{Q}m)^{m+1}}{\Gamma(m+1)} exp\Big(-m\frac{\bar{Q}}{Q}\Big) Q^{-(2+m)}\,, \tag{4.5}$$

where $\Gamma(\alpha)$ is the gamma function. The effect of changing m in this distribution is that extreme events are lessened with greater values (Fig. 4.2). The value of m is related to κ of Molnar et al., 2006, with $\kappa = m + 1$, and as such typical values for m are between zero and five.

We define the probability of a particular discharge as

$$\mathbb{P}_k = \int_{\bar{Q}_{k-1,k}}^{\bar{Q}_{k,k+1}} Pdf(Q)dQ\,, \tag{4.6}$$

where $\bar{Q}_{\alpha,\beta}$ is the average between Q_α and Q_β (Fig. 4.3). For $k = 1$ the lower limit of integration becomes 0, while the upper limit for $k = n_Q$ becomes $+\infty$.

To avoid integrating numerically for each probability the Pdf can be integrated analytically into a cumulative distribution function. From Lague et al., 2005 the cumulative distribution function is

$$Cdf_{\bar{Q},m}(Q) = 1 - \gamma(m\bar{Q}/Q, m+1)\,, \tag{4.7}$$

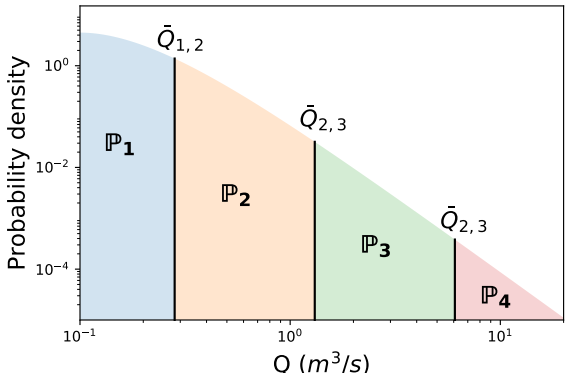

Figure 4.3: Definition of probabilities for each discharge. Here $m = 1$ and $\bar{Q} = 0.3$.

where $\gamma(\beta, \alpha)$ is the lower incomplete gamma function. As such, Eq. 4.6 becomes

$$\mathbb{P}_k = Cdf(\bar{Q}_{k-1,k}) - Cdf(\bar{Q}_{k,k+1})\,. \tag{4.8}$$

In this form $\mathbb{P}_1 = Cdf(\bar{Q}_{k,k+1})$ and $\mathbb{P}_{n_Q} = 1 - Cdf(\bar{Q}_{k-1,k})$.

4.3.3 Hydraulics

To calculate hydraulic parameters we develop an interface between the cross-section evolution code and SWMM. This interface constructs SWMM input files from the cross-sections geometries, runs a simulation to steady state, and reads the value for head at each cross-section. These simulations are run for each discharge, Q_k, per time step.

SWMM defines channel geometry through three types of objects: nodes, links, and curves. Nodes represent the junction between sections of the conduit, outlets (outfalls), or storage. Parameters specified at junctions are the height of the bottom of the junction (invert elevation in SWMM terminology), which we consider to be $Z_{min,i}$, and maximum water depth at which overland flooding occurs. The maximum depth parameter allows the total head to be limited to realistic values. To translate the model geometry to SWMM $n_{cs} + 1$ junction nodes are specified, and one outlet node

at the most downstream location representing base level. Each junction may also have an inflow defined, where water enters the conduit. We consider only the upstream-most junction to have an inflow with the value Q_k. Parameters set at the outlet are the type of outlet and height. The type of outlet is set to a fixed head condition, with the value being set to B. Values read from nodes after a simulation are the steady state head, h, at each junction and the total discharge that reaches the downstream-most junction as limited by the maximum depth parameter. This discharge is stored as the temporary discharge at a time step for erosion calculations.

Links represent lengths of conduit sub-sections. Links have two set of parameters: the first set are the length and Manning friction factor, and the second are geometry parameters consisting of the type of geometry of the cross-section, the maximum width of the cross-section, and the height. We use the custom geometry type to translate the freely updating cross-sections to SWMM. Custom geometries are specified as a shape defined by the widths at a series of heights in the cross-section. Widths and heights are normalized by the total height of the cross-section. Each cross-section l_i is translated to this format by sampling widths at equidistant heights from the bottom of the cross-section to the total height $Z_{max,i} - Z_{min,i}$. The geometry of the model is translated to SWMM with n_{cs} links with the custom geometry determined by cross-sections l_i at each time step. An additional link of length dL connects the downstream-most cross-section of the conduit to base level. The geometry of this extra link is prescribed to be the same as the downstream most cross-section.

Simulations are run using the Python module SWMM5-Python for each Q_k per time step, with dynamic wave routing that solves the full 1-D Saint-Venant Equations. We assume that each Q_k reaches a steady state and therefore simulations are run with 15 minute sweeps for a total of 24 hours to ensure simulations reach steady state. Head values at each junction, $h_{k,i}$, are recorded

from the last sweep step and friction slope for each cross-section is calculated,

$$S_{f_{k,i}} = \frac{h_{k,i} - h_{k,i+1}}{dL}. \tag{4.9}$$

4.3.4 Shear stress estimation and erosion

We use the method described in Wobus et al., 2006, Wobus et al., 2008, and Cooper and Covington, in prep(b), termed the WTA method, to estimate boundary shear stress, τ_b, for use in the erosion step. The WTA method consists of several steps: determine the height of the free-surface in the vadose case or the energy slope in the phreatic case, compute bed-normal velocity gradients, solving a force balance, and computing τ_b. This method allows the calculation of shear stress given only discharge, geometry, and roughness length, z_0.

To determine the height of the free-surface in the vadose case three equations are solved iteratively at free-surface heights until computed discharge equals prescribed discharge. These are, the continuity equation,

$$Q = \bar{u}A\,, \tag{4.10}$$

the Chézy equation,

$$\bar{u} = C\sqrt{RS_f}\,, \tag{4.11}$$

and a logarithmic approximation of the Chézy friction factor,

$$C = 2.5\sqrt{g}\ln\left(\frac{0.37R}{z_0}\right). \tag{4.12}$$

Wobus et al., 2006 considers water height to be at normal depth, and as such S_f is equal to the slope of the floor, S_0. For the phreatic case A, P, and R are known from the general cross-section and S_f is calculated. To determine whether a cross-section is under vadose or phreatic conditions we compute a maximum discharge by computing discharge at heights through the cross-section. If the

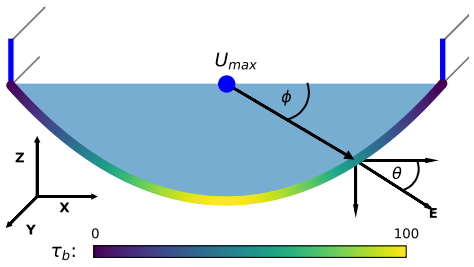

Figure 4.4: Schematic of the WTA method. U_{max} represents the position of maximum velocity. Colored floor is the normalized shear stress distribution.

prescribed discharge is greater than this maximum discharge phreatic conditions are assumed. This procedure is used in the test of multiple discharges with a single cross-section, however, we solve for height of the free-surface and friction slope using the SWMM interface in multiple cross-section simulations.

Velocity gradients are solved with a modified form of the law of the wall using the position and magnitude of the downstream maximum velocity, U_{max},

$$\left.\frac{du}{dr(p_{k,i,j})}\right|_{z_0} = \frac{U_{max_{k,i}}}{z_0} ln(r(p_{k,i,j})/z_0)^{-1} \cdot sin(\phi - \theta)\,. \tag{4.13}$$

To find the value of $U_{max_{k,i}}$ we assume the integrated law of the wall over all $p_{k,i,j}$ equals the average velocity. Angles ϕ and θ are illustrated in Figure 4.4. To translate between roughness length, z_0, and the Manning roughness coefficient used in SWMM, we combine the logarithmic fit of the Chézy friction factor with its relation to the Manning roughness coefficient,

$$C = n^{-1} R^{1/6}\,, \tag{4.14}$$

where n is the Manning roughness coefficient, resulting in the equation

$$n = \frac{R^{1/6}}{2.5\sqrt{g}} \ln\left(\frac{0.37R}{z_0}\right)^{-1}\,. \tag{4.15}$$

This equation allows the translation between hydraulic parameters in SWMM and those used in the WTA method.

From velocity gradients, boundary shear stress is computed,

$$\tau_b(p_{k,i,j}) = \varphi \rho A \left(\frac{du}{dr(p_{k,i,j})} \right)^2, \tag{4.16}$$

where φ is a force balance term,

$$\varphi = \frac{gS}{\sum_{i=1}^{n_p} \left(\frac{du}{dr(p_{k,i,j})} \right)^2 dl(j)}. \tag{4.17}$$

Here $dl(j)$ is the distance between $p_{k,i,j}$ and $p_{k,i,j-1}$.

Erosion rate at each point is calculated per discharge with a shear stress power law equation,

$$E_k(p_{i,j}) = K \tau_b(p_{k,i,j})^a, \tag{4.18}$$

where K is a constant that incorporates factors of erodibility and the size of a time step. Erosion rate for all discharges is computed by the sum of per discharge erosion rate weighted by the probability of that discharge over the general cross-section,

$$E(l_{i,j}) = \sum_{k=1}^{n_Q} \mathbb{P}_k E_k(l_{i,j}). \tag{4.19}$$

4.4 Results

4.4.1 Hydraulics, shear stress, and erosion

To test the ability of SWMM to model the hydraulics at all stages of cave development we test a single, 300 m long, conduit with 5 keyhole shaped cross-sections, as in Figure 4.1. This keyhole shape was generated via simulation of a single cross-section with $Q = 1$, $S = 0.017$ $z_0 = 0.01$ and an initial radius of $1m$. Length of the sub-conduits are 60 meters. For each scenario

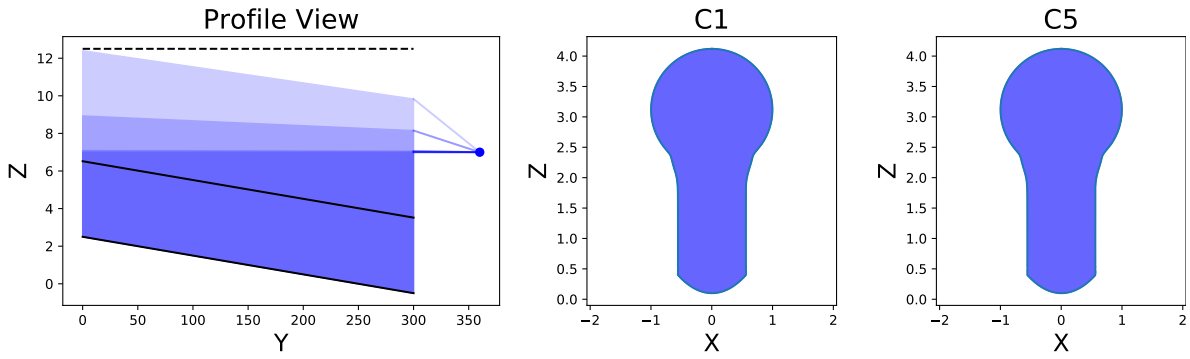

Figure 4.5: Head in the conduit when base level is above the entire conduit. Base level is indicated by a blue circle 60 meters downstream of the conduit. Progressive filling indicates head at different discharges. Colored lines are the potentiometric surface past the conduit.

base level represents a fixed head 60 meters downstream of the last junction node. The initial prescribed slope in the geometry is $S = 0.01$. Manning friction factor is set to 0.04, a common value for caves (Palmer, 2007). The ground surface is set to 12 m above the datum, which is the initial bottom of the downstream-most junction node. Four discharge values are equally spaced logarithmically from $1 - 100$, with $Q_1 = 1.0$, $Q_2 = 4.6$, $Q_3 = 21.5$, and $Q_4 = 100$. We test four scenarios of base level position to evaluate the ability of SWMM to handle the change in base level as the system evolves. The positions of base level are: entirely above the conduit, between the Z_{max} of the upstream- and downstream-most node, between Z_{max} and Z_{min} of the downstream-most cross-section, and below Z_{min} of the downstream-most cross-section. This simulation does not evolve the cross-section through time. The results of these model runs are shown in Figures 4.5-4.8.

In each case the largest discharge is limited by the surface. The limited discharges are $Q = 39$, $Q = 48$, $Q = 66$, and $Q = 70$ for cases 1, 2, 3, and 4, respectively. In most cases the friction slope is highest in the length between the down-stream most junction and base level, however, in the 3rd case when base level is between the floor and ceiling of the down-stream most section of

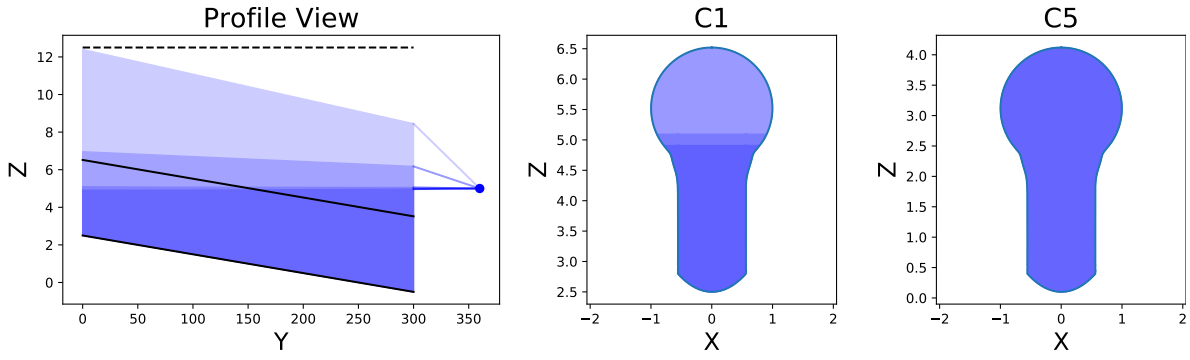

Figure 4.6: Head in the conduit when base level is above part of the conduit.

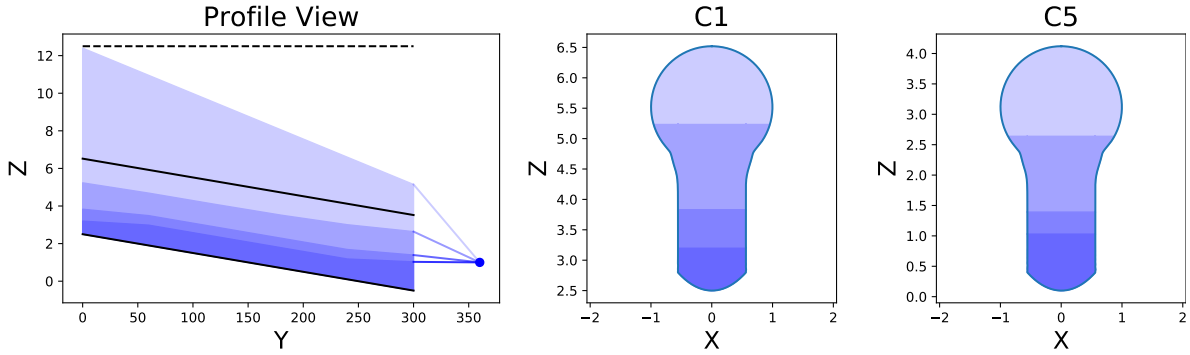

Figure 4.7: Head in the conduit when base level is in between the top and bottom of the downstream cross-section.

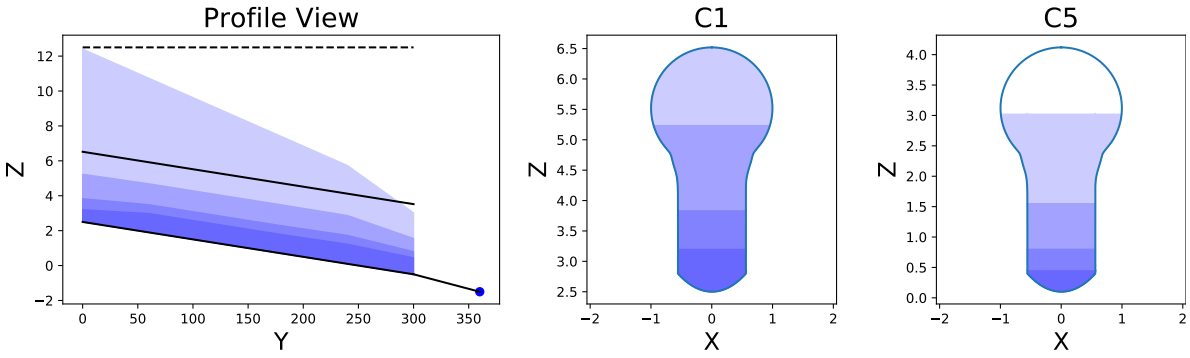

Figure 4.8: Head in the conduit when base level is below the entire conduit.

conduit the highest friction slope is located in upstream sections. In case 4 the down-stream most junction maintains a free-surface for large discharges. The limited discharge, $70m^3/s$, as well as the second highest discharge, $21.5m^3/s$ exceeds the maximum discharge capable if prescribed the same slope and roughness in a single cross-section ($\approx 20m^3/s$), with roughness value obtained from the Manning roughness coefficient, 0.04, and equation 4.15. While $21.5m^3/s$ exceeds the maximum discharge in the single cross- section case, the water height solved for is the normal depth per Chaudhry, 2007, whereas in the multiple cross-section case depth does not need to be normal.

From the hydraulic parameters shear stress is estimated via the WTA method. With head known water depth/height of the free-surface does not need to be found by the minimization method of Wobus et al., 2008, 2006, and the heads calculated from SWMM are used. In the free-surface case water depth is calculated as $h_{k,i} - Z_{min,i}$ and parameters A, P, and R are calculated from the wetted cross-section. For the conduit-full/phreatic case these parameters are calculated from the general cross-section. Per discharge distribution of shear stress for the upstream-most section of conduit in case 4 is shown in Fig. 4.9. This particular case and section are chosen as it captures all discharges including one in phreatic conditions, contains a limited upper discharge, and at least one discharge reaches normal depth where energy slope is parallel to the floor slope. The shear stress distribution for this setting shows an increase in shear stress and wetted perimeter as discharge increases. Shear stress ranges from 4-8 Pa for the lowest discharge, and from nearly 0 to 300 Pa for the highest. The highest shear stresses are located near the top of the wetted portion of the cross-section in the free-surface case, or near the centroid in the conduit-full case. At the vertical walls in the canyon part of the keyhole shear stress decreases. Along the floor shear stress increases from the canyon portion.

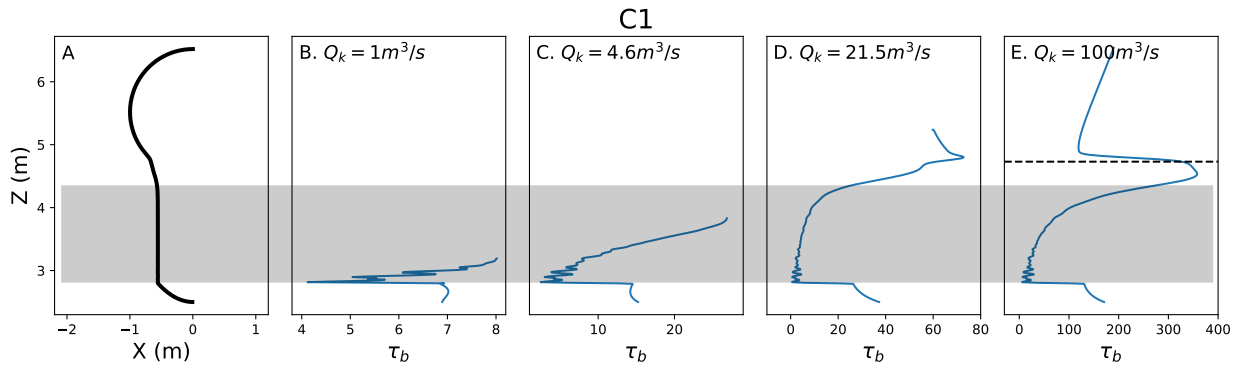

Figure 4.9: Distribution of boundary shear stress around the perimeter of C1 in case 4 for logarithmically spaced discharges. Horizontal gray box highlights the area on the shear stress distributions within the canyon part of the keyhole. In E the discharge is limited by the ground surface, and the discharge that enters the conduit is $70m^3/s$, and the horizontal dashed line indicates the vertical position of the maximum velocity location.

The distribution of erosion is also determined from the shear stress distribution (Fig. 4.10). For this purpose we use the probability distribution parameters $\bar{Q} = 3m^3/s$ and $m = 2$, resulting in $\mathbb{P}_1 = 6.4 * 10^{-1}$, $\mathbb{P}_2 = 3.5 * 10^{-1}$, $\mathbb{P}_3 = 1.1 * 10^{-2}$, and $\mathbb{P}_4 = 1.5 * 10^{-3}$, for $Q = 1$, $Q = 4.6$, $Q = 21.5$, and $Q = 100$, respectively. While the highest discharge is larger than the limit set by the imposed ground surface, $\mathbb{P}_4$ is not changed and we assume the discharge partitions between the conduit and surface flow. The highest amounts of erosion are focused along the floor of the conduit, and along the walls in the canyon section of the keyhole near the free-surfaces/centroid for each discharge. Peaks in Fig. 4.10a near the free-surfaces are artifacts of low $n_Q = 4$, however, with higher n_Q peaks are smoothed as the locations of free-surfaces are throughout the canyon portion of the keyhole (Fig. 4.10b). Despite large shear stresses higher in the cross-section during large discharges (Fig. 4.9e), erosion length is the smallest in these sections as the probabilities of such discharges are orders of magnitude less than those close to $\bar{Q}$. Note that the mean discharge value here is smaller than that used to form the keyhole geometry, and as such erosion lengths are high within the canyon part of the keyhole, which would cause widening in an evolution simulation.

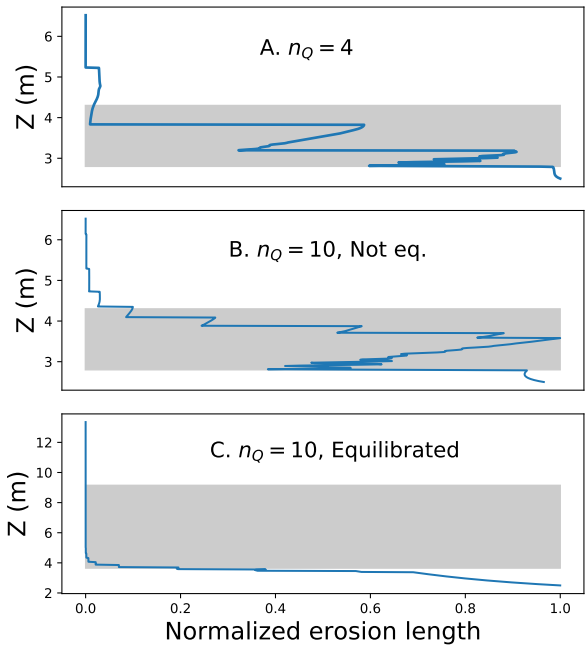

Figure 4.10: Distribution of probability weighted erosion around the perimeter of C1 in case 4 normalized by the largest value of erosion to remove the effect of K for $n_Q = 4$ (A), and $n_Q = 10$ (B and C). Gray horizontal boxes indicate the location of the canyon portion of the keyhole. For A and B the width of the canyon is not yet equilibrated with discharge, and as such erosion is largely focused on the walls of the canyon causing widening. The cross-section in C is equilibrated and as such erosion is dominantly focused on the floor. Peaks near free surface/centroid position are artifacts from the discrete discharges.

When an equilibrated keyhole cross-section for $\bar{Q}$ is used with the same geometry arrangement and settings as in case 4, erosion is dominant on the floor, with minimal widening at the bottom of the canyon (Fig. 4.10c).

4.4.2 Single cross-sections with variable discharge

As a first test of the effect of variable discharge on cross-section evolution we run simulations varying the parameter n_Q (Fig. 4.11). For such simulations the height of the free-surface is solved by minimizing equations 4.10- 4.12 with a set slope, $S = S_f = 0.017$, roughness length, $z_0 = 0.01m$, and power in the erosion law, $a = 1/2$. Distribution parameters of average discharge

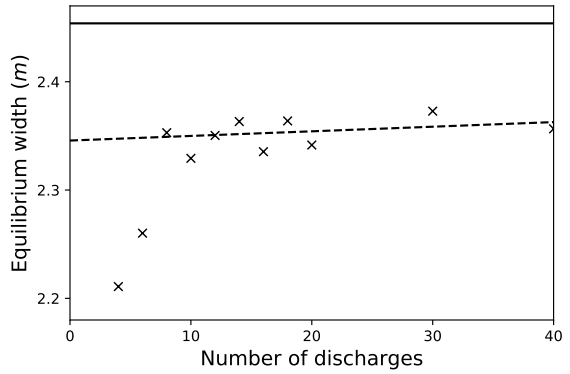

Figure 4.11: Graph on the effect of changing n_Q, with $\bar{Q} = 1m^3/s$ and $m = 2$. Solid line indicates the equilibrium width obtained when a simulation is run without a probabilistic discharge. Dashed line is a line fit to simulation results where $n_Q > 10$, demonstrating that past this value for n_Q equilibrium width does not vary substantially.

and m are set to 1.0 m^3/s and 2.0, respectively. Individual discharges, Q_k, are spaced equally in log-space from $0.1 - 32m^3/s$. If a particular discharge is greater than the maximum discharge water height is not calculated and instead S_f is calculated using equations 4.10-4.12 with the wetted cross-section equal to the general. These simulations are run until a free-surface is formed even at the largest Q_k. A single simulation of only one discharge, $Q = \bar{Q}$, with the same parameters is also run until width is stable over 100 time steps.

To explore the scaling of probabilistic discharge parameterized by $\bar{Q}$ and m we run simulations with a single cross-section varying these parameters (Fig. 4.12). The set of $\bar{Q}$ for simulations are: 0.15; 0.3; 0.6; 1.2; 2.4; 5.0; 7.5; and 15.0 m^3/s and the set of m simulated are: 0.5; 1; 2; 3; 5; and 10. Q_k is spaced equally in log-space from $0.1 - 32m^3/s$ with $n_Q = 20$, and probabilities are calculated per $\bar{Q}$, m pair. Parameters S, z_0, and a are the same as the test of varying n_Q. Similarly, simulations are run until a free-surface can be maintained for even the largest discharge value. A second set of simulations are run with only $\bar{Q}$, a probability of 1, and the same parameters as above.

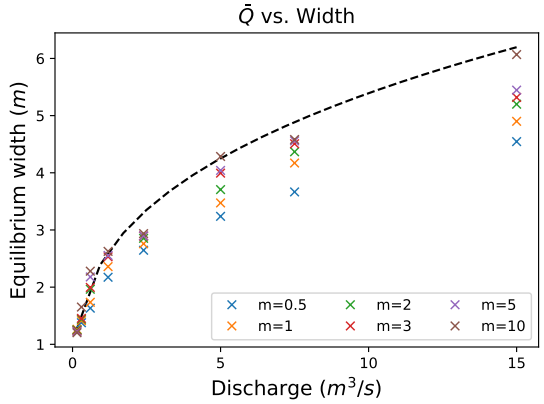

Figure 4.12: Discharge versus equilibrium width for a variety of m. Dashed line is a curve fit to simulations run without probabilistic discharge.

The results of these simulations show that the parameter m results in differing curves in the relationship between mean discharge and equilibrium width. As m increases, simulating smaller probabilities of extreme events both large and small, equilibrium width increases for a given $\bar{Q}$. The largest widths are obtained when $m \to +\infty$ and the probability $\mathbb{P}_{\bar{Q}} = 1$, simulated by only considering $\bar{Q}$. Power law curves fit to each simulation result in an exponent between 0.3 for the smallest value of m and 0.35 for the single discharge, $\bar{Q}$.

4.4.3 Multiple cross-sections with variable discharge

To test the multiple cross-section and base level change aspect of the model we test hypotheses of keyhole passage formation. Initial geometry in these simulations is a 100 meter long, 0.05 meter radius tube, with a slope of 0.03, consisting of 10 individual cross-sections. We choose the 0.05 meter radius as this is a typical stopping radius/width in speleogenesis models exploring the initial stages of cave development (e.g., Dreybrodt et al., 2005). For tests not varying discharge or the distribution of discharge we set $\bar{Q} = 1m^3/s$, $m = 2$, and sample 10 discharges equally in logarithmic space between $0.5m^3/s$, and $10m^3/s$. We choose a Manning roughness coefficient of

0.4, and calculate z_0 using 4.15. The power in the erosion law, a, is set to $1/2$ representing transport limited dissolution. In addition to the typical erosion step we smooth the erosion distribution with a univariate spline of order 1 and a smoothing factor of 0.006 to eliminate the stair steps due to discrete discharges (Fig. 4.10). The ground surface is set to 20 meters above the initial floor of the inlet junction. Initial base level position and base level drop per time step are set per simulation to explore the effects of these values on keyhole formation. Simulations are run until cross-sections either form a canyon shape, or obtain a keyhole shape.

For the first simulations we hold base level constant at various positions near the initial conduit. For the first simulation base level is set to 3 meters, near the top of the initial conduit. As the conduit enlarges head drops to a nearly flat gradient, establishing a free-surface in the upstream most parts. While a free-surface is established the low gradient combined with the position of base level produces a backwater. This backwater minimizes shear stress and incision all but stops (Fig. 4.13a). With a static base level of 1 meter the free-surface does maintain a gradient in the upstream portions of the cave with a backwater in the downstream sections. While a vadose canyon forms, a keyhole does not (Fig. 4.13b). With a static base level below the initial conduit, at -1 meter, the entire cave develops a free-surface and no backwater. Again, a vadose canyon that is not keyhole shaped forms (Fig. 4.13c).

For the second set of simulations we start with a base level at 3 meters and drop base level at various rates. We first set base level drop rate to be a static 0.1 meter per time step. In this case base level drop is initially similar to conduit enlargement when shear stresses are high, and becomes faster than enlargement once the conduit has established a larger radius and shear stress drops. In early stages of this simulation hydraulic gradient becomes gradual as conduit enlargement occurs (Fig. 4.14a), and the free-surface in upstream portions of the conduit are in backwater conditions.

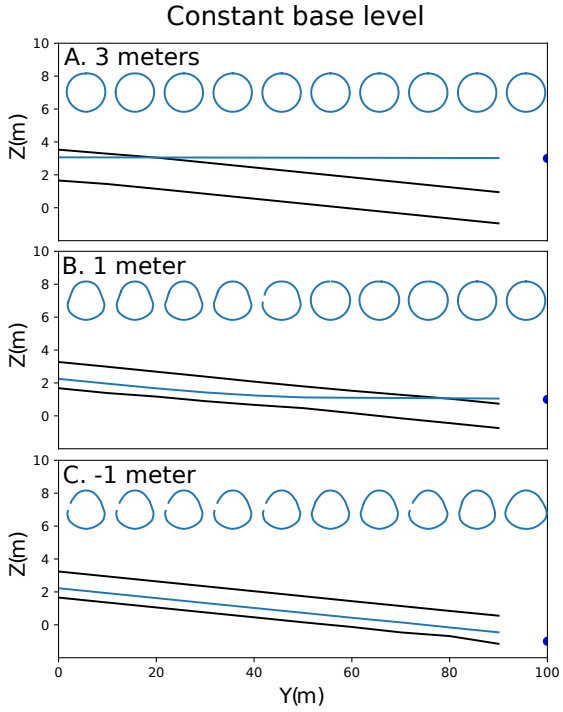

Figure 4.13: Evolution of the multiple cross-section model with a constant base level of 3 meters (A), 1 meter (B), and -1 meter (C). Inset cross-sections are in order 1-10 from left to right. These cross-sections are not to the same scale as the profile and are only to visualize shape. Blue line indicates position of head through the conduit for $\bar{Q} = 1m^3/s$, and the blue dot indicates the position of base level.

As base level continues to fall the free-surface becomes parallel to the passage floor, increasing hydraulic gradient and shear stress, though a backwater is still maintained in the downstream portions. At this point the floor slope changes from the initial slope as a non-keyhole canyon begins incising (Fig. 4.14b). Eventually, the entire conduit maintains a hydraulic gradient that is parallel to the floor, and the new floor slope is observed through the entire conduit. The geometry at this point starts with a canyon with the remnant of a phreatic tube at the upstream portion, with the remnant being overprinted in the dowstream direction. At the downstream end, a phreatic type cross-section is still maintained until the canyon completely cuts through the conduit (Fig. 4.14c). The second simulation drops base level at twice the highest calculated erosion rate per time step in the conduit. Dynamics and geometry of this simulation are the same as the first simulation of this type (Fig. 4.14c). In the last simulation of this type base level is dropped ten times the highest calculated erosion rate per time step. At this high rate of base level drop the dynamics are again the same, however, the floor slope is greater (Fig. 4.15).

The last set of simulations explore the effect of changing the parameters related to discharge during conduit evolution in attempt to simulate a keyhole shape passage. As the vadose canyon section of keyhole passages is narrower than the phreatic tube we drop mean discharge and the extremity parameter. Base level in these simulations begin at 3 meters, and drops at twice the highest rate of incision in the conduit per time step. Despite changing the parameters controlling the probability distribution, we do not change the actual discharges and they remain selected logarithmically spaced between $0.5m^3/s$ and $10m^3/s$. In these simulations we change the probability parameters once the free-surface has been established for the nearest discharge to $\bar{Q}$. For the first simulation $\bar{Q} = 3m^3/s$ while the conduit is entirely phreatic, and $\bar{Q} = 0.5m^3/s$ once the free-surface is established at $3m^3/s$. We hold $m = 3$ for the entire simulation. In this simulation a canyon is cut

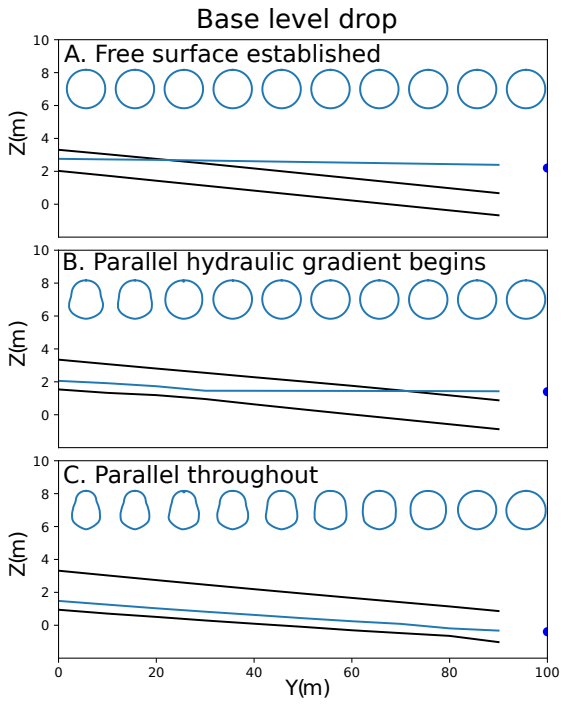

Figure 4.14: Evolution of the multiple cross-section model with dropping base level, starting with a base level at 3 meters. Base level drop is set constant at 0.1 m per time step in A and B, and twice the maximum erosion rate in C.

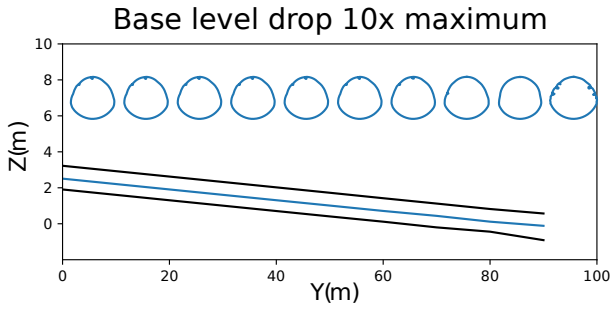

Figure 4.15: Evolution of the multiple cross-section model with base level dropping at 10 times the maximum erosion rate in the conduit. This simulation results in a higher floor slope than those with lower rates of base level fall.

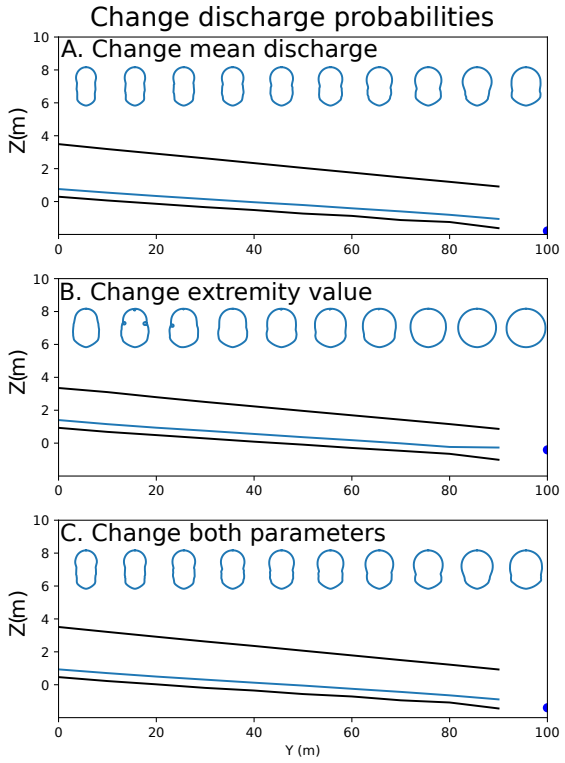

Figure 4.16: Geometry of the evolved conduit when $\bar{Q}$ is changed from $3m^3/s$ to $0.5m^3/s$ (A), m is changed from 5 to 0.5. (B), and both are changed (C). Simulations where $\bar{Q}$ changes successfully produce a keyhole shaped passage.

into the floor of the phreatic tube portion, and a keyhole forms (Fig. 4.16a). This keyhole begins in the upstream most section, migrates in the downstream direction as the conduit evolves. For the second simulation $\bar{Q}$ is held constant at $1m^3/s$ and m is changed from 5 to 0.5 once a free-surface is established. In this simulation a canyon is formed, however, it is the same width as the phreatic tube and no keyhole forms (Fig. 4.16b). For the last simulation we change both $\bar{Q}$ and m, with $\bar{Q}$ changing from $3m^3/s$ to $0.5m^3/s$, and m from 5 to 0.5. This simulation also results in a keyhole that propagates in the downstream direction (Fig. 4.16c).

4.5 Discussion

The model developed here successfully simulates erosion in cave bedrock channels with weighting by probability of discharge controlled by two parameters: the mean discharge $\bar{Q}$, and an extremity exponent, m. We also successfully model equilibrium widths when variable discharge is taken into account within a single cross-section. Finally, the model also allows the simulation of vadose canyons forming in a conduit defined by multiple cross-sections. Each of these components present valuable contributions to both speleogenesis and surface bedrock channel evolution.

4.5.1 Effect of probabilistic weighting on erosion

While the result that shear stress is higher at higher discharges (Fig. 4.9) is obvious as hydraulic gradient increases with discharge, the distribution of erosion around a channel is not necessarily intuitive when probabilistic weighting is taken into effect. As seen in Fig. 4.10a,b erosion in channels not yet equilibrated in width is dominant in areas that have not yet achieved the eventual width, and along the channel floor. In equilibrated channels (Fig. 4.10c) erosion is dominant on the floor. These areas of highest erosion are eroded at all discharges, however areas that are only eroded by the highest discharges have the smallest magnitude of erosion. The result of the highest regions having the least erosion follows that observed in Turowski et al., 2008 for surface bedrock channels. While the distribution of erosion is similar to that of surface channels, the discharges where the most erosion occurs is different. The modeled erosion rates from Turowski et al., 2008 show that the highest discharges, indicated by the highest water positions, produce the most erosion. In our model the most erosion occurs in discharges near to the mean discharge. The difference between these models is the mechanism of erosion; in Turowski et al., 2008 erosion

is due to the tools effect at high discharges, while cover dominates lower discharges, preventing erosion. As such, there exists a threshold at which a discharge can produce geomorphic work. In our model the mechanism of erosion is dissolution, where threshold discharges for geomorphic work are minimal (Covington et al., 2015).

While the tool and cover effect also plays a role in cave evolution (Cooper and Covington, in prep[b]; Farrant and P. L. Smart, 2011), we do not model it in this study. It may be likely that if it is included similar thresholding may arise. Additionally, the inclusion of sediment transport may impact equilibrium width, as increased cover is known to widen channels (Finnegan et al., 2007; Johnson and Whipple, 2010; Nelson and Seminara, 2011; Turowski et al., 2007; Yanites and Tucker, 2010). As our model does not include sediment, the equilibrium widths simulated should not be treated as an exact function of discharge to width, though the results can be interpreted as general rules.

4.5.2 Effect of variable discharge on equilibrium widths

Figure 4.12 demonstrates that variable discharge impacts the equilibrium widths obtained in bedrock channels. Widths obtained through probabilistically weighted erosion are smaller than those obtained when simulating erosion with a single discharge as done in previous studies (e.g Wobus et al., 2008, 2006). While equilibrium widths are smaller, power law fits to simulations reveal that equilibrium width scales with mean discharge to the power of $0.3 - 0.35$. These values are similar to those analytically derived (e.g Finnegan et al., 2005; Wobus et al., 2008), and modeled numerically (Cooper and Covington, in prep[b]; Wobus et al., 2006). Such values also fall within those observed in the field of $0.3 - 0.5$ (Finnegan et al., 2005; Turowski et al., 2007).

Besides $\bar{Q}$, parameters explored that effect equilibrium width are n_Q (Fig. 4.11), and m (Fig. 4.12). The number of discharges and probabilities plays an important control on actually reaching an equilibrium width. For low (< 10) n_Q equilibrium widths are smaller than those for larger values. As n_Q becomes larger, equilibrium widths are actually obtained and the width does not change with n_Q. As such, $n_Q > 10$ was used in simulations to explore scaling relationships. The effect of m is that as the value increases equilibrium widths approach those of singular value simulations with only $\bar{Q}$. The equilibrium widths obtained when erosion is weighted by probability are lower than those in the singular value case. While for smaller values of m the probabilities of larger discharges is higher, the smaller discharges are more likely. Additionally, the probabilities of large discharges is so small that their influences are minor in regions where only those discharges reach (Fig. 4.10). As m becomes large both small and large discharge effects are suppressed, and discharge values near $\bar{Q}$ become increasingly probable. As $m \to \infty$ the probability of $\bar{Q} \to 1$, and no other discharges occur.

The study by Molnar et al., 2006 allows further interpretation of these modeling results as they relate m to climate. In arid environments, large variations in discharge can occur relative to the mean discharge, and thus m is small, whereas in humid environments variability is more constrained. As such, it can be expected that for a given mean discharge, widths of channels in arid environments are narrower than their humid counterparts.

4.5.3 Multiple cross-section evolution and keyhole passages

When the single cross-section model is extended into multiple cross-sections that represent a conduit the evolution of the cave profile can be simulated. We use this model in an attempt to duplicate keyhole passages, a type of cave passage where a vadose canyon of smaller width incises

into a larger phreatic tube. We tested several hypotheses of keyhole formation: 1) the transition from phreatic to vadose conditions generate a keyhole, even without base level change, as the conduit becomes a more efficient route for water and a free-surface establishes, 2) the transition from phreatic to vadose conditions, combined with base level dropping, and 3) the transition from phreatic to vadose conditions, combined with base level drop and change in the probability of discharge as governed by climate. The only simulations that successfully form a keyhole are those where the probability of discharge changes. Additionally, only simulations where $\bar{Q}$ is dropped do keyholes form (Fig. 4.16a,c), despite smaller m producing smaller equilibrium widths in the single cross-section model (Fig. 4.12). Simulations where keyholes successfully form reveal that they propagate in the downstream direction, first forming in the most upstream portion when the hydraulic gradient becomes parallel to floor slope, creating the highest shear stresses in this portion. This represents the propagation of a knickpoint downstream. Interestingly, in thise case, the knickpoint propagates in the opposite direction of surface channels where they travel in the upstream direction (e.g., Cook et al., 2013; Crosby and Whipple, 2006; Lague, 2014; Loget and Van Den Driessche, 2009; Seidl et al., 1994).

While the other sets of simulations do not create keyholes, they do reveal some dynamics of profile evolution in caves. The simulations where the rate of base level fall is changed shows that faster drops in base level create steeper floors in vadose canyons. This result is identical to that seen in surface bedrock channels, where increasing base level rates result in steeper channels, with slope scaling to base level drop rate to the $1.3-1.5$ power (Whipple and Tucker, 1999; Wobus et al., 2006).

While the possibilities for simulation of a single conduit were not exhausted, this model shows several important results for both caves and bedrock channels. Additionally, SWMM can

simulate flows not only in single conduits, but in conduit networks, allowing this model to be extended into a network model in the future.

4.6 Conclusion

The model developed here successfully simulates several aspects of speleogenesis in turbulent flow. The first aspect is the ability to model the flow itself. Secondly, the model constructions the distribution of erosion in canyons, showing both similarities and differences to erosion in surface bedrock channels. By allowing cross-sections to freely evolve using the erosion calculated from shear stress generated by varying discharges, weighted by the probability of those discharges, equilibrium widths are successfully established, showing similar scaling to models considering only the mean discharge. Lastly, a speleogenesis model combining erosion, the ability for cross-sections to evolve at all points, and variable discharge in a conduit with flow determined by the storm water management software, SWMM, allows the simulation of single conduit evolution coupled with changes in base level. This model was used to test various hypotheses on the formation of keyhole type passages.

Simulations of the distribution of erosion weighted by discharge probability showed that erosion is focused on the walls of a canyon and the floor for non-equilibrated channels, and on the floor for equilibrated ones. This focusing occurs despite the highest discharges producing high shear stresses in upper parts of the canyons, as the probability of high discharges is low. These simulations also show that lower discharges, near the mean discharge, do most of the geomorphic work when the erosion mechanism is dissolution, opposite that observed in bedrock channels where tool and cover effects are provided by sediment.

The freely updating single cross-section model with variable discharge shows a similar scaling of equilibrium width to discharge in canyons, however, the magnitude of widths is lower for the variable discharge model. The magnitude of the width is affected by a parameter of the discharge distribution that changes the probability of extreme events; when more extreme events occur, such as in arid environments, equilibrium widths are lower.

The multiple cross-section model is part of the forefront of current speleogenesis models, combining a recent speleogenesis model for cross-section development in turbulent flow with common features in bedrock channel models. We used this model to test multiple hypotheses of keyhole formation, which can only be adequately simulated when taking into account variable discharge, base level change, and the ability of a model to transition between conduit-full conditions and free-surfaces. Keyholes are successfully simulated only when average discharge is changed in the probability distribution. These modeled keyholes propagate downstream, the opposite of that observed in surface channels. This model can be used in the future for realistic simulations of a variety of cave geometries, and allow the exploration of relationships that can only be obtained through numerical models.

4.7 References

Anthony, D. M. and D. E. Granger (2004). "A Late Tertiary origin for multilevel caves along the western escarpment of the Cumberland Plateau, Tennessee and Kentucky, established by 26Al and 10Be". In: *Journal of Cave and Karst Studies* 66.2, pp. 46–55.

— (2006). "Five million years of Appalachian landscape evolution preserved in cave sediments". In: *Perspectives on karst geomorpology, hydrology, and geochemistry - A tribute volume to Derek C. Ford and William B. White*. Ed. by R. S. Harmon and C. M. Wicks. Vol. 404. Special Paper. Geological Society of America, pp. 39–50.

— (2007). "A new chronology for the age of Appalachian erosional surfaces determined by cosmogenic nuclides in cave sediments". In: *Earth Surface Processes and Landforms* 32.6, pp. 874–887.

Audra, P. and A. N. Palmer (2011). “The pattern of caves: controls of epigenic speleogenesis”. In: *Géomorphologie: relief, processus, environnement* 17.4, pp. 359–378.

Barbour, J. R., C. P. Stark, C. W. Lin, H. Chen, M. J. Horng, C. P. Ko, T. C. Yi, T. T. Tsai, W. S. Chang, S. P. Lee, et al. (2009). “Magnitude-frequency distributions of boundary shear stress along a rapidly eroding bedrock river”. In: *Geophysical Research Letters* 36.4.

Bonacci, O. (2001). “Analysis of the maximum discharge of karst springs”. In: *Hydrogeology Journal* 9.4, pp. 328–338.

Campbell, C. W. and S. M. Sullivan (2002). “Simulating time-varying cave flow and water levels using the Storm Water Management Model”. In: *Engineering Geology* 65 (2-3), pp. 133–139.

Chaudhry, M. H. (2007). *Open-channel flow*. Springer Science & Business Media.

Cook, K. L., J. M. Turowski, and N. Hovius (2013). “A demonstration of the importance of bedload transport for fluvial bedrock erosion and knickpoint propagation”. In: *Earth Surface Processes and Landforms* 38.7, pp. 683–695.

Cooper, M. P. and M. D. Covington (in prep[a]). “Cave meanders as a record of erosional mechanism”. In:

— (in prep[b]). “Numerical modeling of paragenetic gallery formation in caves”. In:

Covington, M. D. (2014). “Calcite dissolution under turbulent flow conditions: a remaining conundrum”. In: *Acta Carsologica* 43.1, pp. 195–202.

Covington, M. D., J. D. Gulley, and F. Gabrovšek (2015). “Natural variations in calcite dissolution rates in streams: Controls, implications, and open questions”. In: *Geophysical Research Letters* 42.8, pp. 2836–2843.

Covington, M. D., A. J. Luhmann, C. M. Wicks, and M. O. Saar (2012). “Process length scales and longitudinal damping in karst conduits”. In: *Journal of Geophysical Research* 117.F1, pp. 1–19. ISSN: 0148-0227. DOI: 10.1029/2011JF002212. URL: http://www.agu.org/pubs/crossref/2012/2011JF002212.shtml.

Covington, M. D., C. M. Wicks, and M. O. Saar (2009). “A dimensionless number describing the effects of recharge and geometry on discharge from simple karstic aquifers”. In: *Water Resources Research* 45.11, W11410. DOI: 10.1029/2009WR008004.

Crave, A. and P. Davy (2001). “A stochastic “precipiton” model for simulating erosion/sedimentation dynamics”. In: *Computers & Geosciences* 27.7, pp. 815–827.

Crosby, B. T. and K. X. Whipple (2006). “Knickpoint initiation and distribution within fluvial networks: 236 waterfalls in the Waipaoa River, North Island, New Zealand”. In: *Geomorphology* 82.1-2, pp. 16–38.

Dasher, G. R. (1994). *On Station*. Huntsville, Alabama: National Speleological Society.

Davy, P. and A. Crave (2000). “Upscaling local-scale transport processes in large-scale relief dynamics”. In: *Physics and Chemistry of the Earth, Part A: Solid Earth and Geodesy* 25.6-7, pp. 533–541.

DiBiase, R. A. and K. X. Whipple (2011). “The influence of erosion thresholds and runoff variability on the relationships among topography, climate, and erosion rate”. In: *Journal of Geophysical Research: Earth Surface* 116.F4.

Dreybrodt, W. (1988). *Processes in karst systems, physics, chemistry, and geology*. New York, USA: New York, NY (USA); Springer-Verlag, p. 288.

— (1996). “Principles of early development of karst conduits under natural and man-made conditions revealed by mathematical analysis of numerical models”. In: *Water Resources Research* 32.9, pp. 2923–2935.

Dreybrodt, W., F. Gabrovšek, and D. Romanov (2005). *Processes of Speleogenessis: A Modeling Approach*. Vol. 4. Ljubljana, Slovenia: ZRC Publishing, p. 376.

Dufresne, D. P. and C. W. Drake (1999). “Regional groundwater flow model construction and wellfield site selection in a karst area, Lake City, Florida”. In: *Engineering Geology* 52.1-2, pp. 129–139.

Farrant, A. R. and P. L. Smart (2011). “Role of sediment in speleogenesis; sedimentation and paragenesis”. In: *Geomorphology* 134.1, pp. 79–93.

Finnegan, N. J., G. Roe, D. R. Montgomery, and B. Hallet (2005). “Controls on the channel width of rivers: Implications for modeling fluvial incision of bedrock”. In: *Geology* 33.3, pp. 229–232.

Finnegan, N. J., L. S. Sklar, and T. K. Fuller (2007). “Interplay of sediment supply, river incision, and channel morphology revealed by the transient evolution of an experimental bedrock channel”. In: *Journal of Geophysical Research* 112.F3, pp. 1–17. ISSN: 0148-0227. DOI: 10.1029/2006JF000569. URL: http://www.agu.org/pubs/crossref/2007/2006JF000569.shtml.

Ford, D. C. and R. O. Ewers (1978). “The development of limestone cave systems in the dimensions of length and depth”. In: *Canadian Journal of Earth Sciences* 15.11, pp. 1783–1798.

Gabrovšek, F., P. Häuselmann, and P. Audra (2014). "'Looping caves' versus 'water table caves': The role of base-level changes and recharge variations in cave development". In: *Geomorphology* 204, pp. 683–691.

Gabrovšek, F., B. Peric, and G. Kaufmann (2018). "Hydraulics of epiphreatic flow of a karst aquifer". In: *Journal of Hydrology* 560, pp. 56–74.

Gallegos, J. J., B. X. Hu, and H. Davis (2013). "Simulating flow in karst aquifers at laboratory and sub-regional scales using MODFLOW-CFP". In: *Hydrogeology journal* 21.8, pp. 1749–1760.

Ghasemizadeh, R., X. Yu, C. Butscher, F. Hellweger, I. Padilla, and A. Alshawabkeh (2015). "Equivalent porous media (EPM) simulation of groundwater hydraulics and contaminant transport in karst aquifers". In: *PloS one* 10.9, e0138954.

Granger, D. E., D. Fabel, and A. N. Palmer (2001). "Pliocene- Pleistocene incision of the Green River, Kentucky, determined from radioactive decay of cosmogenic 26Al and 10Be in Mammoth Cave sediments". In: *Geological Society of America Bulletin* 113.7, pp. 825–836.

Granger, D. E., J. W. Kirchner, and R. C. Finkel (1997). "Quaternary downcutting rate of the New River, Virginia, measured from differential decay of cosmogenic 26Al and 10Be in cave-deposited alluvium". In: *Geology* 25, pp. 107–110.

Granger, D. E. and L. Siame (2006). "A review of burial dating methods usingˆ 2ˆ 6Al andˆ 1ˆ 0Be". In: *Special Papers-Geological Society of America* 415, p. 1.

Groves, C. G. and J. Meiman (2005). "Weathering, geomorphic work, and karst landscape evolution in the Cave City groundwater basin, Mammoth Cave, Kentucky". In: *Geomorphology* 67 (1-2), pp. 115–126.

Halihan, T. and C. M. Wicks (1998). "Modeling of storm responses in conduit flow aquifers with reservoirs". In: *Journal of Hydrology* 208.1-2, pp. 82–91. ISSN: 0022-1694. DOI: DOI: 10.1016/S0022-1694(98)00149-8.

Hartshorn, K., N. Hovius, W. B. Dade, and R. L. Slingerland (2002). "Climate-driven bedrock incision in an active mountain belt". In: *Science* 297.5589, pp. 2036–2038.

Hill, M. E., M. T. Stewart, and A. Martin (2010). "Evaluation of the MODFLOW-2005 conduit flow process". In: *Groundwater* 48.4, pp. 549–559.

Johnson, J. P. and K. X. Whipple (2010). "Evaluating the controls of shear stress, sediment supply, alluvial cover, and channel morphology on experimental bedrock incision rate". In: *Journal of Geophysical Research* 115.F02018.

Kaufmann, G., F. Gabrovšek, and J. Turk (2016). "Modelling cave flow hydraulics in Postojnska jama, Slovenia/Modeliranje toka podzemeljske Pivke v Postojnski jami, Slovenija". In: *Acta Carsologica* 45.1, p. 57.

Kirby, E. and K. X. Whipple (2012). "Expression of active tectonics in erosional landscapes". In: *Journal of Structural Geology* 44, pp. 54–75.

Lague, D. (2010). "Reduction of long-term bedrock incision efficiency by short-term alluvial cover intermittency". In: *Journal of Geophysical Research: Earth Surface* 115.F2.

— (2014). "The stream power river incision model: evidence, theory and beyond". In: *Earth Surface Processes and Landforms* 39.1, pp. 38–61.

Lague, D., N. Hovius, and P. Davy (2005). "Discharge, discharge variability, and the bedrock channel profile". In: *Journal of Geophysical Research (Earth Surface)* 110.F9, pp. 4006–+. DOI: 10.1029/2004JF000259.

Lauritzen, S.-E. and J. Lundberg (2000). "Solutional and erosional morphology of caves". In: *In: Klimchouk, A., Ford, DC, Palmer, Arthur N. & Dreybrodt, Wolfgang,(eds), Speleogenesis. Evolution of Karst Aquifers. National Speleological Society, Huntsville*, pp. 408–426.

Loget, N. and J. Van Den Driessche (2009). "Wave train model for knickpoint migration". In: *Geomorphology* 106.3-4, pp. 376–382.

Miller, S. R., P. B. Sak, E. Kirby, and P. R. Bierman (2013). "Neogene rejuvenation of central Appalachian topography: Evidence for differential rock uplift from stream profiles and erosion rates". In: *Earth and Planetary Science Letters* 369, pp. 1–12.

Molnar, P., R. S. Anderson, G. Kier, and J. Rose (2006). "Relationships among probability distributions of stream discharges in floods, climate, bed load transport, and river incision". In: *Journal of Geophysical Research: Earth Surface* 111.F2.

Nelson, P. A. and G. Seminara (2011). "Modeling the evolution of bedrock channel shape with erosion from saltating bed load". In: *Geophysical Research Letters* 38.17.

Olsson, J. and P. Burlando (2002). "Reproduction of temporal scaling by a rectangular pulses rainfall model". In: *Hydrological Processes* 16.3, pp. 611–630.

Olsson, J. and J. Niemczynowicz (1996). "Multifractal analysis of daily spatial rainfall distributions". In: *Journal of Hydrology* 187.1-2, pp. 29–43.

Opdyke, B. N., G. Gust, and J. R. Ledwell (1987). "Mass transfer from smooth alabaster surfaces in turbulent flows". In: *Geophysical Research Letters* 14.11, pp. 1131–1134. ISSN: 0094-8276. DOI: 10.1029/GL014i011p01131.

Palmer, A. N. (1984). “Geomorphic interpretation of karst features”. In: *Groundwater as a geomorphic agent. Allen and Unwin, Boston, Massachusetts. 390pp*, pp. 173–209.

— (1987). “Cave levels and their interpretation”. In: *National Speleological Society Bulletin* 49.2, pp. 50–66.

— (1991). “Origin and morphology of limestone caves”. In: *Geological Society of America Bulletin* 103.1, pp. 1–21.

— (2007). *Cave Geology*. Dayton, OH: Cave Books.

Perne, M., M. D. Covington, and F. Gabrovšek (2014). “Evolution of karst conduit networks in transition from pressurised flow to free surface flow”. In: *Hydrology and Earth System Sciences Discussions* 11.6, pp. 6519–6559. DOI: 10.5194/hessd-11-6519-2014. URL: http://www.hydrol-earth-syst-sci-discuss.net/11/6519/2014/.

Peterson, E. W. and C. M. Wicks (2006). “Assessing the importance of conduit geometry and physical parameters in karst systems using the storm water management model (SWMM)”. In: *Journal of Hydrology* 329 (1-2), pp. 294–305.

Prelovšek, M., J. Turk, and F. Gabrovšek (2008). “Hydrodynamic aspect of caves”. In: *International Journal of Speleology* 37.1.

Roberts, G. G. and N. White (2010). “Estimating uplift rate histories from river profiles using African examples”. In: *Journal of Geophysical Research: Solid Earth* 115.B2.

Rossman, L. A. (2010). *Storm water management model user’s manual, version 5.0*. National Risk Management Research Laboratory, Office of Research and Development, US Environmental Protection Agency Cincinnati.

Scanlon, B. R., R. E. Mace, M. E. Barrett, and B. Smith (2003). “Can we simulate regional groundwater flow in a karst system using equivalent porous media models? Case study, Barton Springs Edwards aquifer, USA”. In: *Journal of hydrology* 276.1-4, pp. 137–158.

Seidl, M. A., W. E. Dietrich, and J. W. Kirchner (1994). “Longitudinal profile development into bedrock: An analysis of Hawaiian channels”. In: *The Journal of Geology* 102.4, pp. 457–474.

Smart, C. C. (1988). “A deductive model of karst evolution based on hydrological probability”. In: *Earth Surface Processes and Landforms* 13.3, pp. 271–288.

Snyder, N. P., K. X. Whipple, G. E. Tucker, and D. J. Merritts (2003). “Importance of a stochastic distribution of floods and erosion thresholds in the bedrock river incision problem”. In: *Journal of Geophysical Research: Solid Earth* 108.B2.

Springer, G. S. (2004). “A pipe-based, first approach to modeling closed conduit flow in caves”. In: *Journal of hydrology* 289.1, pp. 178–189.

Stark, C. P. (2006). “A self-regulating model of bedrock river channel geometry”. In: *Geophysical Research Letters* 33.4.

Stock, G. M., D. E. Granger, I. D. Sasowsky, R. S. Anderson, and R. C. Finkel (2005). “Comparison of U–Th, paleomagnetism, and cosmogenic burial methods for dating caves: implications for landscape evolution studies”. In: *Earth and Planetary Science Letters* 236.1-2, pp. 388–403.

Sun, A. Y., S. L. Painter, and R. T. Green (2005). “Modeling Barton Springs segment of the Edwards aquifer using MODFLOW-DCM”. In: *Sinkholes and the Engineering and Environmental Impacts of Karst*, pp. 163–177.

Svensson, C., J. Olsson, and R. Berndtsson (1996). “Multifractal properties of daily rainfall in two different climates”. In: *Water Resources Research* 32.8, pp. 2463–2472.

Szymczak, P. and A. J. C. Ladd (2011). “The initial stages of cave formation: Beyond the one-dimensional paradigm”. In: *Earth and Planetary Science Letters* 301.3, pp. 424–432.

Tucker, G. E. and R. L. Bras (2000). “A stochastic approach to modeling the role of rainfall variability in drainage basin evolution”. In: *Water Resources Research* 36.7, pp. 1953–1964.

Turowski, J. M., N. Hovius, H. Meng-Long, D. Lague, and C. Men-Chiang (2008). “Distribution of erosion across bedrock channels”. In: *Earth Surface Processes and Landforms: The Journal of the British Geomorphological Research Group* 33.3, pp. 353–363.

Turowski, J. M., D. Lague, and N. Hovius (2007). “Cover effect in bedrock abrasion: A new derivation and its implications for the modeling of bedrock channel morphology”. In: *Journal of Geophysical Research: Earth Surface* 112.F4.

Whipple, K. X. (2004). “Bedrock Rivers and the Geomorphology of Active Orogens”. In: *Annual Review of Earth and Planetary Sciences* 32, pp. 151–185. DOI: 10.1146/annurev.earth.32.101802.120356.

Whipple, K. X. and G. E. Tucker (1999). “Dynamics of the stream-power river incision model: Implications for height limits of mountain ranges, landscape response timescales, and research needs”. In: *Journal of Geophysical Research* 104.B8.

White, W. B. (1988). *Geomorphology and Hydrology of Karst Terrains*. New York, USA: Oxford University Press.

Whittaker, A. C., P. A Cowie, M. Attal, G. E. Tucker, and G. P. Roberts (2007). “Bedrock channel adjustment to tectonic forcing: Implications for predicting river incision rates”. In: *Geology* 35.2, pp. 103–106.

Wobus, C. W., J. W. Kean, G. E. Tucker, and R. S. Anderson (2008). “Modeling the evolution of channel shape: Balancing computational efficiency with hydraulic fidelity”. In: *Journal of Geophysical Research: Earth Surface (2003–2012)* 113.F2.

Wobus, C. W., G. E. Tucker, and R. S. Anderson (2006). “Self-formed bedrock channels”. In: *Geophysical Research Letters* 33.18.

Worthington, S. R. H. (2005). “Evolution of caves in response to base-level lowering”. In: *Cave and Karst Science* 32.1, p. 3.

Yanites, B. J. and G. E. Tucker (2010). “Controls and limits on bedrock channel geometry”. In: *Journal of Geophysical Research* 115.F04019, pp. 1–17.

5 Conclusions

The components of this dissertation provide a first step for understanding speleogenesis past the breakthrough stage, when turbulent flow develops, sediment is transported, and the bulk of cave morphology forms. Notably, this dissertation establishes the first accurate model of cross-section evolution within caves including a variety of settings: phreatic tubes, paragenetic galleries, both meandering and non-meandering vadose canyons, and keyhole passages. The third project extends the freely updating 2D cross-section model to one of a single conduit in the form of a series of cross-sections representing sub-reaches. The code-base for these simulations is available to download and adapt for future use.

Besides the production of accurate simulations of cross-section geometries, each project contributes to the field of speleogenesis and to bedrock channels in general. The first project models the process of paragenesis, where cave development proceeds upwards under phreatic conditions coupled with a sediment cover. This process has only so far been understood in a conceptual framework, with minimal physical modeling, and no physical models of the formation of paragenetic galleries. The successful simulation of the process reveals dynamics of paragenetic gallery formation that have been hypothesized in conceptual models. While duplication via a model developed from first principles on its own provides a valuable contribution to the field, the first project also explores results that can only be obtained through modeling. The ability to simulate paragenetic galleries with prescribed discharge and sediment supply over large timescales that can not be observed in the field enables the exploration of how geometry responds to these input parameters. The scaling relationship derived analytically from the governing equations is verified through a set of simulations, and the establishment of such a scaling relationship can be used to constrain past

conditions of sediment supply and discharge from the simple measurement of paragenetic gallery width. This relationship shows that equilibrium width in paragenetic galleries scales with discharge to the 1/2 power, and weakly (1/6 power) to the inverse of sediment supply. Interestingly, this inverse scaling with sediment supply is the opposite of what is observed and modeled for surface bedrock channels.

The numerical model of cross-section evolution adds additional evidence that our understanding of erosion in soluble bedrock channels is incomplete; paragenetic galleries and vadose canyons that reach a stable width, as seen ubiquitously in the field, do not form unless erosion is a function of shear stress. For erosion to scale with shear stress these types of passages must form by mechanical erosion, or transport limited dissolution, contradicting predictions of only reaction rate limited dissolution occurring in turbulent flow. The cross-section model developed in this first study, combined with the observation that shear stress indicating bedforms, scallops, have different sizes on opposing walls around a meander bend provide a potential way of resolving the type of erosion seen in various cave settings. The second study in this dissertation combined cross-section models of meanders where shear stress on opposing walls and the incision angle of the wall was recorded, with measurements of 3D scanned, well scalloped, meander bends in a gypsum cave, Parks Ranch Cave in New Mexico, and a limestone cave, Copperhead Cave, in Arkansas. Simulations revealed that different powers in a shear stress erosion law, reflective of erosion process, produced different relationships between shear stress/scallop ratio, and incision angle. Statistical interpretation of the field data in both Copperhead Cave and Parks Ranch Cave indicate that the power in the shear stress erosion law is between 0.5 and 2.5, with a best fit of approximately 1 for Parks Ranch Cave, and 0.5 for Copperhead Cave. These values arise through a mix of dissolution and mechanical erosion. The lack of plucked blocks in these caves suggested that abrasion is the

dominant mechanical process, though plucking of individual grains may be important, however no models exist suggesting the scaling of grain plucking to shear stress. Dissolution in either case can be reaction rate limited or transport limited to produce such a scaling of erosion to shear stress.

This study also produced a valuable tool in bedrock channel simulations, as well as a tool for estimating discharge from scallops in vadose settings. Statistical fitting of scallop sizes estimated by the shear stress approximation method to scallops measured around a meander bend in Parks Ranch Cave showed that the method developed for straight reaches successfully approximates shear stress in a non-straight type cross-section by shifting the position of maximum velocity, validating its veracity in the meander cross-section evolution model. This fitting minimizes the difference between scallop size calculated from by discharge and slope and that of the measured scallop distribution in the channel. The minimized value of discharge and slope from this method successfully reconstructed water height as indicated by the change in angle of passage walls, and the slope from minimization matched measured floor slope.

The last study in this dissertation extends the speleogenesis model developed for simulating paragenesis and vadose canyons in several, more realistic ways. First, the cross-section model is extended into a series of cross-sections representing sub-lengths of an individual conduit (considered to be 2.5 dimensional), with water height determined by the storm water management software, SWMM. This model combines a feature widely implemented in surface bedrock channel models, but mostly neglected in speleogenesis models, the ability for base level to evolve. Lastly, hydraulic parameters for multiple discharges are calculated, and erosion is weighted by the probability of a particular discharge as determined by a two parameter discharge distribution. For the last feature, the implementation in this study appears to be the first in a cross-section model where the cross-section can freely evolve at all points, and therefore is a valuable contribution not only to speleo-

genesis models, but to bedrock channels in general. The variable discharge feature, combined with a single cross-section reveals the importance of the distribution parameters of average discharge and one controlling the probability of extreme events. Such simulations showed that width of vadose canyons/surface bedrock channels including variable discharge scales the same as if only the single, average discharge is considered. However, the actual magnitude of width is smaller than the single, average discharge. As the extremity parameter increases, simulating less importance of extreme events, width magnitude approaches the single discharge case. As high variability occurs in arid environments and less variability occurs in more humid environments, these results show that equilibrium widths are likely smaller per average discharge in arid environments.

The 2.5D nature of the model, combined with base level changes allows the simulation of many cave passage geometries. As a first use of this type of speleogenesis model keyhole type passages were successfully simulated from an initial, post-breakthrough, phreatic tube when mean discharge falls during conduit evolution. This model shows potential for many future speleogenesis models, and the capability of SWMM to simulate not only single conduits, but networks of pipes, allows further extension to model network geometries, such as branchwork or maze caves, post-breakthrough.

Overall this dissertation presents a contribution to speleogenesis models and to understanding erosion in caves. It also opens up future lines of work. To resolve the issue of the type of dissolution in caves more field work is recommended using measurements scalloped, meandering channels with a set incision angle. An extremely valuable test of the meander method would be to perform measurements in a glacier cave, as the scaling with erosion is known. Further, experiments to quantify the scaling of erosion to shear stress for individual grain plucking would help in understanding the erosional processes in gypsum and limestone caves. The importance of grain plucking

can also be explored by collecting field samples and using microscopy as plucked grains leave a signature fingerprint. Finally, the model developed in last study show promise for simulating realistic geometries not only at the cross-section level, but the reach level as well.